NMR IMAGING INVESTIGATIONS OF SWELLING HPMC TABLETS

by

GLENN WONG HUP AUN

B. Sc., The University of British Columbia, 1999

A THESIS SUBMITTED IN PARTIAL FULFILMENT OF
THE REQUIREMENTS FOR THE DEGREE OF

MASTER OF SCIENCE

in

THE FACULTY OF GRADUATE STUDIES

(Department of Chemistry)

We accept this thesis as conforming
to the required standard

THE UNIVERSITY OF BRITISH COLUMBIA

November 2001

In presenting this thesis in partial fulfilment of the requirements for an advanced degree at the University of British Columbia, I agree that the Library shall make it freely available for reference and study. I further agree that permission for extensive copying of this thesis for scholarly purposes may be granted by the head of my department or by his or her representatives. It is understood that copying or publication of this thesis for financial gain shall not be allowed without my written permission.

Department of CHEMISTRY

The University of British Columbia
Vancouver, Canada

Date NOVEMBER 27, 2001

Abstract

The use of controlled release formulations in the pharmaceutical industry offers several advantages over rapid release formulations. An important feature of controlled release formulations is the ability to release a drug for an extended period of time at a controlled rate. One example is hydroxypropylmethylcellulose (HPMC) which is a hydrophilic polymer that has the unique property that when exposed to water, it undergoes a volume expansion or swells resulting in a polymer concentration gradient. A drug combined with HPMC into a tablet has a drug diffusion behaviour that is determined by this HPMC concentration gradient. To gain further insight in terms of providing concentration information, NMR imaging was employed in the present work to investigate the swelling of pure HPMC tablets.

One-dimensional swelling experiments exposed only one side of a flat face HPMC tablet to water and therefore limited the swelling to only one direction. These swelling experiments were carried out at the physiological temperature of 37 °C and at various temperatures to determine if a correlation existed between temperature and the swelling rate. The results indicated a dependence of the swelling rate on temperature with an increase in temperature resulting in a greater swelling rate.

To provide a more realistic understanding of these swelling systems, a three-dimensional swelling experiment was also carried out to monitor the polymer concentration gradients in three-dimensions. In contrast to the one-dimensional swelling, the three-dimensional swelling of a pure HPMC tablet involved the water penetration into both flat faces and sides. Results indicated that the rate of expansion favoured the vertical swelling direction over the radial direction as expected.

In an effort to predict the swelling behaviour, a mathematical model was employed to

simulate the one-dimensional swelling of a series of tablets of different thicknesses. Evaluation of the model was done by comparing the theoretical to the experimental results. The mathematical model was limited in its ability to predict the swelling in one-dimension. It assumed that the swelling was a homogeneous, single component system which did not reflect the one-dimensional experimental results that indicated a less homogeneous and a more heterogeneous swelling process.

TABLE OF CONTENTS

List of Tables

List of Figures

List of Abbreviations

BVT	Bruker Variable Temperature unit
FID	Free Induction Decay
HPMC	Hydroxypropylmethylcellulose
i.d.	Inner Diameter
NMR	Nuclear Magnetic Resonance
o.d.	Outer Diameter
rf	Radio Frequency
S.D.	Standard Deviation
T_E	Time-to-echo, time between 90° pulse and maximum amplitude of the echo
T_R	Repetition time, delay between repeats of an NMR experiment

Acknowledgements

I would like to extend my gratitude to my research supervisor, Dr. Colin Fyfe for his guidance and input during the course of my research. I would like to thank Dr. Andrew Lewis for his help and patience especially during the initial stages of my work. I would like to thank Dr. Charles Haynes of the Department of Biotechnology for his assistance in the modeling of the tablets and Nooshie for writing the program. I would like to thank Dr. Robert Miller of the Department of Pharmaceutical Sciences for the preparation of the tablets. I would like to thank all the Fyfe group members, past and present for their friendship and kindness. Finally, I would like to thank my Mom, Dad, and Brother for all their support.

Chapter 1

Introduction

1.1 Controlled Release Formulations

Controlled drug delivery by solid dosage forms such as tablets is advantageous for both the patient and the pharmaceutical industry. These delivery systems when used correctly, can deliver a drug at a predetermined rate for a definite time period while maintaining a therapeutic level where the concentration of the drug released does not reach a toxic level. The release of the drug can extend for a prolonged period of time in which case only one tablet needs to be ingested. A study done in 1979 estimated that 50% of the 1.8 billion prescription medications issued annually in the United States are not taken correctly [1]. Incorrect use of medications can result in an overdose-underdose cycle of drug concentration that is due to the ingestion of rapid-release formulations which are taken at regular intervals. These rapid-release formulations when ingested incorrectly at shortened intervals, lead to an increase in drug concentration that could reach a toxic level. On the other hand, prolonged intervals between ingestion leads to a continual decrease in drug concentration. The drug concentration eventually drops below the therapeutic level resulting in an ineffective drug treatment. By administering a single controlled release tablet, the patient is relieved from the constant ingestion of medication and at the same time therapeutic drug concentrations are attained and then maintained for an extended period.

Controlled release technology provides a benefit not only to the patient but also to the pharmaceutical industry. The cost of developing a controlled release formulation is greater than a conventional formulation but increases the efficiency of the drug and is less expensive than the development of a new drug. In addition to the cost, since drug patents expire after several years, a new drug delivery system may give continued benefits for the pharmaceutical company [2]. The long term goal is to tailor a drug treatment to the needs of a group of patients where the rate

of drug release, location, and timing are factors that can be directly controlled.

1.2 Swelling Controlled Delivery Systems

Swelling controlled delivery systems involve the use of a group of hydrophilic polymers that has a unique swelling behaviour when exposed to water. Cellulose ethers are a broad class of hydrophilic polymers that include hydroxypropylmethylcellulose (HPMC; Figure 1.1) which is the polymer investigated in this thesis. Due to its wide availability, low cost, low toxicity, and

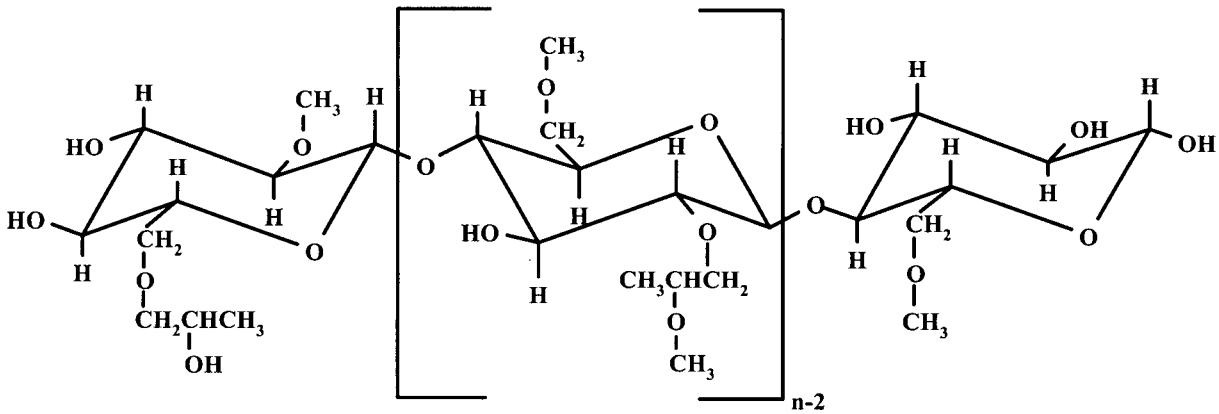

Figure 1.1 Structure of hydroxypropylmethylcellulose.

FDA approval, it is a popular choice for hydrophilic matrices. The HPMC as received is in the form of a powder. Pressing the HPMC powder along with the drug into capsules or tablets gives a form of drug delivery that can be administered orally. When a hydrophilic polymer such as HPMC is exposed to water, the mobility of the polymer chains increases, leading to a net disentanglement of these chains with the final outcome being the destruction of the polymer network. This leads to volume expansion of the tablet and what is termed swelling. The swelling of the tablet results in a polymer concentration gradient with a higher polymer concentration in the region of the tablet farthest from the water environment. The region of polymer surrounding the tablet that is approximately less than 15% HPMC is described as a gel region [3]. This gel region depending on the extent of the polymer chain disentanglement and the chemical structure of the drug can either inhibit or promote the diffusion of drug. The drug

release will depend on the effect of water penetration, polymer hydration, and drug diffusion out of the gel.

1.3 Investigations of the Swelling of HPMC

Various types of analytical methods have been employed to study these swelling controlled drug release systems. The most common technique involves the suspension of a tablet/capsule in a flow cell. Water is continually flowing through the cell in a closed loop and samples of liquid are assayed by UV/Vis spectrophotometry to monitor the total drug concentration released [4, 5, 6]. A more direct technique involves swelling a tablet for a specific time and then slicing the tablet and drying the identical slices to a constant weight. The water and polymer concentrations in each of the original slices of the swollen tablet can then be determined [7].

In situ imaging is a non-destructive technique which allows a tablet to be monitored without disturbing the polymer gel layer. The obvious imaging technique is optical photography which allows the dimensional changes of a tablet to be monitored [4, 5, 8]. The techniques listed above fail to provide both the ability to study the swelling characteristics in a non-destructive manner and to determine the concentrations of the water or the polymer in the swelling tablet. A technique that can be employed which meets the above two points is NMR imaging. Preliminary NMR imaging studies were concerned with the dimensional changes of a swollen HPMC tablet and the water penetration into the matrix [9, 10]; however, these investigations failed to provide concentration information for the swelling process.

1.4 Nuclear Magnetic Resonance

Nuclear magnetic resonance was first reported in 1946 [11, 12] and is a well established tool for the elucidation of chemical structures of molecules. The theory of NMR is extensively discussed in several books [13, 14, 15, 16]. The following description is meant only to be sufficient to understand the experiments described in this thesis.

It has been known since the 1920's that atomic nuclei have an angular momentum generated from their inherent rotation or spin. In the case of hydrogen, this results in a magnetic dipole as shown in Figure 1.2 (a). The proton when placed in a magnetic field B_o behaves similarly to a spinning top in that the magnetic dipole rotates about a precessional orbit at its Larmor frequency as shown in Figure 1.2 (b).

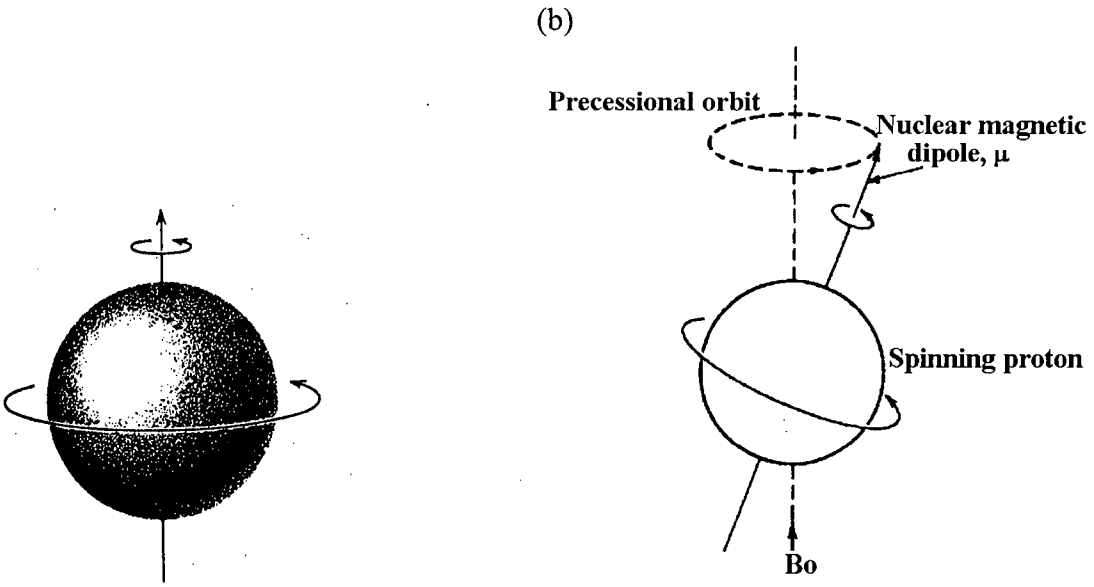

Figure 1.2 Description of a proton (a) Rotating on its nuclear axis generating a magnetic dipole (b) In a magnetic field B_o precessing about its precessional orbit.

A nucleus of spin, I, can exist in 2I + 1 spin states. Protons are spin ½ and thus have two spin states: spin "up" ($m_I = +½$) and spin "down" ($m_I = -½$). In a magnetic field, B_0, there is an excess of protons in the spin "up" state determined by the Boltzmann equation as shown in

Figure 1.3 (a). The magnetic behaviour of the entire population of protons can be defined macroscopically using a net magnetization vector as shown in Figure 1.3 (b) parallel to the main magnetic field defined as the z-axis. By application of a radio frequency pulse, it is possible to rotate the net magnetization vector about any desired axis. An rf field, B_1, applied for the time required to rotate the net magnetization from the z-axis to the x, y plane is said to have performed a 90° rotation and is termed a '90° pulse.' This magnetization in the x, y plane begin to rotate and in doing so generates an electromotive force that can be detected. The signal that is detected is called the free induction decay (FID). When the magnetization is tipped to the x, y plane, each proton not only feels the main magnetic field but also the magnetic properties of neighbouring protons. The protons will acquire a range of varying precessional frequencies causing a decay of the signal. The decay is a first order process and the rate is described in terms of the T_2 relaxation time.

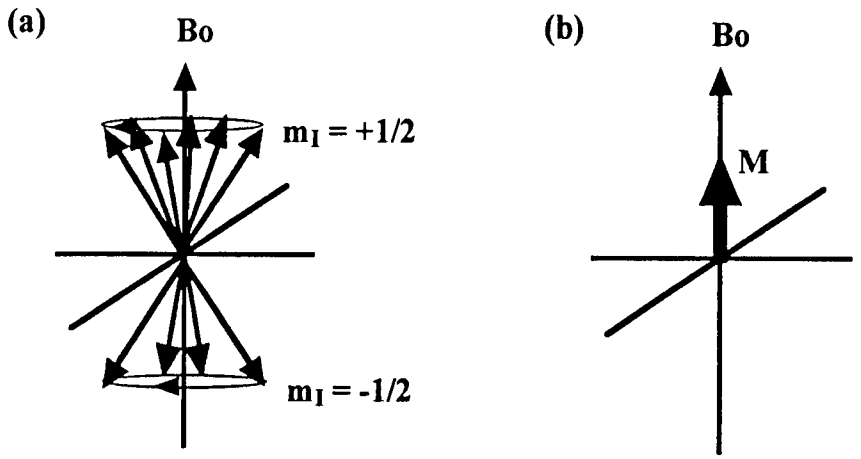

Figure 1.3 Magnetic behaviour of protons in a magnetic field B_o (a) An excess of spins in spin "up" state ($m_I = + ½$) in a field B_o (b) The simplified depiction of the excess of spins in the spin "up" state as represented by a net magnetization vector (M) in a field B_o.

1.5 Relaxation Processes

There are two relaxation times to consider when carrying out NMR experiments: T_1 (spin-lattice) and T_2 (spin-spin) relaxation times. The T_1 relaxation time arises from the disturbance of the spin states by a rf pulse that results in a non-Boltzmann population distribution. This disturbance in population will eventually return to the Boltmann distribution by a first order process, the rate of which is described by the T_1 value. The most commonly used pulse sequence to measure T_1 is the inversion recovery sequence [17] shown in Figure 1.4 (a). After a 180° pulse, the net magnetization is inverted from the +z-axis to the –z-axis as shown by the vector description in Figure 1.4 (b). After a delay period, τ, in which the net magnetization relaxes toward its equilibrium value along the +z-axis, B_o, a 90° pulse tips the net magnetization to the x, y plane so that the sign and the magnitude of the magnetization can be detected. In Figure 1.4 (b) the τ interval is too short for recovery and the net magnetization vector is still along the –z-axis. Following the 90° pulse, the net magnetization is in the x, y plane and is detected as having a small negative intensity when plotted as a function of relative intensity versus τ as shown in Figure 1.4 (c). This pulse sequence is repeated for various τ values and the T_1 value is obtained by fitting the intensities of the resulting signal to Equation 1.1. Knowledge of T_1 is important in obtaining quantitatively reliable data as the delay between successive repetitions (T_R) of a pulse sequence should be five times T_1 to allow for the complete return of the spin population to Boltzmann equilibrium.

$$I[t] = I_0 + Ae^{\left(-\frac{\tau}{T_1}\right)} \qquad (1.1)$$

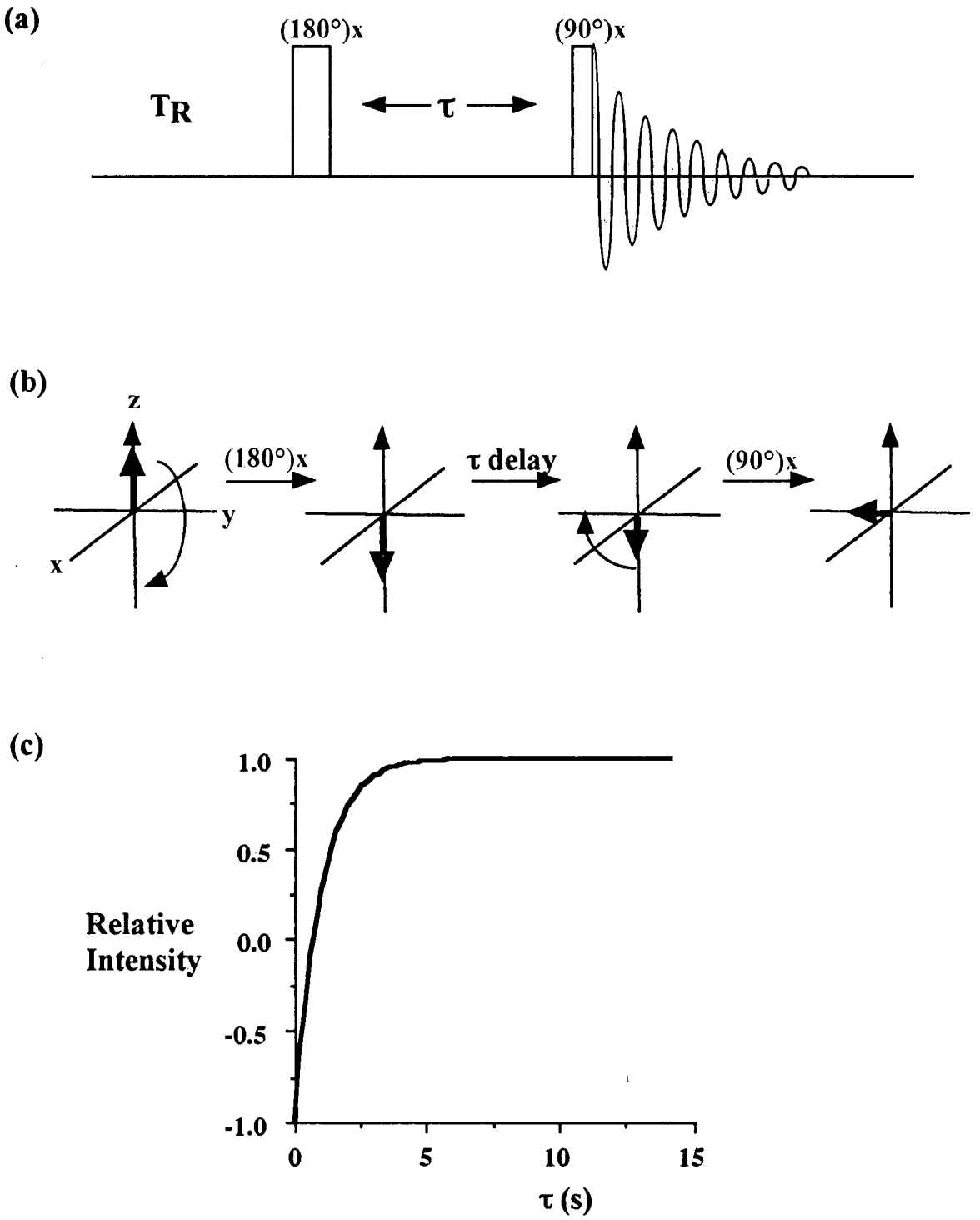

Figure 1.4 Method for measuring T_1 spin-lattice relaxation times (a) Inversion recovery pulse sequence (b) Vector description of the net magnetization as a consequence of the inversion recovery pulse sequence (c) Plot of equation 1.1 illustrating the effect of τ on the signal intensity.

Although in theory the T_2 relaxation time can be determined from the decay of the FID, inhomogeneities in the magnetic field dominate the rate of decay and the true T_2 cannot be measured directly from the FID. The T_2 (spin-spin) relaxation time describes the length of time that the magnetization can be manipulated and detected in an NMR experiment and is responsible for the decay of the FID. A pulse sequence used to measure T_2 is the spin-echo sequence [18] as shown in Figure 1.5 (a). After a 90° pulse, the net magnetization is tipped in the x, y plane as shown in Figure 1.5 (b). During the τ delay, the nuclear spins start to dephase which results in a decrease in the signal's maximum intensity due the field inhomogeneities that causes a range of Larmor precessional frequencies. After a 180° pulse, the vectors are rotated to a new position where the faster rotating vectors (F) now lag behind the slower ones (S). As such, after a delay 2τ, the different precessional frequencies of the vectors are now refoccused. The refocused vector has, however, decreased in magnitude as a result of true T_2 dephasing which cannot be refocused. The relationship between T_E (2τ) and the intensity of the signal is shown in Figure 1.5 (c). The longer the T_E, the greater the reduction in signal intensity. By varying T_E , T_2 can be determined by fitting the signal intensity as a function of T_E to Equation 1.2. A second pulse sequence that can also be used to measure T_2 is the multi-echo sequence. The key difference between the spin-echo and multi-echo methods is the acqusition time. Further required details of this sequence will be discussed in Chapter 2.

$$I[t] = Ae^{\left(-\frac{T_E}{T_2}\right)} \tag{1.2}$$

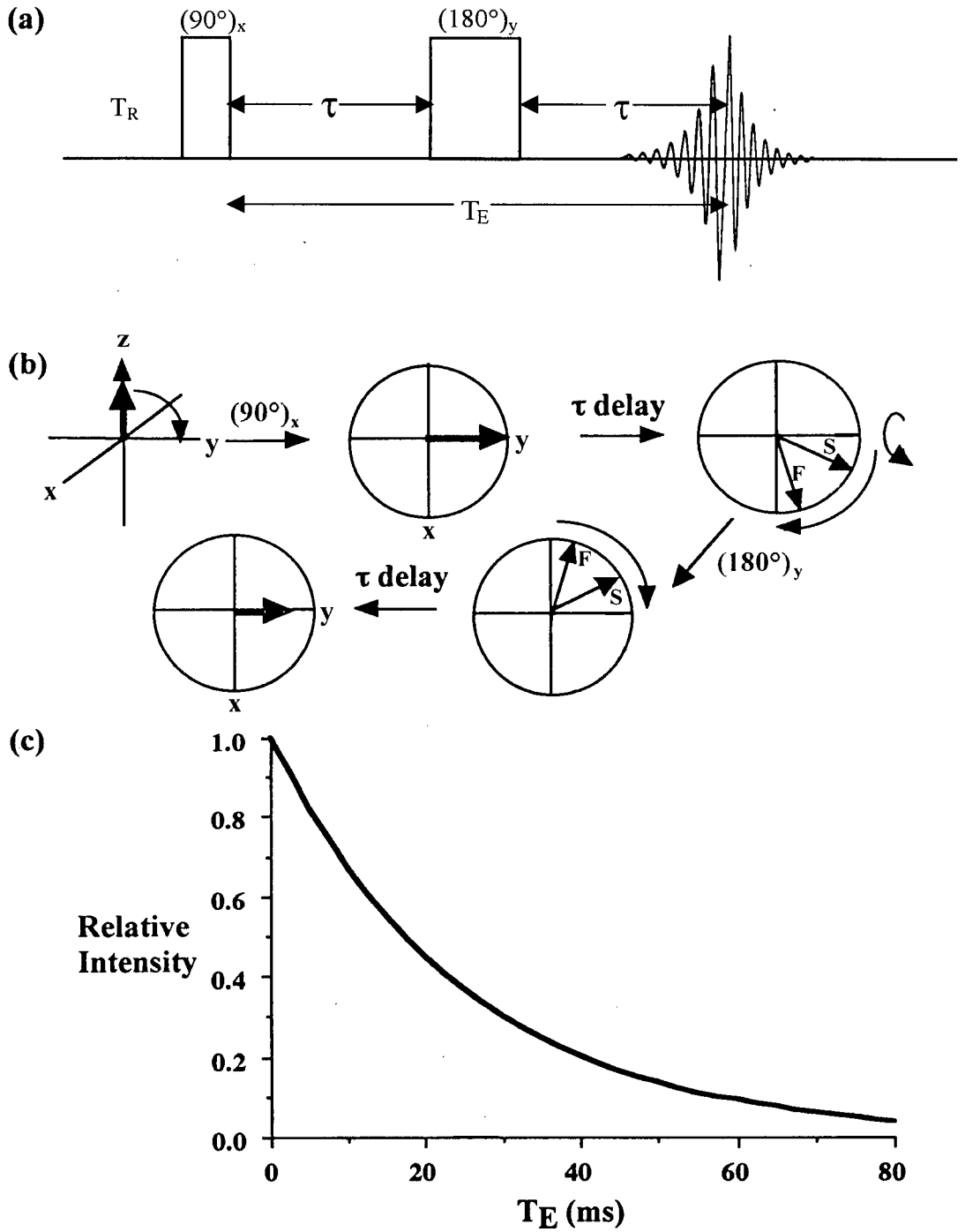

Figure 1.5 Method for measuring T_2 spin-spin relaxation times (a) Spin-echo pulse sequence (b) Vector description of the net magnetization vector as a consequence of the spin-echo pulse sequence. F and S represent the fast and slow precessing vectors respectively (c) Equation 1.2 plotted to illustrate the effect of T_E on the signal intensity.

1.6 Previous Work on the Swelling of HPMC Using NMR Imaging

Previous work on the swelling of HPMC using NMR imaging was carried out in this laboratory by Dr. Almira Blazek [3]. The combination of NMR imaging and NMR spectroscopy yielded a detailed description of the swelling and drug release behaviour of these systems. Her work was based on the one-dimensional swelling of HPMC tablets at 22 °C where only one of the tablet faces was exposed to water preventing the exposure of the remaining face and the sides to water and consequently, the water penetration into the tablet was limited to only this face of the tablet. Thus the swelling of the tablet was limited to only the vertical direction. The reasons this one-dimensional and not the three-dimensional swelling was investigated were the simplification of the subsequent analysis and the interpretation of data. In the case of a swelling tablet, a polymer concentration gradient exits. The goals of her thesis were to monitor this concentration gradient as a function of the time the tablet was in the water environment and to track the release of drug from the tablet. The main reason the polymer concentration gradient or the swelling profile was monitored was because the release of the drug is dependent on the polymer concentration. The determination of these swelling profiles makes it possible to predict the drug release profile. One of the biggest limitations in her work was the efficiency in acquiring and processing of the data due to the imaging equipment available. The acquisition of T_2 relaxation times was done with a spin-echo pulse sequence which took a long time to complete due to the T_R of water.

1.7 Current Work on the Swelling Property of HPMC Using NMR Imaging and the Goals of this Thesis Research

One great improvement in the current work on the swelling property of HPMC involves the capability of implementing a new pulse sequence with the current equipment. This sequence called multi-echo is more efficient in the acquiring and processing of the data. In Chapter 2, the T_2 relaxation times of known HPMC and water mixtures are determined by both the spin-echo and the multi-echo pulse sequence. However, more emphasis is placed on the multi-echo pulse sequence since it will be used in the one-dimensional swelling of HPMC tablets found in Chapter 3. The previous swelling investigations were carried out at only 22 °C and Chapter 3 extends this to swelling experiments at three temperatures (32 °C, 37 °C, and 47 °C). These variable temperature experiments can provide an insight into the swelling behaviour by allowing for the determination of an activation barrier for specific polymer concentrations. In addition to the one-dimensional swelling of HPMC tablets, a three-dimensional swelling experiment is described in Chapter 4. Whereas the one-dimensional swelling involves the penetration of water and the subsequent increase in volume of the polymer in only the vertical direction, the three-dimensional swelling involves the penetration of water and subsequent swelling in both the vertical and radial directions. In Chapter 5, the results from the swelling experiments particularly for the case of one-dimensional swelling HPMC tablets are compared to various models to test their applicability and validity.

Chapter 2

Determination of [HPMC]/T_2 Correlations

2.1 Introduction

In mixtures of polymer and water, direct NMR measurements on the polymer are not feasible due to its characteristic broad spectral lines. However, the characteristics of the polymer can be inferred indirectly through the interactions with the water. There are at least 2 possible states in which water can exist. A species in a free state which has no interactions with the polymer and a species in the "bound state" which can have varying degrees of bonding interactions with the polymer. In order to quantitatively study the swelling behaviour of HPMC in terms of the polymer concentration, the ^{1}H relaxation times of the water must be measured. More specifically, the water spin-spin (T_2) relaxation time must be correlated to the concentration of HPMC. Thus, T_2 values measured for known HPMC concentrations are necessary in order to provide a basis for this correlation. Along with the water ^{1}H spin-spin relaxation times, the ^{1}H water spin-lattice (T_1) relaxation times are measured for different polymer concentrations in order to obtain quantitatively reliable results.

2.2 Preparation of HPMC Mixtures

The HPMC (Methocel K4M premium) was obtained from Dow Chemical Co. as a free flowing white powder. The HPMC mixtures were prepared by weighing out the appropriate amount and mixing it with the appropriate amount of distilled water in a vial. The moisture content of the HPMC powder was determined by thermogravimetric analysis and was found to be 5.4% and this percentage of moisture in the powder was used to correct for the weight of HPMC. Therefore the actual weight % HPMC is:

$$\text{actual weight \% HPMC} = \frac{\text{wt. HPMC - 5.4\% moisture}}{\text{wt. HPMC + wt. distilled water}}$$

The contents in the vial were stirred and the vial was capped. Parafilm was used to seal the vial and it was placed in a refrigerator to allow the mixture to equilibrate. After a week, the mixture was stirred again, sealed, and placed in a refrigerator for another week. According to previous work [3], the gel mixtures were ready for NMR measurements after two weeks of equilibration. This was confirmed three months later when similar measurements were made that showed very small deviations from the original measurements.

2.3 ^{1}H T_1 Relaxation Times for Water in HPMC Mixtures

All the imaging experiments were carried out on a Bruker Avance DRX 360 MHz (8.46 T) spectrometer. The gradient coil system is not located on the probehead but instead is a separate entity permanently mounted to the room temperature shim set inside the bore of the magnet. The probehead consists of a probehead body with interchangeable rf coils of varying diameters (5 mm, 10 mm, 20 mm, and 30 mm) which can be tuned to either ^{1}H or ^{19}F frequencies.

As discussed in Chapter 1, the T_1 values are important in obtaining quantitatively reliable data. In the case of the HPMC mixtures, the T_1 values were obtained by the inversion recovery method [17] shown in Figure 1.4 (a). After a recycle delay time T_R, which is selected to be approximately 5 times T_1, the 180° pulse tips the net magnetization to the –z-axis. After a time τ, a 90° pulse tips the net magnetization from the z axis to the x,y plane where it is detected. The intensity of the signal I[t] is as a function of τ and the determination of T_1 involved a two parameter non-linear fit to Equation 1.1 using Xwinnmr 2.6.

The T_1 and subsequent T_2 determinations were carried out using the same vials as the mixtures were originally prepared in. Before the relaxation times were determined, the mixtures were placed in a water bath at the appropriate temperature and allowed to equilibrate for an hour. The relaxation times were determined using the 20 mm coil. Once inside the magnet, the

temperature was kept constant by a Bruker Variable Temperature (BVT) unit. In this setup, a heating coil coupled with a dewar was inserted into the probehead. A compressed air line was connected to the dewar and together with the heating coil and BVT unit provided a constant air flow at the specific temperature chosen.

The T_1 values determined for the different mixtures at the various temperatures are shown in Table 2.1. As shown in Figure 2.1, there is a clear relationship between the T_1 values and the HPMC concentrations at all temperatures. The dependence is a smooth function of concentration and there is a greater dependence on T_1 at the lower HPMC concentrations. Once the T_1 values are known for the different HPMC concentrations, quantitative measurements to determine the spin-spin relaxation times can now be made using a recycle delay time of 5 times T_1.

Table 2.1 Measured ^{1}H T_1 spin-lattice relaxation time values for the water in different HPMC mixtures at the different temperatures.

% HPMC[a]	T_1 [b] (s) at 32 °C	T_1 [b] (s) at 37 °C	T_1 [b] (s) at 47 °C
0	3.609	3.669	4.324
2.22	3.333	3.321	4.020
4.47	2.952	3.307	3.599
7.05	2.765	2.921	3.371
8.98	2.413	2.550	3.038
13.6	2.072	2.166	2.495
17.8	1.714	1.859	2.119
22.6	1.458	1.588	1.817
27.4	1.233	1.289	1.492
37.0	0.9394	1.054	1.157
46.4	0.7198	0.8016	0.9631
55.2	0.5612	0.6958	0.7262

[a] corrected for 5.4% moisture content

[b] error ± 5%

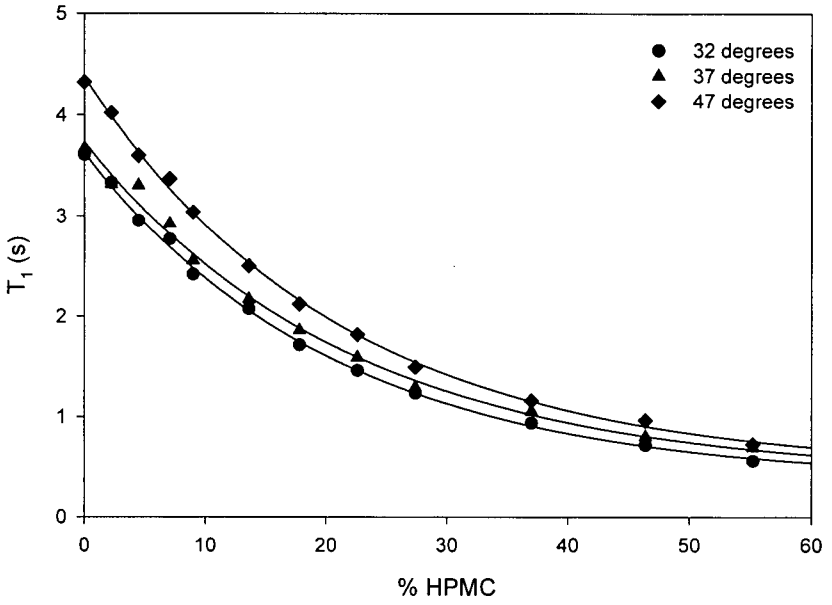

Figure 2.1 The dependence of T_1 on the HPMC concentration.

2.4 ^{1}H T_2 Relaxation Times for Water in HPMC Mixtures Using the Spin-Echo Pulse Sequence

Again after the HPMC mixtures had been equilibrated at the appropriate temperature, the spin-spin relaxation times were measured using the spin-echo pulse sequence [18] shown in Figure 1.5 (a). After a recycle delay T_R, a 90° pulse is applied tipping the net magnetization to the x, y plane. After an evolution time τ, the spins begin to dephase and a 180° pulse is applied. After a second τ interval, the spins are refocused and the signal is detected. T_2 relaxation times were determined by varying the time to echo (T_E) and observing the ^{1}H signal intensity. The signal intensity I[t] was plotted against T_E and a two parameter non-linear fit to Equation 1.2 was carried out using Xwinnmr 2.6. The T_2 values for the different HPMC mixtures at the various temperatures are shown in Table 2.2 and plotted in Figure 2.2. The relaxation times for the

Table 2.2 ^1H T_2 values for water in the different HPMC concentrations at the various temperatures determined by the spin-echo pulse sequence.

% HPMC[a]	T_2 [b] (ms) at 32 °C	T_2 [b] (ms) at 37 °C	T_2 [b] (ms) at 47 °C
2.22	464	414	388
4.47	376	383	316
7.05	272	269	248
8.98	186	176	157
13.6	124	137	119
17.8	92.1	88.3	83.1
22.6	68.8	77.1	73.7
27.4	48.9	51.2	48.7
37.0	23.6	22.2	21.5
46.4	9.68	10.7	12.2
55.2	6.08	6.34	6.1

[a] corrected for 5.4% moisture content
[b] error ± 5%

water component in the HPMC mixtures are very dependent on the mobility of the water within the polymer matrix. The higher the HPMC concentration, the shorter the relaxation times. In mixtures with low HPMC concentrations, the hydrated polymer chains exhibit an increase in mobility that could mean a contribution of hydroxyl or methyl groups to the observed ^1H signal. However, imaging experiments [3] performed with D_2O confirmed that the observed ^1H signal from the polymer has an insignificant effect on the observed ^1H signal. The temperature dependence on the relaxation times is greater at the lower HPMC concentrations. However, the differences in the T_2 values at the various temperatures are very small and within reasonable error. It was assumed that the dependence of T_2 on the HPMC concentration at the three different temperatures fit could be described by a single calibration curve.

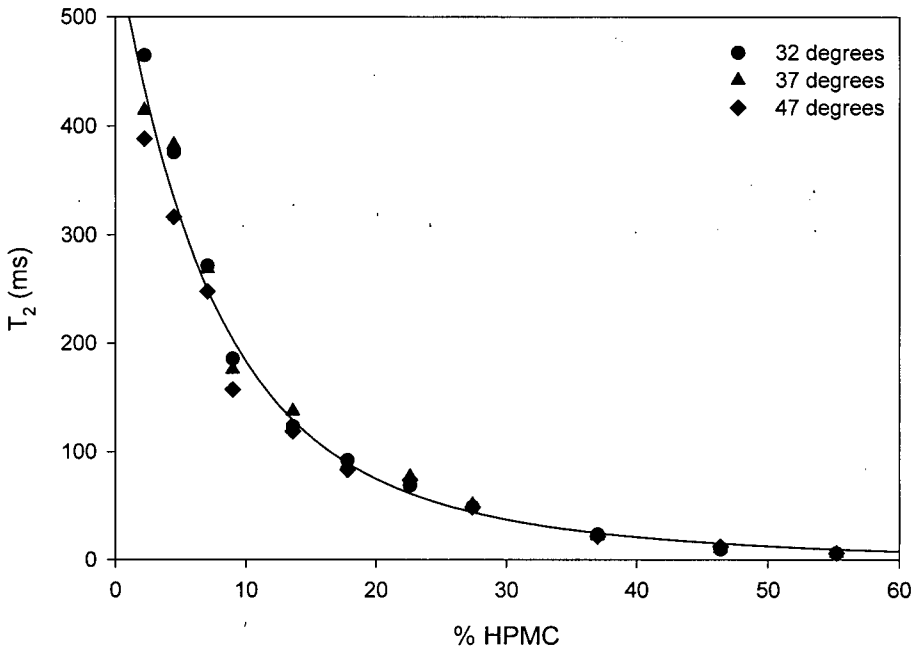

Figure 2.2 Plot of T_2 values vs. % HPMC for the three different temperatures indicated determined by the spin-echo pulse sequence.

2.5 ^{1}H T_2 Relaxation Times for Water in HPMC Mixtures Using the Multi-Echo Pulse Sequence

The multi-echo pulse sequence [19], shown in Figure 2.3 will ultimately be used to determine T_2 values when imaging experiments are performed. Compared to the spin-echo pulse sequence, this pulse sequence is important because of the rapid determination of T_2 as multiple

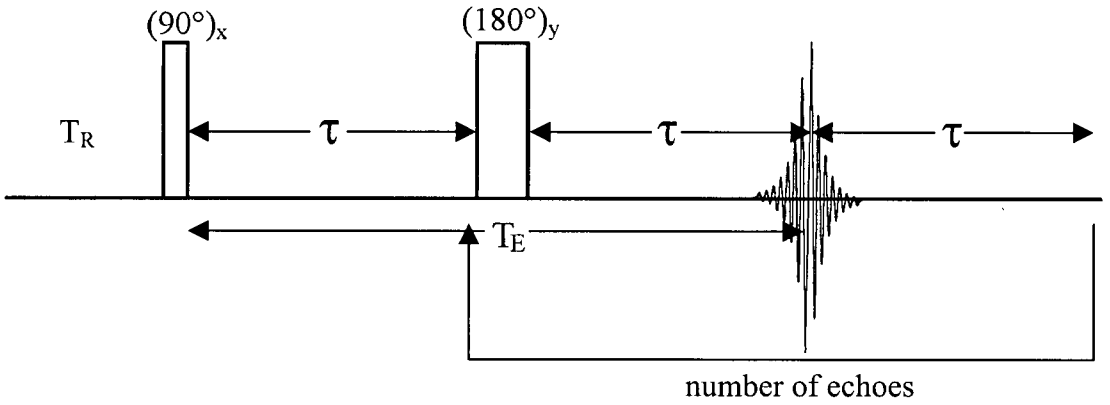

Figure 2.3 Multi-echo pulse sequence for measuring T_2

data points at n x 2τ that are acquired from a single excitation pulse. This rapid determination of T_2 translates to an improvement in efficiency that will be significant when the one-dimensional swelling of HPMC tablets are investigated in Chapter 3 and in particular for the three-dimensional swelling experiments in Chapter 4. A drawback to note is that the T_2 values obtained are not true T_2 values. This is due to the presence of stimulated echoes that will be discussed shortly. However, any association between the T_2 values and the HPMC concentrations are valid as long as T_2 is reproducible because this correlation is only an empirical one. Unlike the spin-echo pulse sequence which consists of a single incremented T_E the multi-echo pulse sequence consists of an echo train. After a recycle time T_R, a 90° pulse tips the net magnetization to the x, y plane. After a time τ, the spins dephase and a 180° pulse rotates the spins around the x, y-axes. After 2τ, the spins are refocused and are detected. Up to this point, the pulse sequence is similar to the spin-echo pulse sequence. However, the acquisition of echoes continues and after 3τ, a second 180° pulse rotates the spins around the x, y-axes again. After 4τ, the spins are refocused and are detected. This train of echoes continues and the imaging software stores every echo separately into memory. Each echo that is collected has a decreased signal intensity from the previous echo as the T_E is increased along the echo train. One very big advantage the multi-echo pulse sequence has over the spin-echo is the experimental time. It takes more time to determine the T_2 value using the spin-echo method. However, upon direct comparison of T_2 values obtained by both pulse sequences, the T_2 values differed by as much as a factor of two. One explanation is the presence of stimulated echoes. Any two pulses create an echo. Therefore, after the 90°-180° pulse pair, an echo is created and after the 180°-180° pulse pair, a second echo is created. However, any three pulses create a stimulated echo. In addition to the true echo, there is also intensity from a stimulated echo on top which could cause a very slight increase in the echo's intensity.

Again, after equilibration of the HPMC mixtures at the appropriate temperature, T_2 measurements were carried out. The T_2 values of the various HPMC mixtures were determined using two different experimental protocols with parameters chosen to produce adequate numbers of points for the different T_2 ranges. The first protocol, short echo time, had a T_E of 5.6 ms and this is best for the determination of the T_2 values of the high HPMC concentrations. The second experimental protocol, long echo time, had a T_E of 38.1 ms which was more appropriate for the T_2 determinations at the lower HPMC concentrations as shown in Figure 2.4 . The use of the two different echo times employed will be discussed in more detail in Chapter 3 when the one-dimensional swelling of HPMC tablets is described. T_2 was determined using Equation 1.2 using a two parameter non-linear fit by the imaging software ParaVision 2.1 BII supplied by Bruker. The results of the spin-spin relaxation times for T_E = 5.6 ms and T_E = 38.1 ms are shown in Table 2.3 and Table 2.4 respectively. The resulting fits for the short echo times and

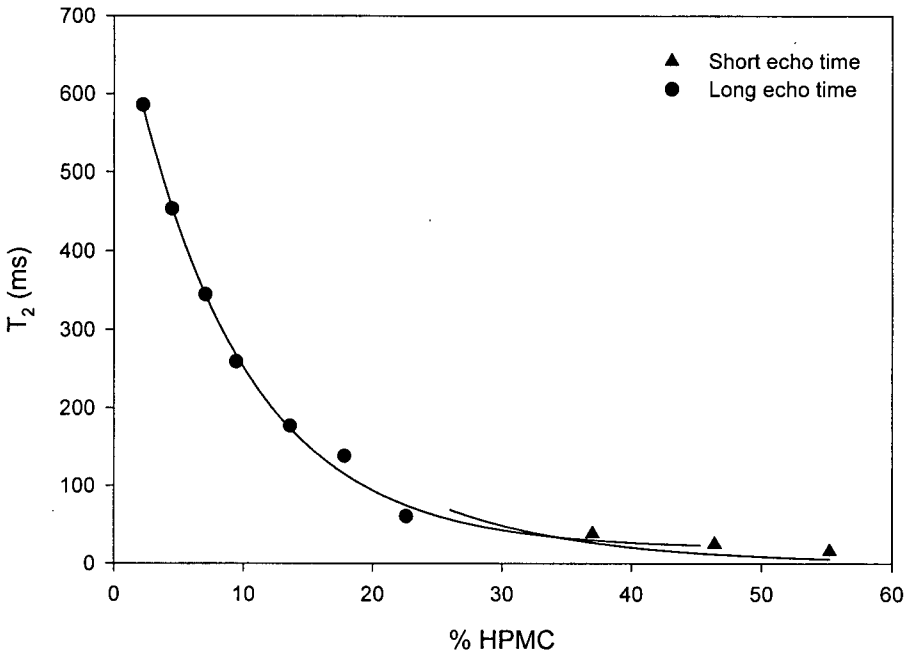

Figure 2.4 ^{1}H T_2 measurements made by the short and long echo time protocols for the two HPMC concentration ranges at 37 °C.

Table 2.3 ^{1}H T_2 values for the water in different HPMC concentrations determined by the multi-echo pulse sequence at the temperatures indicated for T_E = 5.6 ms.

% HPMC [a]	T_2 [b] (ms) at 32 °C	T_2 [b] (ms) at 37 °C	T_2 [b] (ms) at 47 °C
2.22	693	643	476
4.47	585	454	393
7.05	435	345	293
8.98	313	286	207
13.6	220	199	161
17.8	167	159	139
22.6	65.9	71.3	67.5
27.4	50.2	46	44.2
37.0	38.9	38.7	34.9
46.4	26.5	25.1	24.7
55.2	23	16	16.9

[a] corrected for 5.4% moisture content
[b] error ± 5%

Table 2.4 ^{1}H $T2$ values for the water in different HPMC concentrations determined by the multi-echo pulse sequence at the temperatures indicated for T_E = 38.1 ms.

% HPMC[a]	T_2 [b] (ms) at 32 °C	T_2 [b] (ms) at 37 °C	T_2 [b] (ms) at 47 °C
2.22	621	586	436
4.47	502	454	354
7.05	376	345	263
8.98	283	246	179
13.6	191	177	143
17.8	146	138	122
22.6	61.9	61.2	59.7
27.4	42.7	39.6	40.3
37.0	31.4	31.6	28.3
46.4	28.4	28.4	27.1
55.2	23	20.9	21.5

[a] corrected for 5.4% moisture content
[b] error ± 5%

long echo times at the temperatures indicated are shown in Figures 2.5 and 2.6 respectively. The calculated error bars for T_2 values primarily for the less concentrated HPMC concentrations at 32 °C and 37 °C overlap within the experimental limit and therefore the resulting fit included the T_2 values for both temperatures. However, the error bars for T_2 values at 47 °C for the less concentrated HPMC concentrations do not overlap the error bars at 32 °C and 37 °C and as such the fit was carried out included only the T_2 values at 47 °C.

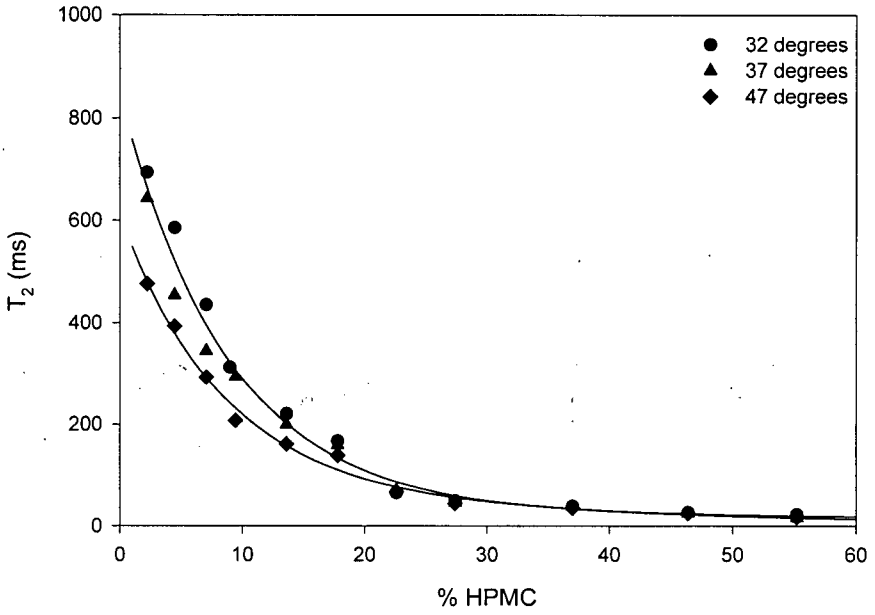

Figure 2.5 The T_2 dependence on % HPMC and temperature when T_E = 5.6 ms determined by the multi-echo pulse sequence.

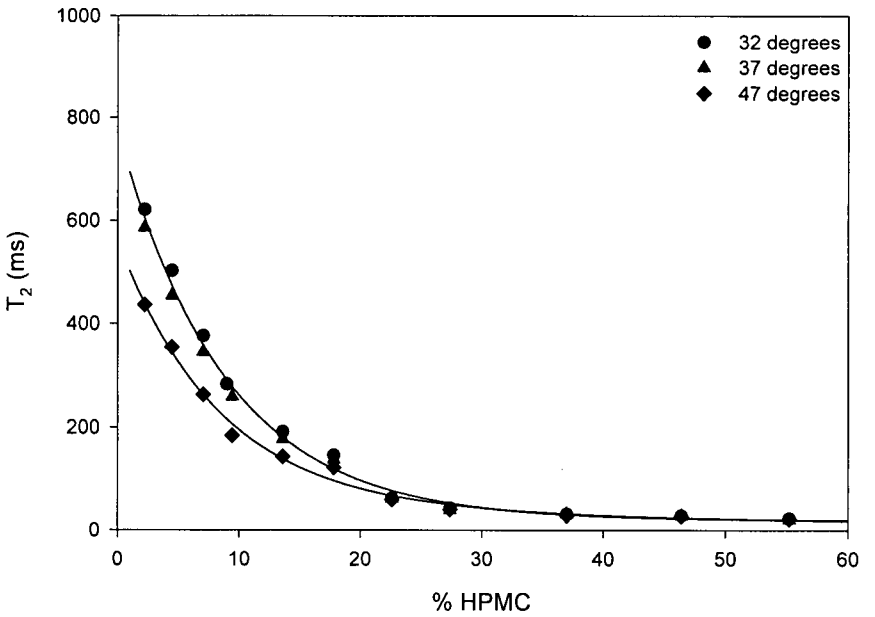

Figure 2.6 The T_2 dependence on % HPMC and temperature when T_E = 38.1 ms determined by the multi-echo pulse sequence.

Equations 2.1 to 2.4 were obtained by fitting the results in Mathematica using non-linear least-squares fitting and correlate the HPMC concentration to the T_2 values measured.

$$[\text{HPMC}] = 70.816\, e^{-(0.04395)(T_{2,H})} + 25.336\, e^{-(0.003091)(T_{2,H})} \quad (2.1)$$

$$[\text{HPMC}] = 177.75\, e^{-(0.07828)(T_{2,H})} + 26.538\, e^{-(0.003662)(T_{2,H})} \quad (2.2)$$

$$[\text{HPMC}] = 69.431\, e^{-(0.046)(T_{2,H})} + 24.523\, e^{-(0.004196)(T_{2,H})} \quad (2.3)$$

$$[\text{HPMC}] = 67.449\, e^{-(0.06986)(T_{2,H})} + 39.777\, e^{-(0.007358)(T_{2,H})} \quad (2.4)$$

Equation 2.1 involved fitting the T_2 relaxation times from the short echo time protocol for polymer mixtures equilibrated to 32 °C and 37 °C. The results from the T_2 determination of the polymer mixtures using the long echo time at 32 °C and 37 °C were fitted yielding Equation 2.2. Equations 2.3 and 2.4 were generated by measuring the T_2 values for the different polymer mixtures at 47 °C using the short echo time and long echo time protocols respectively.

At HPMC concentrations approximately less than 35%, the T_2 values determined are reproducible particularly when the long echo time protocol is used to measure T_2 due to the long T_E and a greater number of echoes collected. At HPMC concentrations approximately greater than 35%, there is a limited dependence of T_2 on HPMC concentration and the polymer mixture is heterogeneous. As such, T_2 values determined are considered semi-quantitative. Since T_2 is short, it was advantageous to use the short echo time protocol to determine T_2 for the higher HPMC concentrations. Equations 2.1 to 2.4 will be significant when the one-dimensional and subsequent three-dimensional swelling of HPMC tablets are investigated quantitatively.

To determine if there was statistically a correlation between the quantitative and semi-quantitative HPMC concentration regions, the standard deviation (S.D.) of the fit at 37 °C for T_E = 38.1 ms was calculated. T_2 values that were less than 3 times S.D. would be considered unreliable and should be ignored. In this case, all T_2 values were greater than 3 times S.D.;

however at higher HPMC concentrations and shorter T_2, the maximum difference between 3 times S.D. and T_2 was 32% as shown in Table 2.5. These HPMC concentrations and their corresponding T_2 values would be classified as statistically semi-quantitative. However, as the HPMC concentrations decrease the disparity between T_2 and 3 times S.D. also decreases. These HPMC concentrations would be classified as being statistically more quantitative.

Table 2.5 Disparity between T_2 as determined for T_E = 38.1 ms at 37 °C and 3 x S.D.

% HPMC	Disparity between T_2 and 3 x S.D. (%)
2.22	1.1
4.47	1.5
7.05	1.9
8.98	2.7
13.6	3.8
17.8	4.8
22.6	11
27.4	17
37	21
46.4	23
55.2	32

Chapter 3

Investigation of the Temperature Dependence of the One-dimensional Swelling of HPMC Tablets

3.1 Introduction

The reason why numerous T_2 values were determined in Chapter 2 was to quantify the swelling behaviour of HPMC tablets in terms of the polymer concentration. The swelling of the polymer matrix is a result of the penetration/imbibing of water leading to polymer hydration. This results in an increase in the mobility of the polymer chains leading to volume expansion. The biggest differences between previous one-dimensional swelling studies and the current work are improvements in efficiency, greatly reduced experimental time, and simplicity of the subsequent analysis. The one-dimensional swelling of an HPMC tablet involves the exposure of one side of a flat-faced tablet to water. Thus the imbibing of water and subsequent volume expansion of the polymer matrix is in one direction, along the z-gradient axis greatly simplifying the determination of rate expansion constants. The swelling behaviour of these tablets were investigated at three temperatures (32 °C, 37 °C, and 47 °C).

3.2 One-dimensional Imaging

One-dimensional imaging was first introduced in 1973 [20, 21]. It involves the application of a linear magnetic field gradient that causes a controlled magnetic field inhomogeneity. In Figure 3.1 (a), two tubes of water with varying diameters are placed inside an rf coil. A normal NMR experiment would result in a spectrum containing one sharp peak. However, with the application of a linear magnetic gradient along the x-direction the nuclei to be detected experience different applied magnetic fields along the direction of the gradient. This translates to different Larmor precessional frequencies along the sample. The Fourier transform of the observed signal corresponds to the spin

density projected onto the x-axis as shown in Figure 3.1 (c). Thus, nuclei have been differentiated on the basis of their frequency and phase into strips or voxels. This relationship between resonance frequency and position is the basis of NMR imaging. By combining this gradient application with a pulse sequence such as the multi-echo for determining T_2, T_2 values can be obtained from each voxel efficiently.

3.3 Experimental Setup for One-dimensional Swelling Investigations

The HPMC powder as received was compressed using a rotary tablet press. The appropriate amount of HPMC powder as received was weighed out on a top loading balance and then transferred to the die of a Beta Manesty rotary tablet press. The properties of Type 1 HPMC tablets which are the primary choice of tablets investigated in this Chapter are given in Table 3.1. However, different tablet thicknesses can be obtained by varying the amount of HPMC used and by keeping the peak compression force approximately the same. The properties of two additional HPMC tablets of different thicknesses are also given in Table 3.1. The one-dimensional swelling experiments were carried out in a 15 mm o.d. (12.8 mm i.d.) NMR tube held vertically in the 20 mm rf coil. The setup of the HPMC tablet swelling experiment is shown in Figure 3.2. Fluorinated grease was used to coat the flat surface of the glass support and the edges of the tablet to prevent water from leaking through

Table 3.1 Properties of HPMC tablets.

Type	HPMC (mg)	Compressional force (MPa)	Diameter[a] (mm±0.01)	Thickness[a] (mm±0.01)	Evacuation period (minutes)
1	323	60	12.75	2.66	10
2	165	62	12.75	1.35	5
3	562	56	12.75	3.89	15

[a] as measured with digital calipers

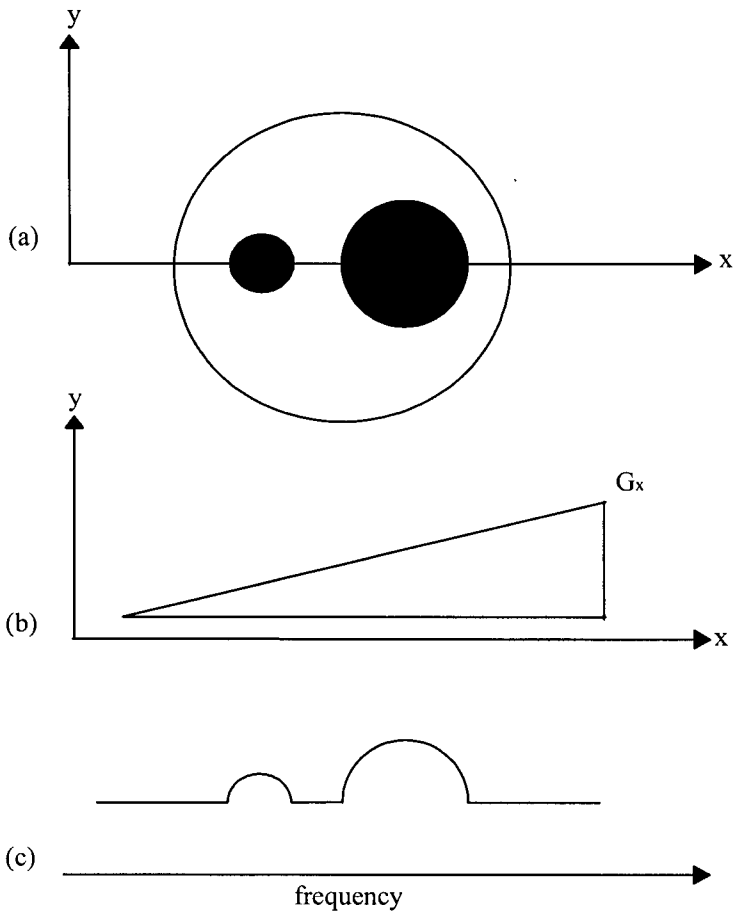

Figure 3.1 One-dimensional imaging of two tubes of water. (a) Two tubes of water of varying diameters as represented by the darkened circles in an rf coil. (b) The application of the x-gradient. (c) The resulting spectrum of (a).

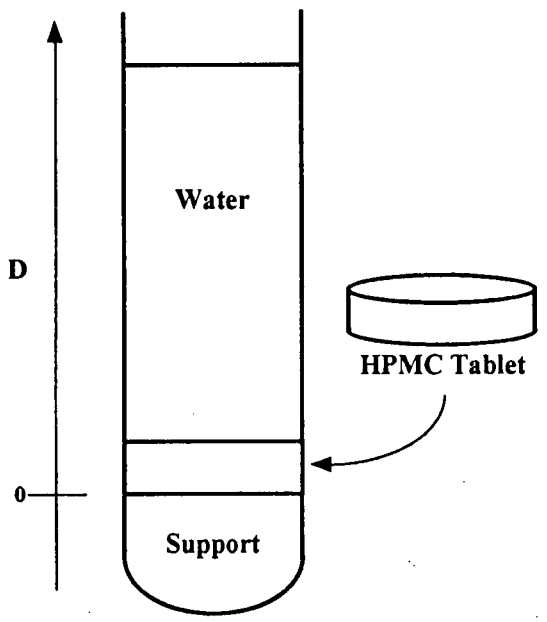

Figure 3.2 Setup of the one-dimensional swelling of an HPMC tablet.

the space between the tablet and the wall of the NMR tube. The tablet was vacuum treated to remove any air which might be trapped in the tablet during the compression of HPMC powder into tablets. The main reason why the tablet was evacuated is that as the matrix swells, air trapped in the pores become air bubbles which occupy space that would otherwise be taken up by polymer. This contributes to an apparent increase in the swollen volume of the polymer invalidating the analysis [3]. The NMR tube was placed in a Schlenk tube as shown in Figure 3.3 and kept under vacuum for a period of time dependent on the thickness of the tablet. Glass rods were also placed inside to prevent the tablet from being moved upwards during the vacuum process. Distilled water at room temperature was used to break the vacuum which prevented the incorporation of air into the tablet. The water was then decanted and replaced with 5 mL distilled water at the temperature chosen. The tube was capped, placed in the coil and a Dewar together with a heating coil were placed inside the probe to control the sample temperature. The heating coil was connected to a BVT unit which controlled the current to the heating coil. A compressed air line was connected to the Dewar thus allowing the passage of warm air to flow to the NMR tube. The determination of T_2 was done using two different experimental protocols as was indicated in Chapter 2 to most efficiently work in two different ranges of T_2. The first protocol (short echo time) had an echo time of 5.6 ms that allowed for the accurate determination of the short T_2 relaxation times corresponding to high HPMC concentrations (40% to 65%). The second protocol (long echo time) consisted of an echo time of 38.1 ms that accurately determined the longer T_2 relaxation times corresponding to the lower HPMC concentrations (< 30%). A summary of the different parameters used in the two different experimental protocols is given in Table 3.2. The reason why this approach was used involves the number of echo acquisitions: using a single short echo time protocol would result in a very large number of echoes being acquired in order to detect the longer T_2 relaxation times. This would mean a greater usage of available disk space on the hard drive. A single longer echo time would accurately determine the longer T_2 values but the

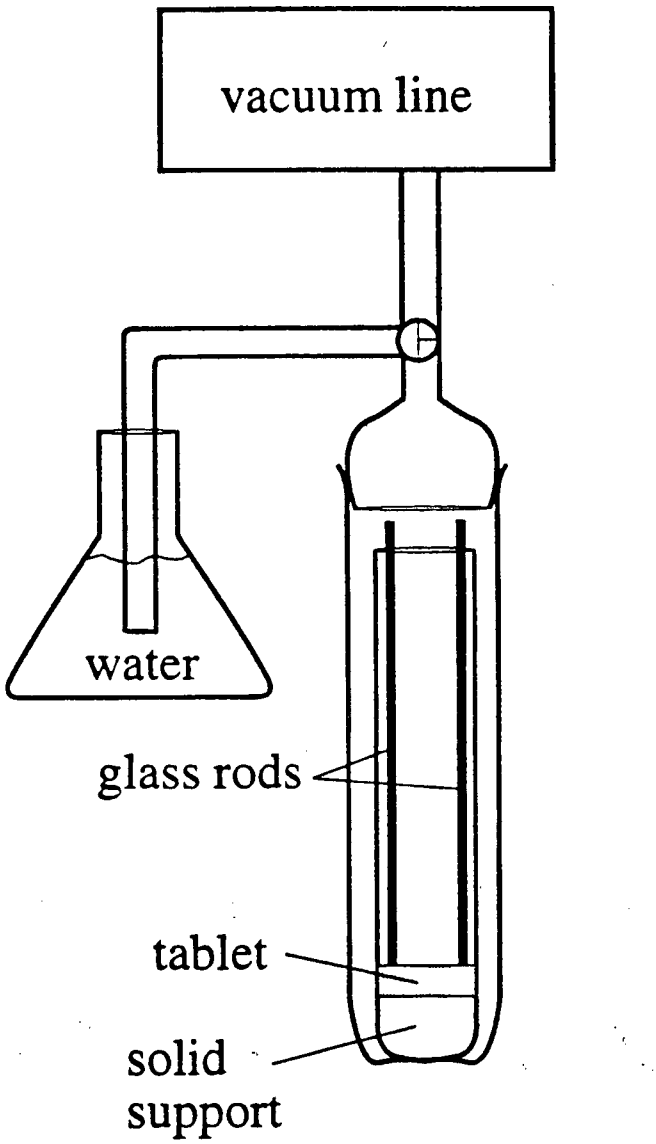

Figure 3.3 A schematic representation of the experimental setup for vacuum treatment of HPMC tablets. Glass rods are inserted into the NMR tube to prevent the tablet from being pulled upwards. The NMR tube is placed in a Schlenk tube that is connected by a three-way valve to a vacuum line and a source of water. The tablet is subjected to a vacuum for a time period depending on the thickness and then water is drawn into the Schlenk tube to break the vacuum. Prior to the placement of the NMR tube inside the magnet for imaging, the glass rods are removed and the water is decanted and replaced with water at the chosen temperature.

determination of the shorter T_2 relaxation times corresponding to the higher HPMC concentrations would involve too few data and be very inaccurate. Each experiment took 3.5 minutes to complete and a pair of experiments lasted 7 minutes. The entire swelling experiment was stopped after 43 hours. Each experimental protocol which had a specific number of echo acquisitions was converted to a single T_2 image of individual T_2 values for all the voxels. The T_2 image was then exported as an ASCII file where it was processed using Microsoft Excel 97 using Equations 2.1 to 2.4.

Table 3.2 Summary of the parameters used in the two different imaging protocols.

	Short echo time	Long echo time
T_E (ms)	5.6	38.1
Number of echoes	50	80
T_R (s)	30	30
Number of points/voxels acquired	96	96

3.4 Results and Discussion of the Temperature Dependence of One-dimensional Swelling of Type 1 HPMC Tablets

One-dimensional imaging was used to quantify the swelling process in terms of HPMC concentration. The one-dimensional swelling of Type 1 HPMC tablets was investigated at different temperatures to determine if a connection between the temperature and the rate of volume expansion or swelling existed. The temperatures chosen in this study were 32 °C, 37 °C, and 47 °C which can also provide an estimate of the activation energy for the swelling. The one-dimensional imaging to determine T_2 employed the multi-echo pulse sequence with the echo train as shown in Figure 3.4.

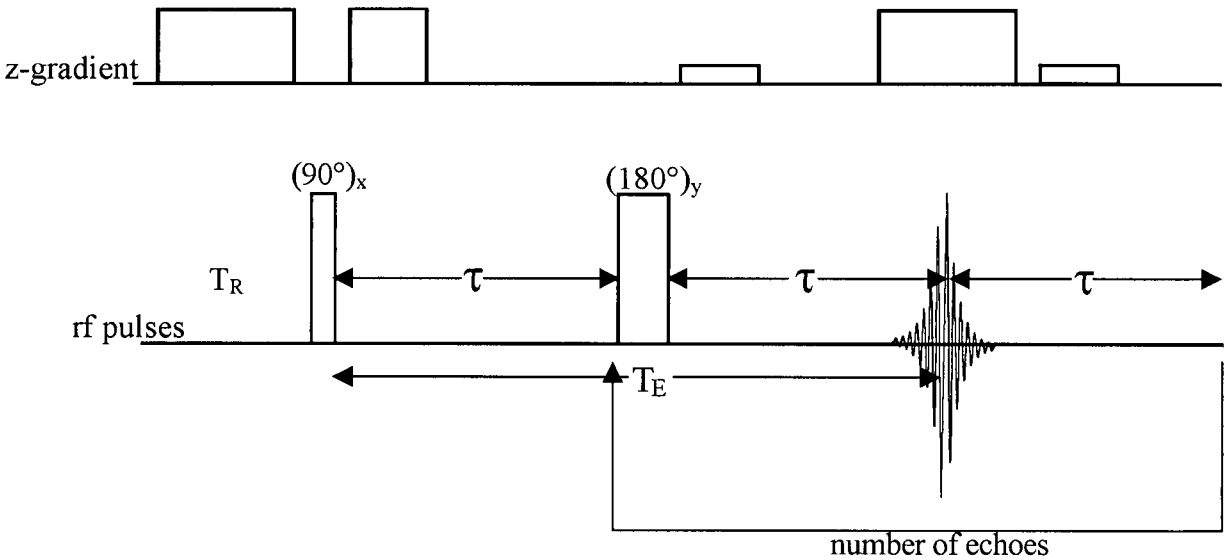

Figure 3.4 Multi-echo pulse sequence used for the one-dimensional imaging.

This pulse sequence is similar to that previously shown in Figure 2.3 but in addition to rf pulses, a gradient along z which in this case is in the same direction as the main magnetic field is applied. The application of the z-gradient gives a linear variation of the magnetic field along the direction of the gradient. The water protons experience different magnetic fields, resulting in different Larmor precessional frequencies and are distinguished from one another within specific volume elements or voxels along the vertical axis of the NMR tube. The z-gradient along with the application of rf pulses and incremented T_E values creates different signal intensities in the voxels as shown in Figure 3.5..

The resulting intensity values were fitted to Equation 1.2 generating T_2 relaxation times for each voxel as shown in Figure 3.6. The resolution or the width of each voxel is 0.3125 mm. Assuming the ^1H T_2 relaxation times previously determined for water in known HPMC concentrations are the same as those in the swelling experiments then the calibration equations, Equations 2.1 to 2.4 are valid. Therefore, T_2 values in each voxel can then be converted to HPMC concentration using Equations 2.1 to 2.4. T_2 values obtained from the short echo time protocol were fitted to Equations 2.1 and 2.3 at the appropriate temperature generating HPMC concentrations. On the other hand, the T_2 values obtained from the long echo time protocol were fitted to Equations 2.2 and 2.4 generating HPMC concentrations appropriate for polymer concentrations approximately less than 30%. Polymer concentrations between approximately 30% and 40% obtained from T_2 values from both short and long echo time protocols were averaged. The resulting profiles in terms of HPMC concentration versus swelling distance of Type 1 HPMC tablets at 32 °C, 37 °C, and 47 °C are shown in Figures 3.7, 3.8, and 3.9 respectively. The individual points on each of the profiles represents the average HPMC weight % of three replicate swelling experiments. In each of the profiles, the original tablet face is indicated by a solid vertical line. The dashed horizontal line indicates the separation of each profile into two regions with one region (<35%) being assigned as being more quantitatively reliable because the systems are more homogeneous. HPMC concentrations greater than 35% are considered semi-quantitative due to the limited dependence on the concentration of HPMC as the T_2 relaxation times are all very short. Although T_2 values are determined for higher polymer concentrations, these have much higher errors and the system is heterogeneous. For these reasons, these values were not used in subsequent analysis pertaining to the one-dimensional modeling found in Chapter 5. The mass balance for a single profile or the summation of the individual concentration points could not be calculated and compared to the original tablet weight because all the individual concentration points were not less than 35% HPMC even after 43 hours of swelling.

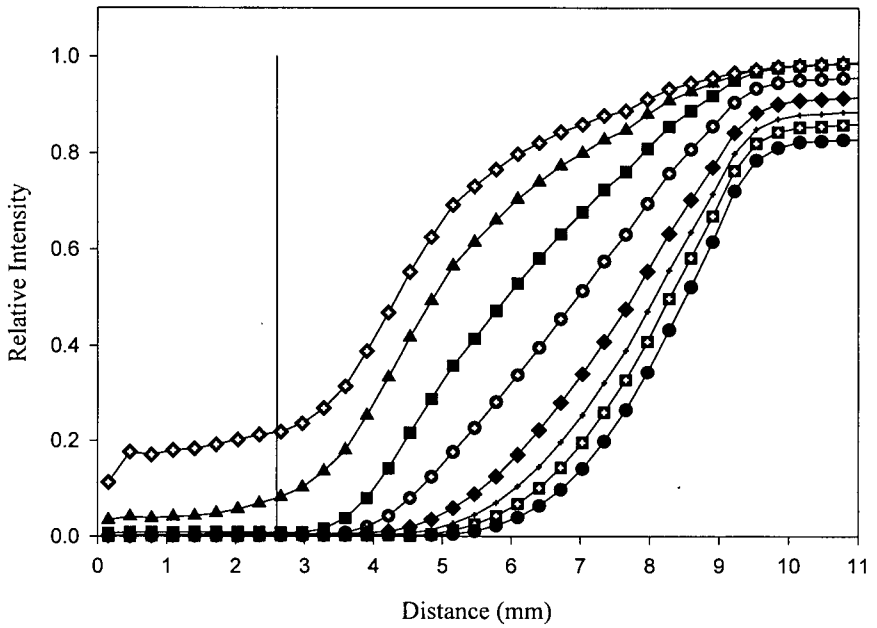

Figure 3.5 Variation of signal intensity as a function of T_E after 28 hours of swelling at 37 °C using the short echo time protocol. The solid vertical line represents the original tablet thickness. T_E=5.6ms (partially filled diamond), T_E= 16.9ms (triangle), T_E=45.1ms (filled square), T_E=84.6ms (partially filled circle), T_E=147ms (filled diamond), T_E=192ms (crosshairs), T_E=231ms (partially filled square), T_E=282ms (filled circle).

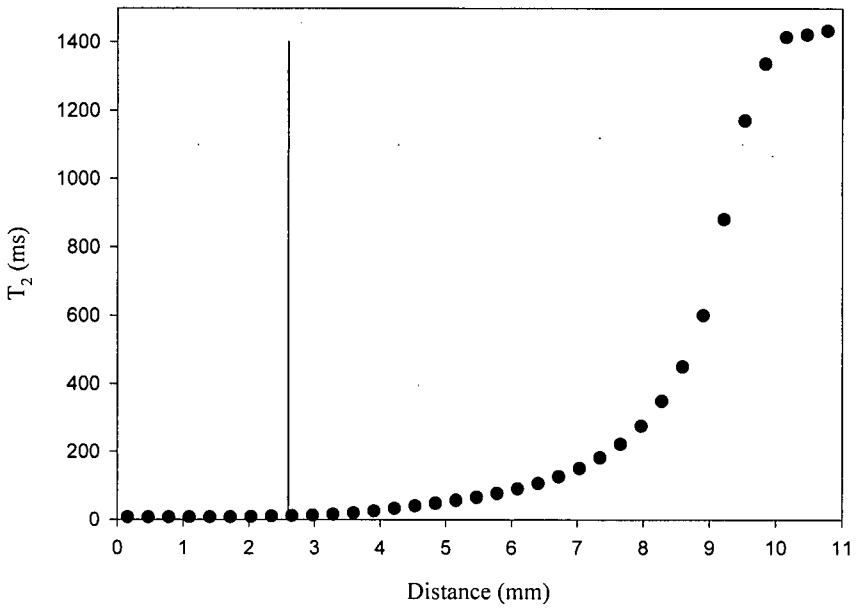

Figure 3.6 Corresponding T_2 values calculated from Figure 3.5.

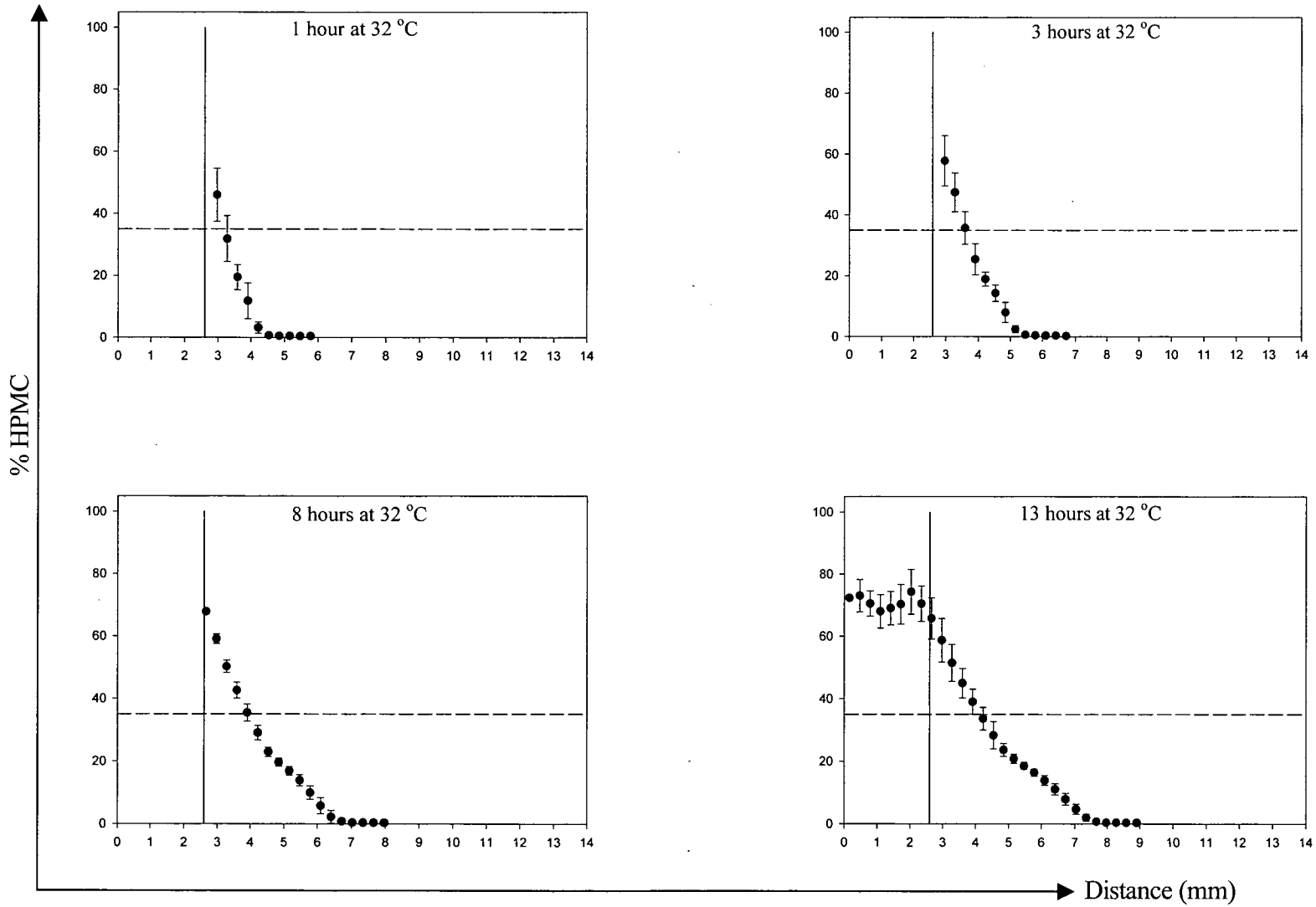

Figure 3.7 Average HPMC weight % swelling profiles of three replicate experiments with corresponding error bars (less than maximum possible errors) of Type 1 tablets at 32 °C. The solid vertical line represents the original tablet thickness and the dashed horizontal line indicates the limit of reliability of the HPMC weight percents. The axes labels for the profiles are the same and are defined by the arrows.

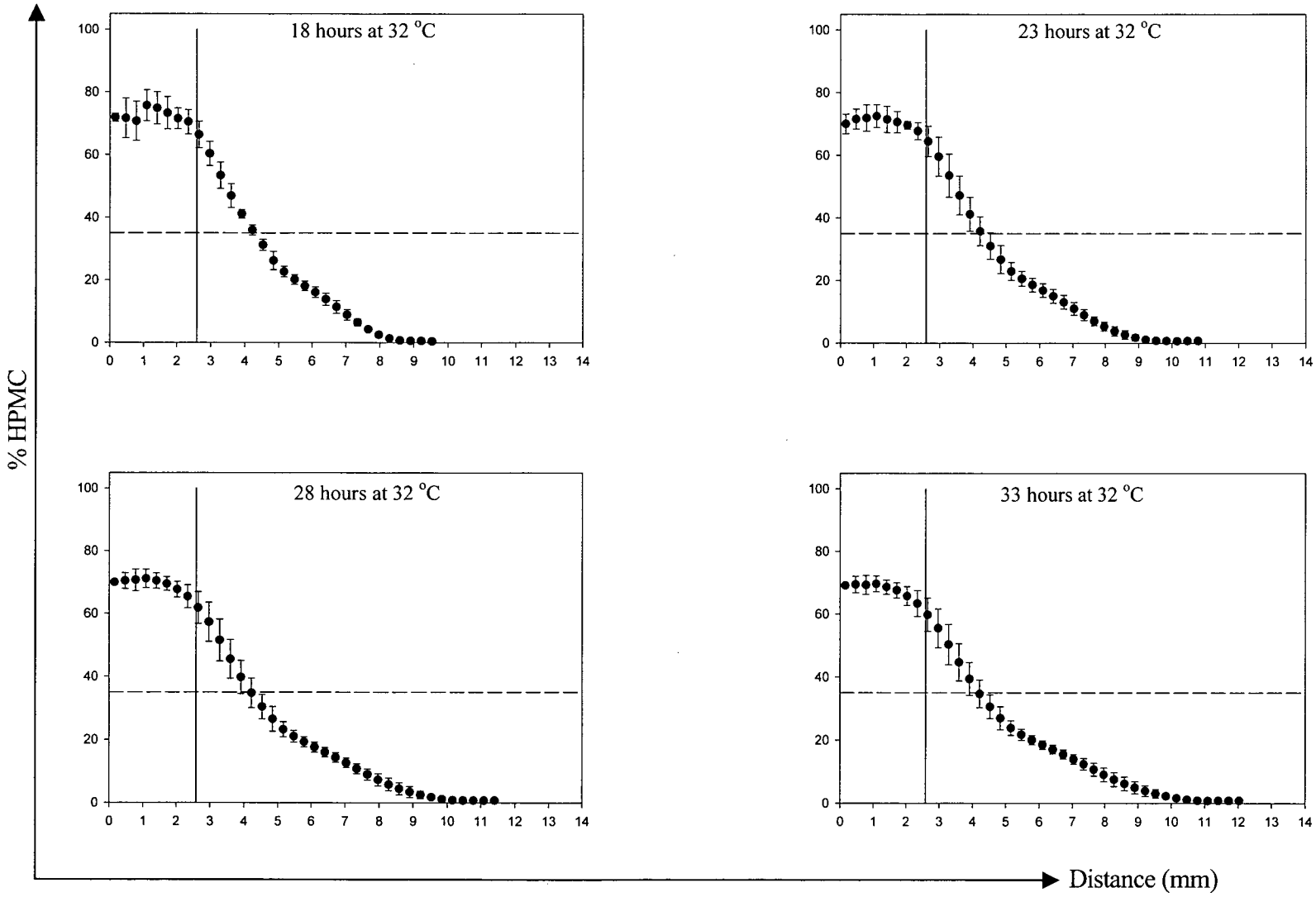

Figure 3.7 continued.

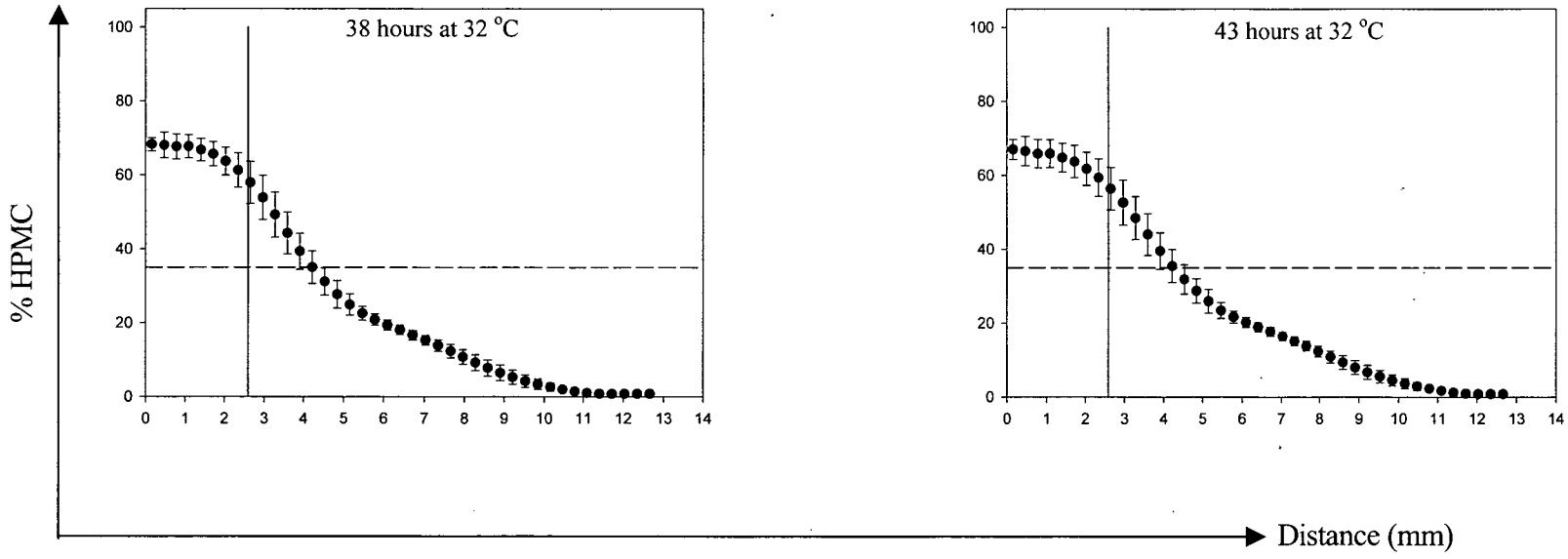

Figure 3.7 continued.

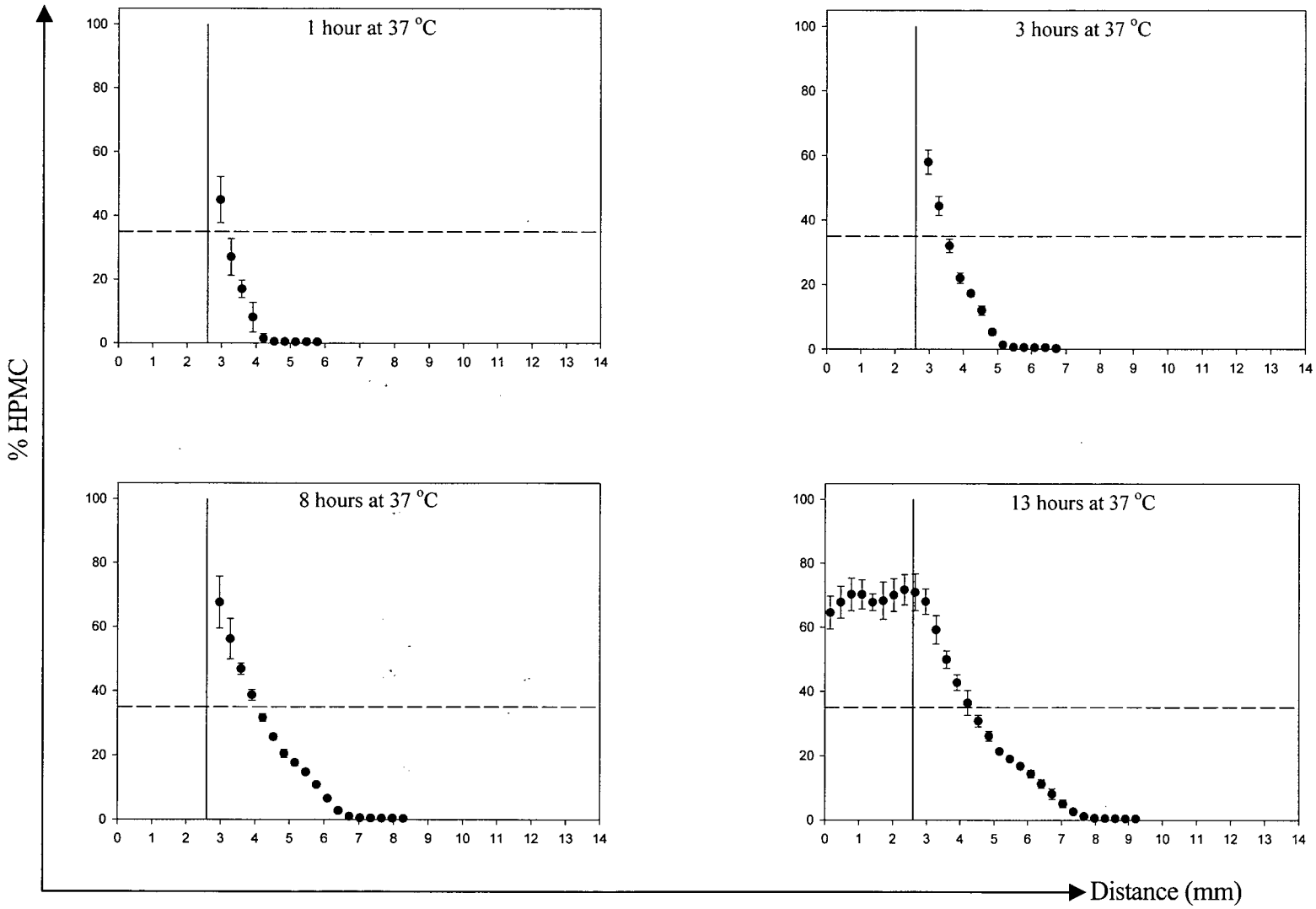

Figure 3.8 Average HPMC weight % swelling profiles of three replicate experiments with corresponding error bars (less than maximum possible errors) of Type 1 tablets at 37 °C. The solid vertical line represents the original tablet thickness and the dashed horizontal line indicate the limit of the reliability of the HPMC weight percents. The axes labels for the profiles are the same and are defined by the arrows.

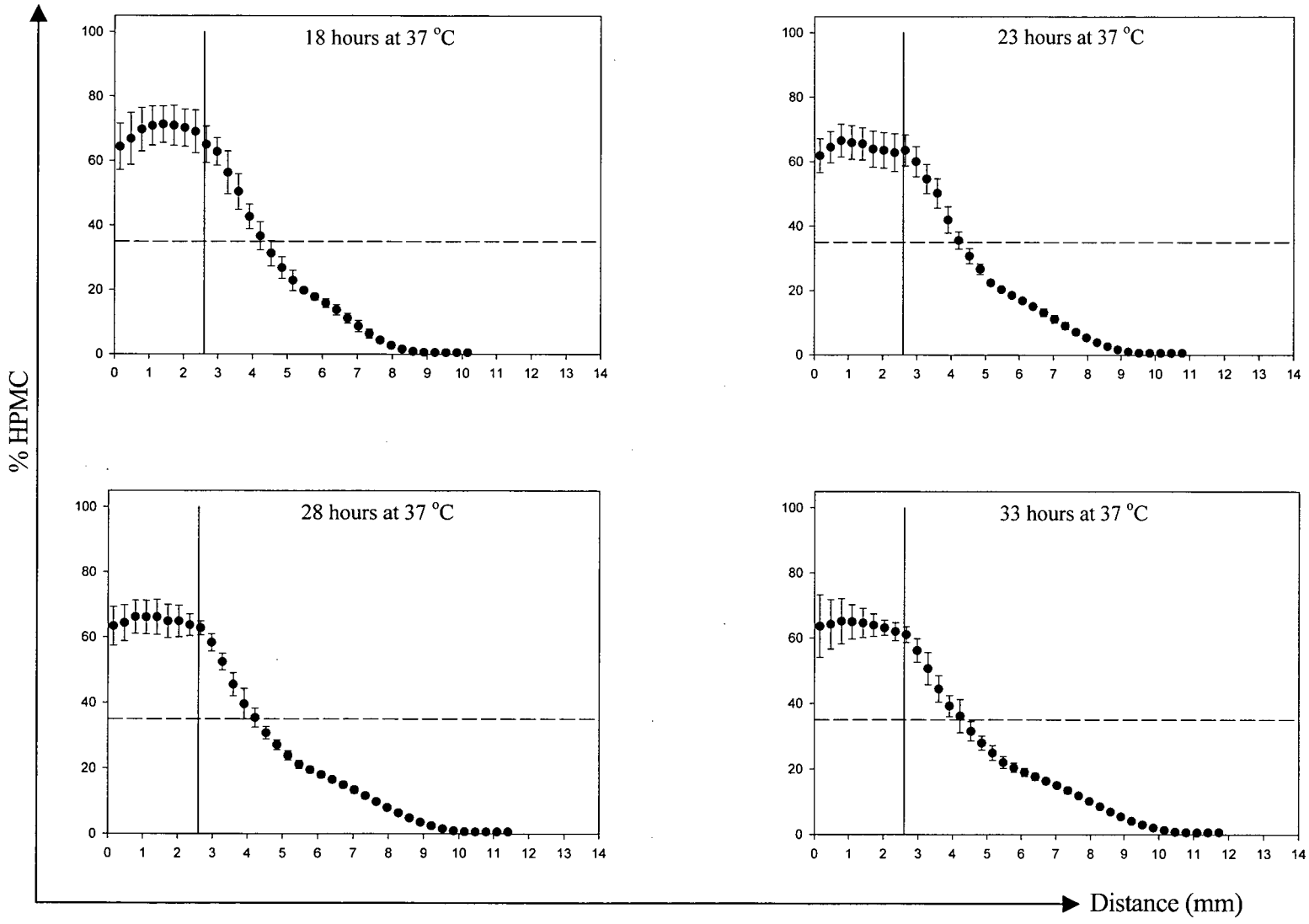

Figure 3.8 continued.

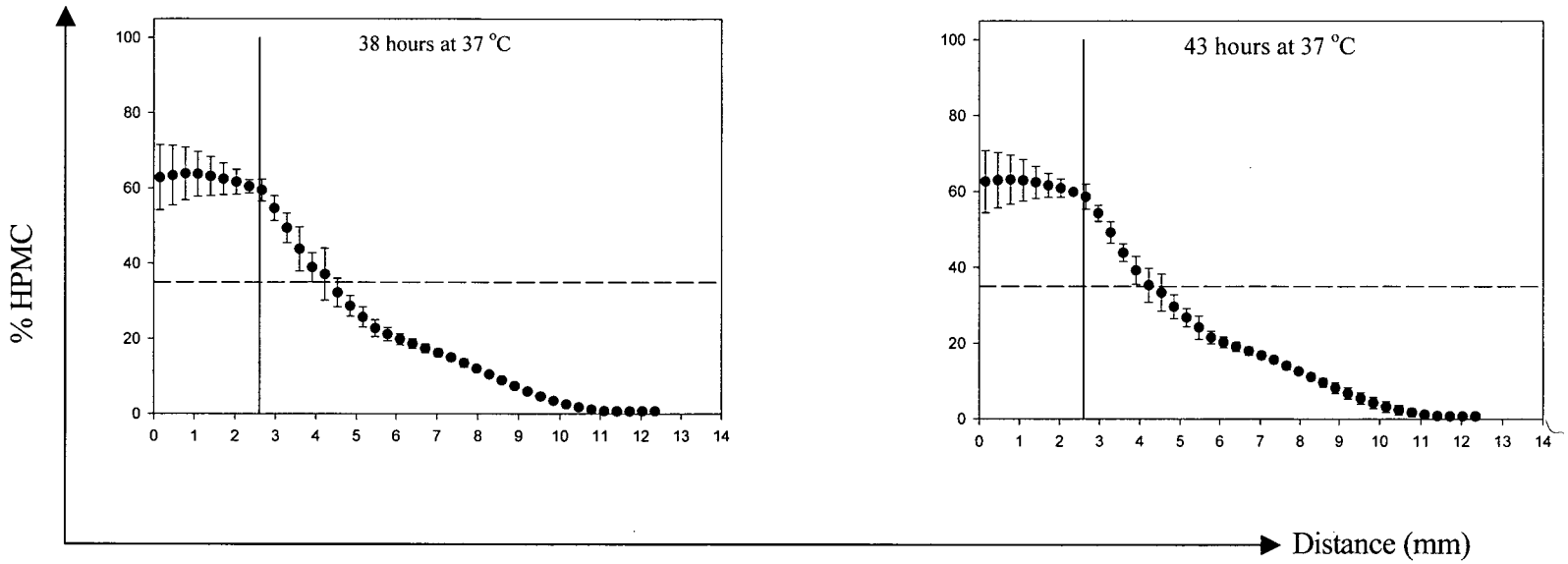

Figure 3.8 continued.

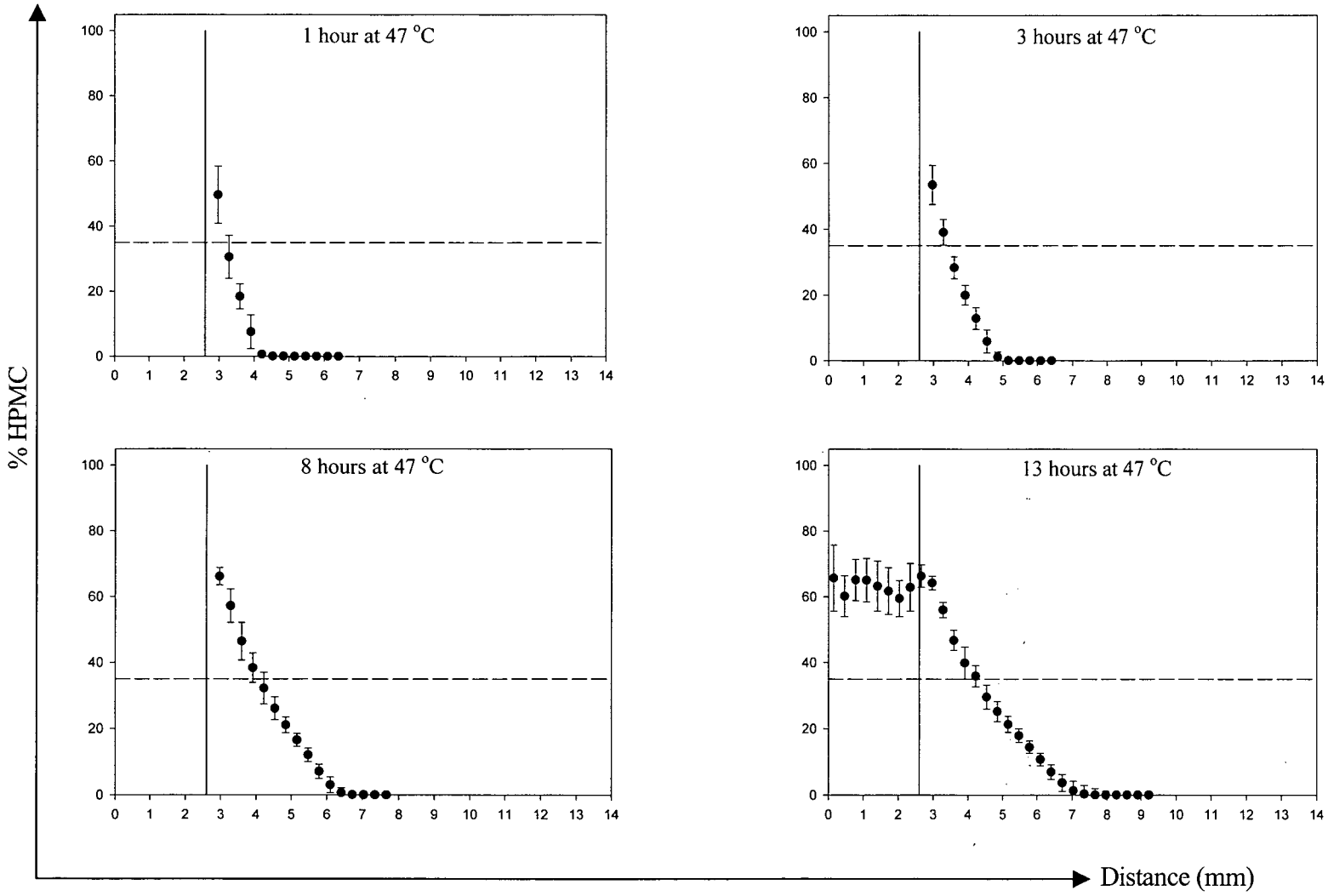

Figure 3.9 Average HPMC weight % swelling profiles of three replicate experiments with corresponding error bars (less than maximum possible errors) of Type 1 tablets at 47 °C. The solid vertical line represents the original tablet thickness and the dashed horizontal line indicate the limit of the reliability of the HPMC weight percents. The axes labels for the profiles are the same and are defined by the arrows.

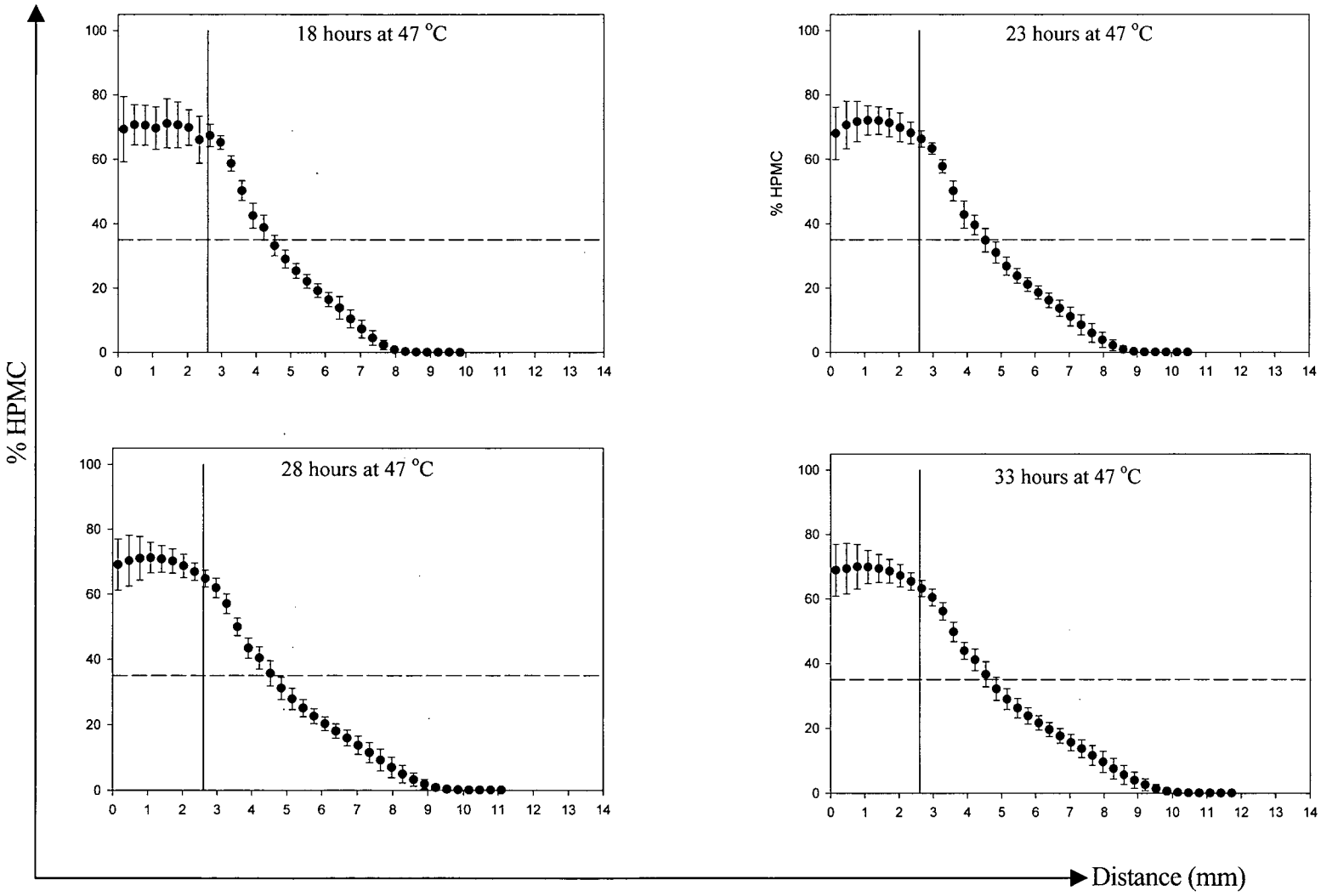

Figure 3.9 continued.

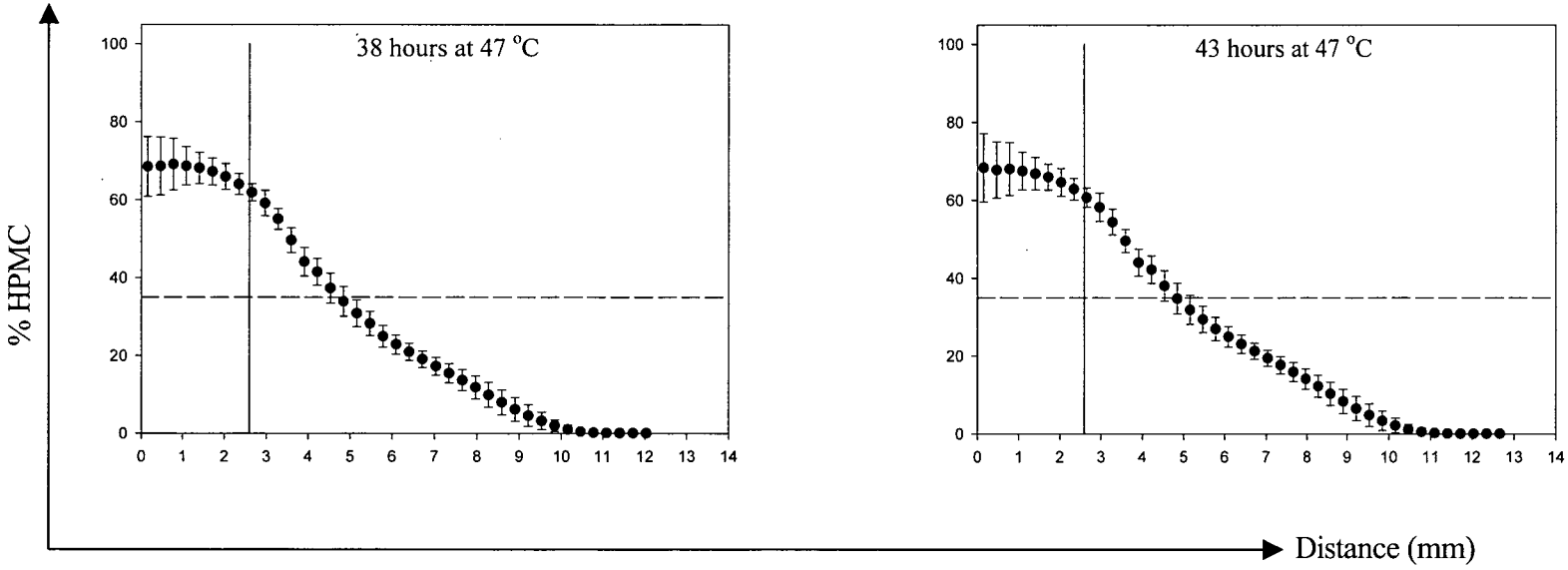

Figure 3.9 continued.

Present in all the profiles is a characteristic "bump" at approximately 25% HPMC. In previous one-dimensional imaging studies, this "bump" was also observed. A possible explanation as to the presence of this "bump" could be the existence of air bubbles due to an insufficient evacuation period. A viable experiment to support or contradict this reason is to evacuate the tablet for an extended period of time. Results indicate that when the HPMC tablet was evacuated for a duration equal to 4 times the normal evacuation period, there was still the presence of the "bump" in the swelling profiles.

At the earlier swelling times (one to eight hours), there is no indication that water has penetrated the core of the matrix at all three temperatures. However, T_2 relaxation times can only be obtained when there is sufficient water present and at high HPMC concentrations, T_2 is too short to be measured. Thus, the calculated HPMC concentrations do not extend as far into the core at the earlier swelling times. From Figures 3.7 to 3.9, at HPMC concentrations less than 30% there is expansion at all swelling times whereas at HPMC concentrations between 30% and 40% there appears to be less expansion at the longer swelling times. At the earliest swelling time, water imbibes the dry matrix leading to hydration. This results in a volume expansion or swelling of the polymer matrix and a concentration gradient is observed. Water penetration occurs more readily at the lower HPMC concentrations resulting in volume expansion. This explains the continuous swelling at HPMC concentrations below 30%. However, the inner core of the tablet which is very concentrated does not change as much at the later swelling times. The penetration of water into this core is limited due to the continuous imbibing of water at the lower HPMC concentrations and subsequent swelling. In this case, at very long swelling times the core of the table should decrease in HPMC concentration due to the constant "stripping away" of polymer. A possible reason why this could occur is the tablet thickness. A thicker tablet would limit the penetration of water at the later swelling times compared to a thinner tablet. Results from swelling experiments of Type 2 and 3 HPMC tablets at 37 °C confirm that the thickness of a tablet affects the ability of water to further penetrate the tablet core. These

profiles are shown in Figures 3.10 and 3.11. The one-dimensional swelling of these tablets were carried out as previously described in Section 3.3 except for the duration of the evacuation period depending on the tablet thickness. A Type 3 tablet which has a thickness of 3.89 mm limited the penetration of water into the tablet core even after 43 hours of swelling. As such, the polymer concentration within the tablet core remained fairly constant without any large deviation in the concentration compared to the preceding swelling times. However, a Type 2 tablet with a thickness of 1.35 mm compared to that of a Type 3 tablet exhibited the opposite behavior. After 43 hours of swelling, the polymer concentration within the core of the Type 2 tablet was less concentrated than the Type 3 tablet which can be attributed to a greater ability of water to penetrate the thinner tablet. Also, the polymer concentration within the core of the Type 2 tablet continued to decrease as the swelling of the tablet proceeded. At 43 hours of swelling, all the individual HPMC concentration points were less than 35% HPMC and the mass balanced the original tablet weight.

It is difficult to conclude if there is a correlation between the temperature and the rate of polymer expansion from visual inspection of the profiles. However, by examining HPMC concentrations at 5% and 10% which is defined as being in the gel state and monitoring the swelling distances of these fronts, expansion rate constants can be obtained. The distances of the 5% and 10% gel fronts are given in Table 3.3 and 3.4 respectively at the three different temperatures.

Table 3.3 Expansion distances of the 5% gel front at the different temperatures.

Swelling time (hours)	Front Distance (mm) at 32 °C	Front Distance (mm) 37 °C	Front Distance (mm) 47 °C
1	3.94	3.90	3.91
3	4.73	4.70	4.68
8	5.90	5.98	5.94
13	6.65	6.64	6.72
18	7.18	7.19	7.36
23	7.58	7.63	7.92
28	7.95	8.10	8.44
33	8.33	8.53	8.92
38	8.71	8.95	9.37
43	9.08	9.25	9.79

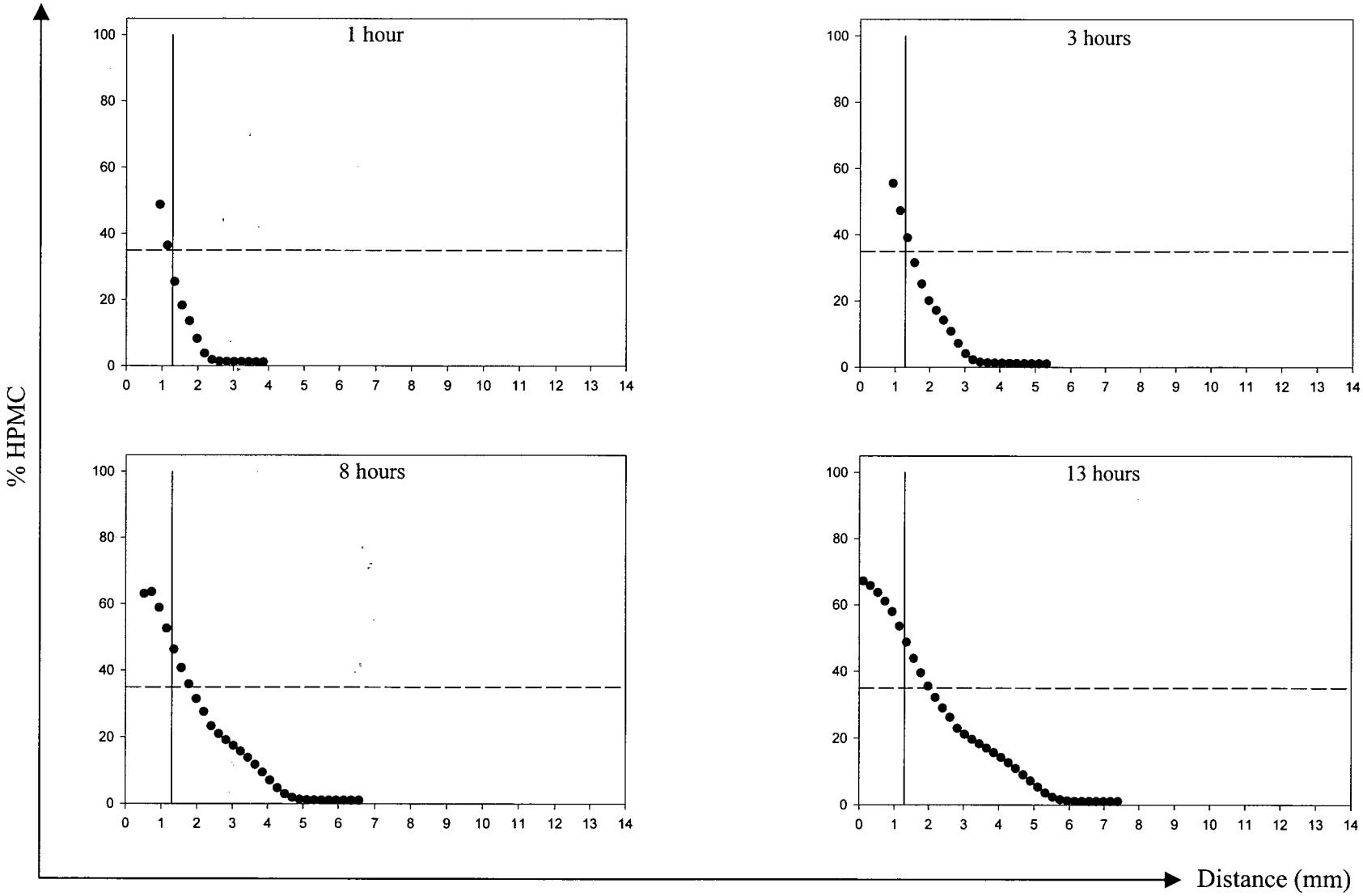

Figure 3.10 One-dimensional swelling profiles of a Type 2 HPMC tablet at 37 °C. The solid vertical line at 1.35 mm indicates the original tablet thickness and the dashed horizontal line at 35% HPMC indicates the limit of reliability. The axes in the plots are defined by the arrows.

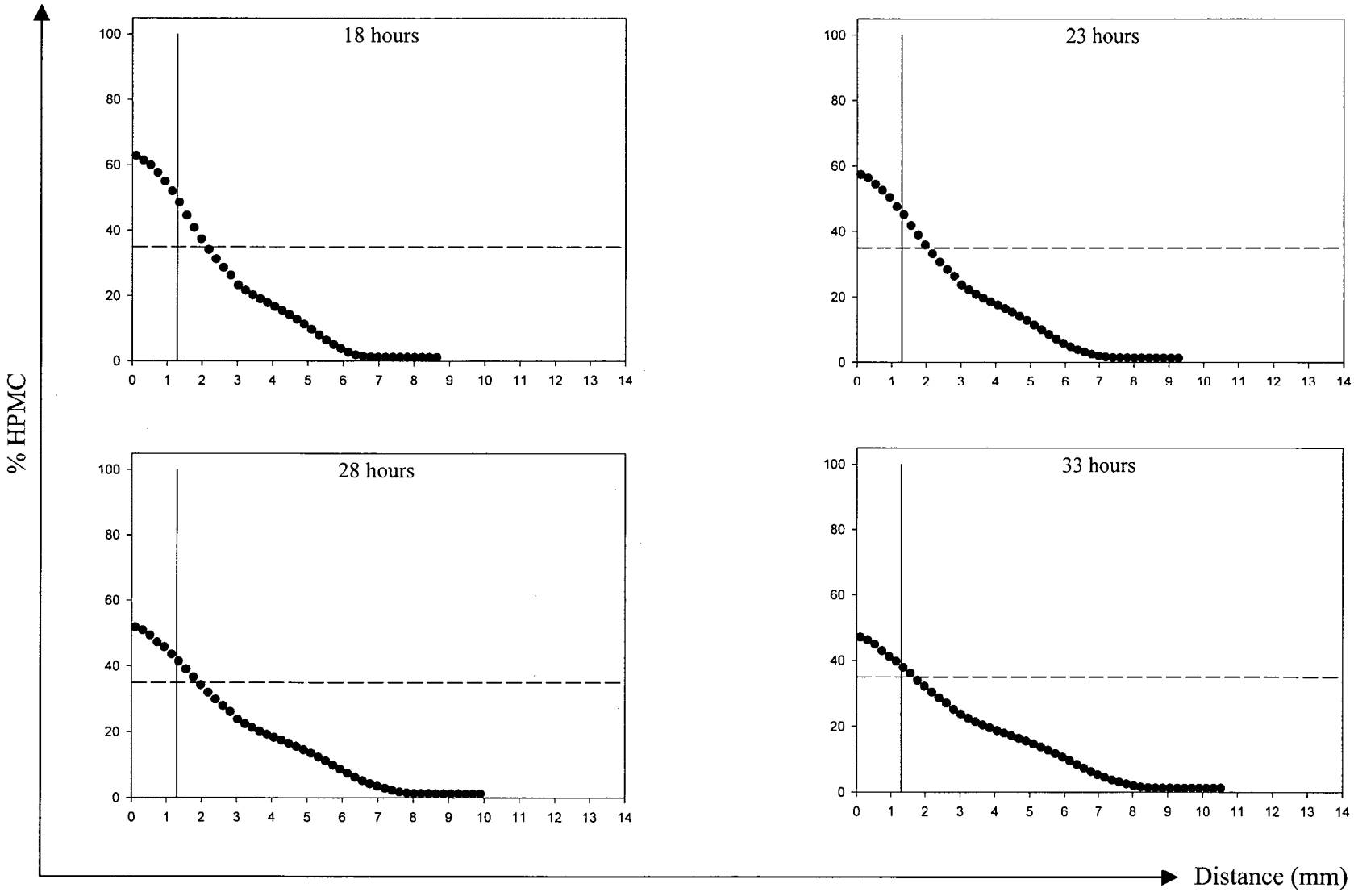

Figure 3.10 continued.

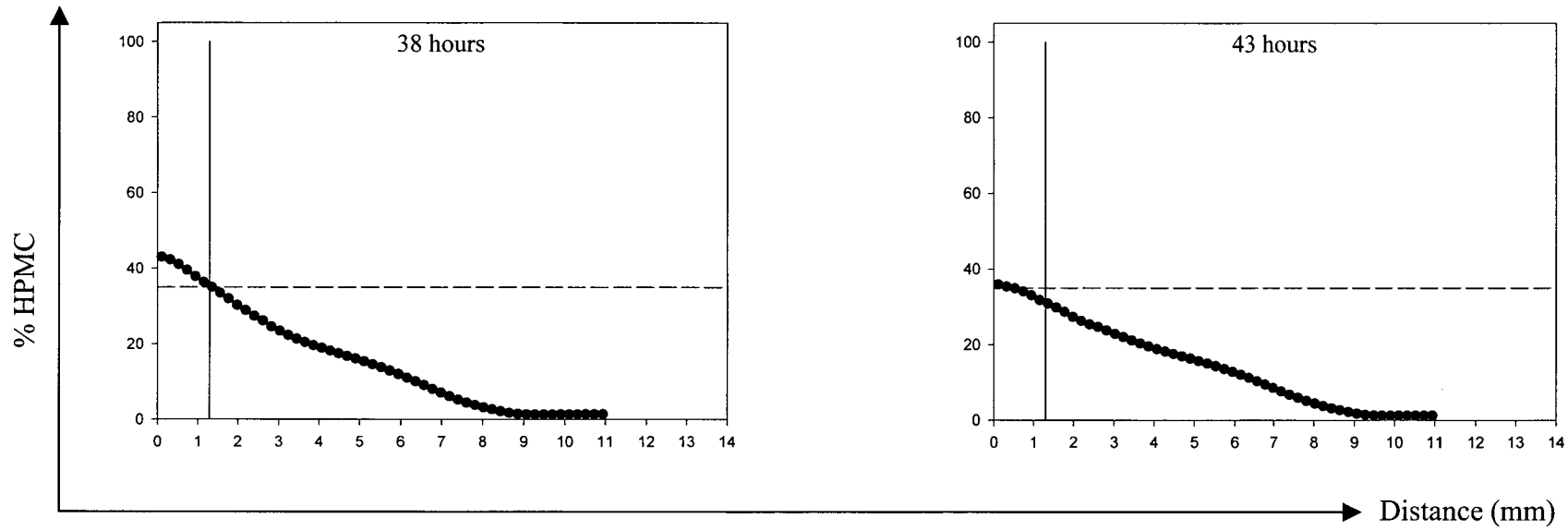

Figure 3.10 continued.

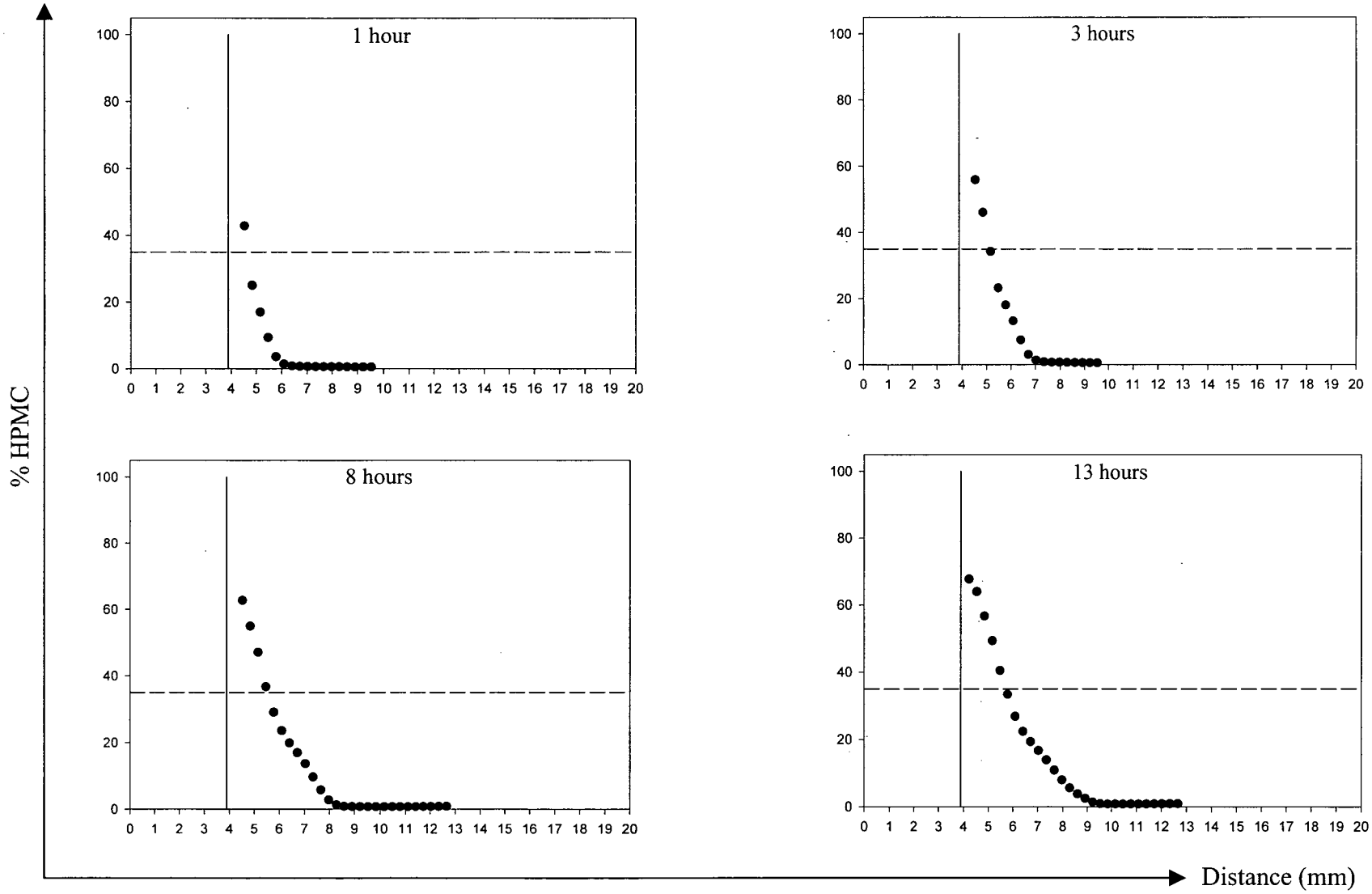

Figure 3.11 One-dimensional swelling profiles of a Type 3 HPMC tablet at 37 °C. The solid vertical line at 3.89 mm indicates the original tablet thickness and the dashed horizontal line at 35% HPMC indicates the limit of reliability. The axes in the plots are defined by the arrows.

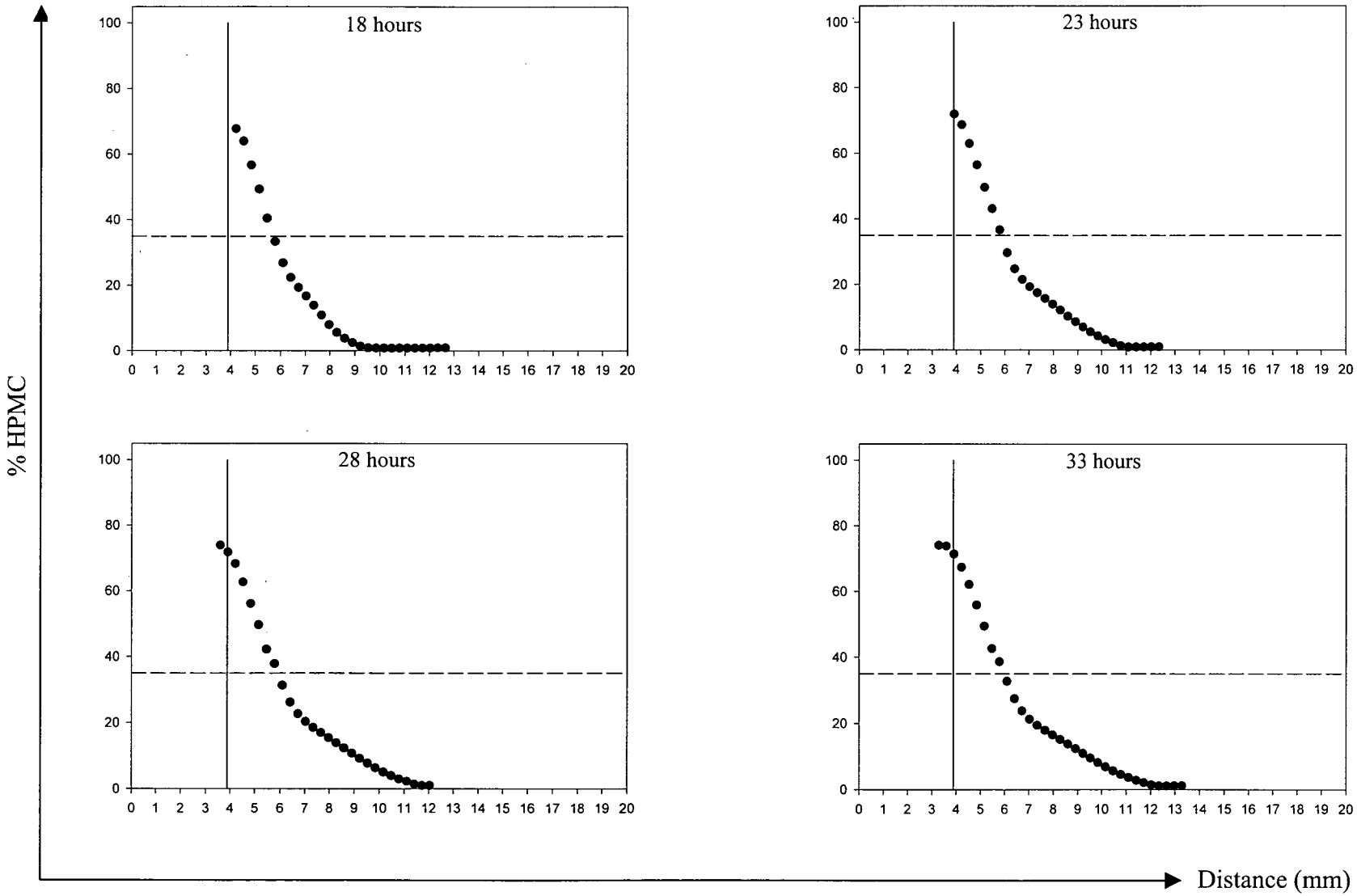

Figure 3.11 continued.

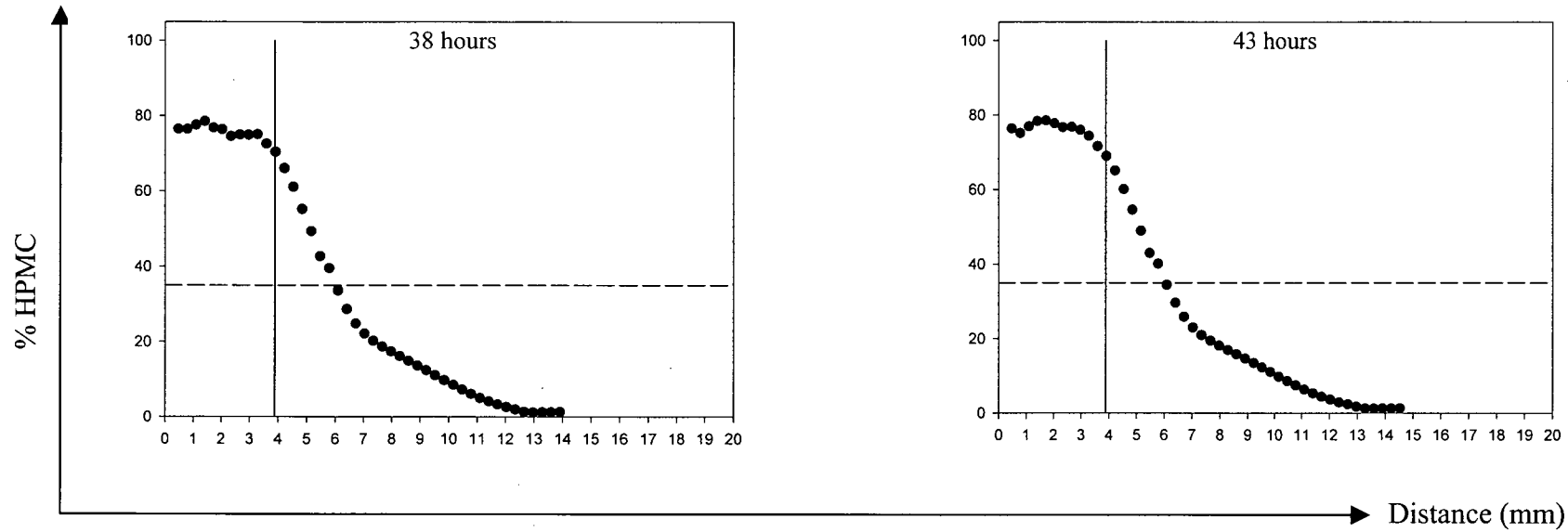

Figure 3.11 continued.

Table 3.4 Expansion distances of the 10% gel front at the different temperatures.

Swelling time (hours)	Front Distance (mm) 32 °C	Front Distance (mm) 37 °C	Front Distance (mm) 47 °C
1	3.76	3.72	3.74
3	4.49	4.47	4.44
8	5.52	5.61	5.58
13	6.17	6.17	6.28
18	6.58	6.56	6.82
23	6.82	6.85	7.27
28	7.08	7.23	7.68
33	7.36	7.60	8.08
38	7.68	7.95	8.46
43	8.00	8.17	8.84

By plotting the distance traveled by the front versus the square root of swelling time, a linear relationship is obtained as shown in Figure 3.12 at the appropriate temperature. The slopes from these graphs ($cm/s^{1/2}$) squared yield rate expansion constants (cm^2/s). The expansion rate constants obtained for the different gel concentrations at the appropriate temperatures are summarized in Table 3.5. At all three temperatures, the less concentrated polymer front is moving at a greater rate than the more concentrated polymer front. Although the rate expansion constants of the three temperatures do not differ by much, there is indeed a correlation between the temperature and the expansion rate of the gel. The rate of gel expansion is greater at the higher temperature and the rate expansion decreases accordingly as the temperature is decreased. The activation energy for the two different gel fronts can

Table 3.5 Summary of rate expansion constants for the 5% and 10% HPMC fronts at the specific temperature.

	Rate Expansion Constant[z] (cm^2/s) at 32 °C	Rate Expansion Constant[z] (cm^2/s) at 37 °C	Rate Expansion Constant[z] (cm^2/s) at 47 °C
5% HPMC	2.27×10^{-6}	2.52×10^{-6}	3.07×10^{-6}
10% HPMC	1.47×10^{-6}	1.67×10^{-6}	2.28×10^{-6}

[a] error ± 4%

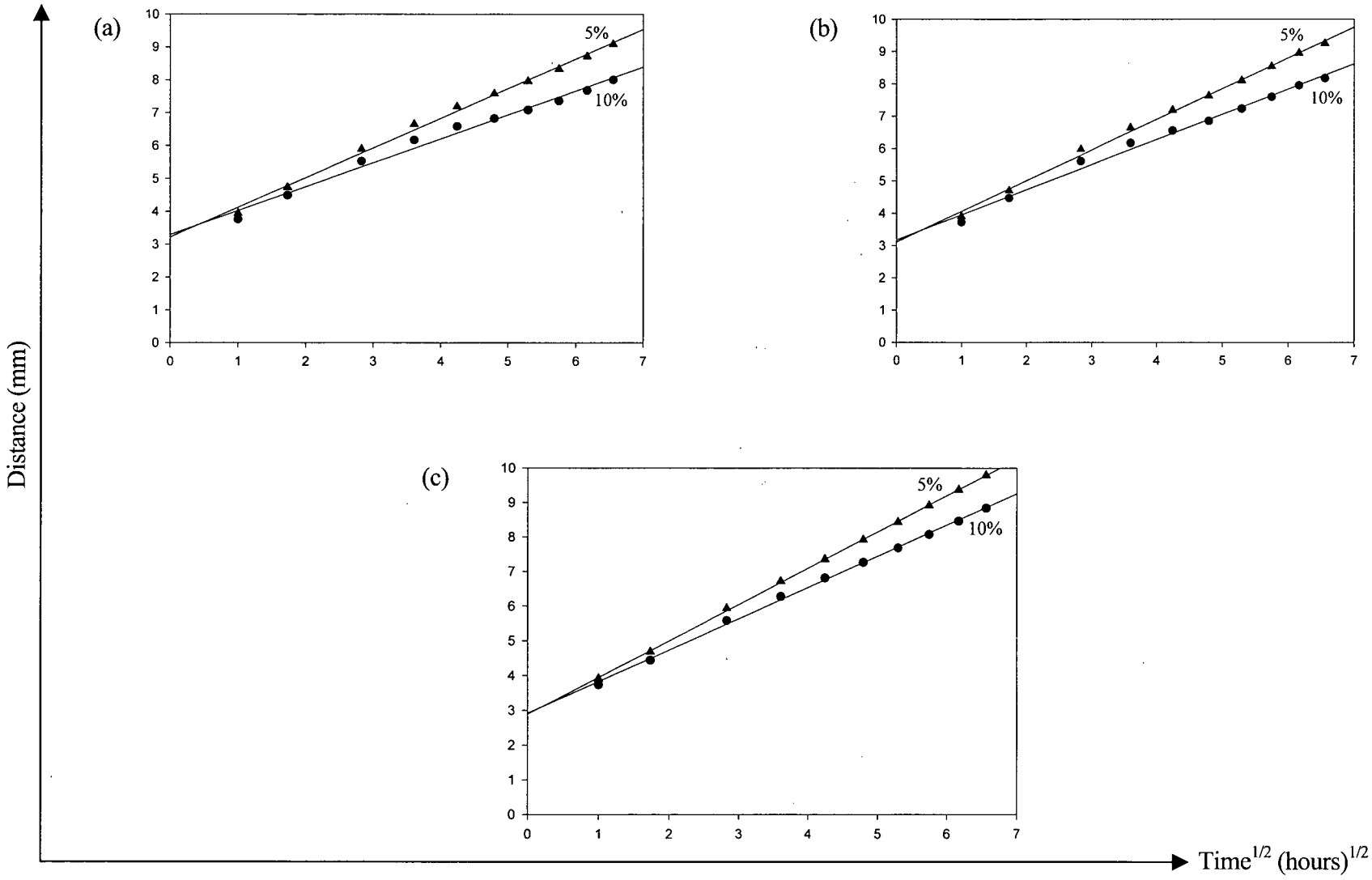

Figure 3.12 The distance of gel expansion from the swelling of Type 1 HPMC tablets as a function of the square root of time. (a) Rate expansion constants at 32 °C (b) Rate expansion constants at 37 °C (c) Rate expansion constants at 47 °C. The axes labels for the plots are the same and are defined by the arrows.

be calculated by using the equation derived from the Arrhenius Equation 3.1.

$$k = Ae^{\left(\frac{-E_a}{RT}\right)} \tag{3.1}$$

By plotting Ln (Expansion rate constant) versus 1/temperature, a linear relationship is obtained as shown in Figure 3.13. The activation energy for the 5% HPMC is (3.93 ± 0.31) x 10^3 cal·mol^{-1} K^{-1} and for the 10% is (5.66 ± 0.45) x 10^3 cal·mol^{-1} K^{-1}. It is clear that the energy barrier for the 5% gel region is lower than the 10% gel region. The energy barrier for the 5% gel region is approximately 1.5 times lower in energy than the 10% gel region. This approximate calculation of the energy barriers is in agreement with the expansion rate constants in that the 5% gel front is moving at a greater rate than the 10% gel front which is attributed to a lower energy barrier.

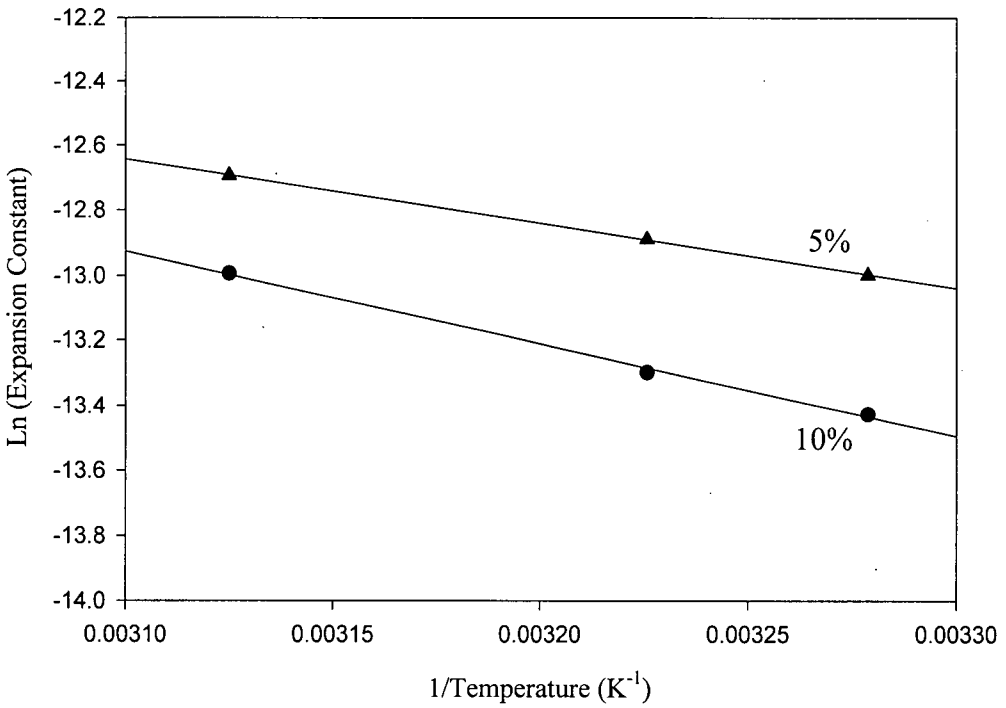

Figure 3.13 The relationship between Ln(Expansion Constant) as a function of 1/temperature for the 5% and 10% gel fronts. Using the equation derived by Arrhenius, the activation energy is obtained.

3.5 Summary

One-dimensional swelling profiles were generated to monitor the swelling of pure HPMC tablets in terms of polymer concentration and distance. Polymer concentrations were determined using calibration equations from Chapter 2 that related known polymer concentrations to their corresponding T_2 relaxation times. One-dimensional swelling of Type 1 HPMC tablets at three different temperatures confirmed that volume expansion for both the 5% and 10% gel fronts was greater at the higher temperature. Calculated activation energies for the 5% gel region was lower as compared to the 10% gel region. Present in all the profiles at all three temperatures was a characteristic "bump" at approximately 25% HPMC. The importance of the "bump" will become more evident when the one-dimensional modeling is described in Chapter 5. The one-dimensional swelling of HPMC tablets provided more insight into the swelling process; however, in order to further investigate the swelling process, the three-dimensional swelling must be considered. By taking advantage of the efficiency of the multi-echo pulse sequence, the three-dimensional swelling of a HPMC tablet is investigated in Chapter 4.

Chapter 4

Investigation of the Three-dimensional Swelling of Type 1 HPMC Tablets

4.1 Introduction

Due to the relative simplicity of the experiment and the subsequent interpretation of the results, the one-dimensional swelling of HPMC tablets was investigated first. Nevertheless, the ultimate goal is to monitor the three-dimensional swelling since this is the outcome of tablets once ingested. Unlike the one-dimensional case which involves the penetration of water into one face of a flat faced HPMC tablet, the three-dimensional swelling would involve the penetration of water into both flat faces and also the sides of the tablet. With the present imaging equipment and the implementation of the new multi-echo pulse sequence, it should be possible to monitor the changes in concentration as the tablet swells. The present chapter describes the investigation of this swelling behaviour and provides concentration information using NMR imaging.

4.2 Two-dimensional Imaging

Two-dimensional imaging is similar to one-dimensional imaging in that there is a division of the entire sample into voxels. Whereas one-dimensional imaging spatially resolves the NMR signal in one direction, two-dimensional imaging spatially resolves the NMR signal in two dimensions. The two-dimensional pulse sequence used to measure T_2 relaxation times within a specific region of sample is shown in Figure 4.1. This pulse sequence is similar to the pulse sequence in Figure 3.4 employed in the one-dimensional investigation of HPMC tablets except for the use of selective pulses and the application of magnetic field gradients in more than one direction.

Slice selection involves the 'selection' of a plane of the sample from which the NMR signal is detected. This involves the combination of a selective pulse along with a linear magnetic field gradient. The application of a linear magnetic field gradient results in a range of

resonance frequencies over the sample and this combined with a selective pulse which has a defined frequency range, results in the excitation of nuclei within a small cross-section or "slice" through the sample as shown in Figure 4.2. A small negative gradient is immediately applied

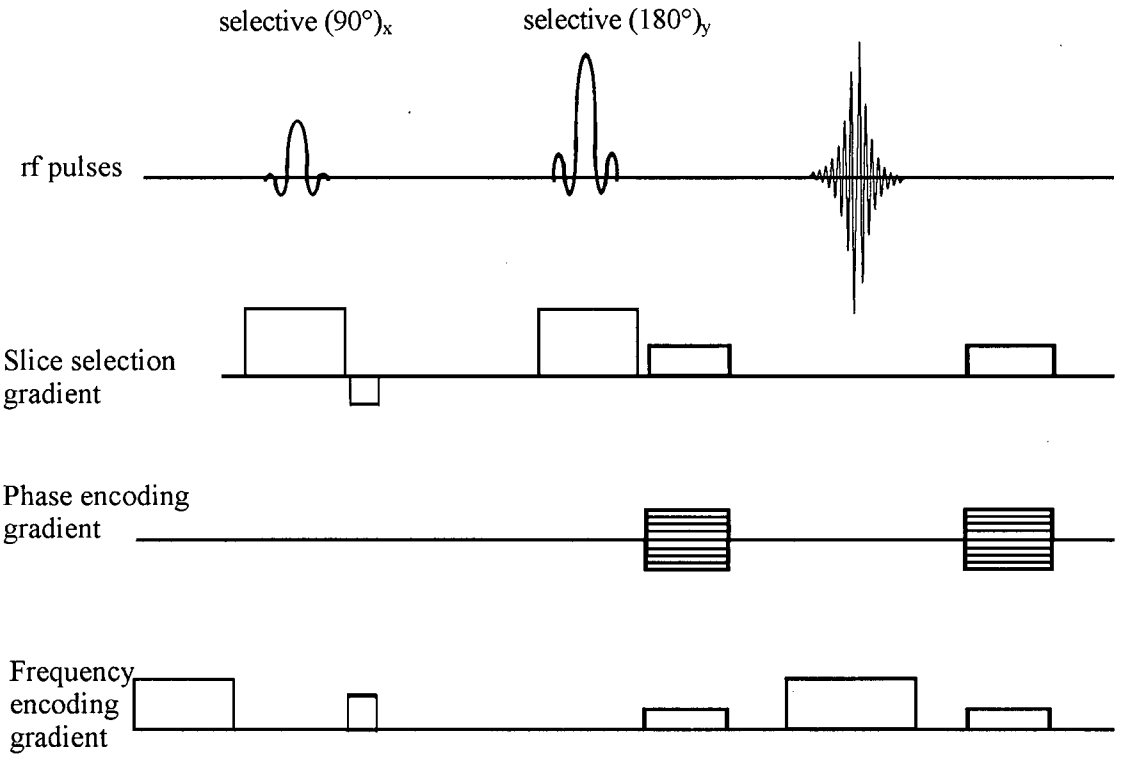

Figure 4.1 Two-dimensional imaging multi-echo pulse sequence used to investigate the three-dimensional swelling HPMC tablets.

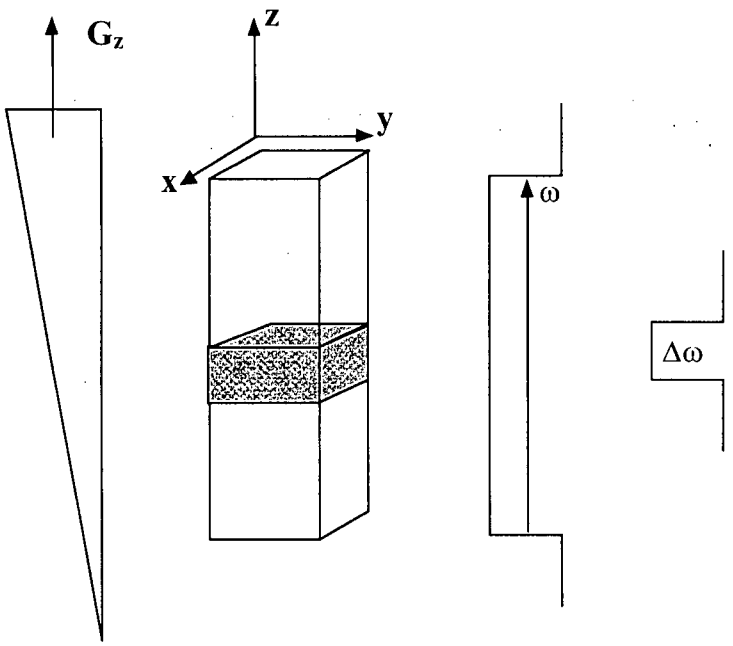

Figure 4.2 The process of slice selection of a sample (a) Application of the z-gradient over the sample (b) Sample (c) Spread of frequency from the sample due to the application of the gradient (d) Excitation width $\Delta\omega$ of the selective pulse corresponding to a specific region in the sample as indicated by the shaded region in (b).

after the slice selection to refocus the magnetization in the slice. The thickness of the slice can be varied by controlling the gradient strength and the frequency distribution of the selective pulse, $\Delta\omega$. Along with the thickness, the orientation of this excited region can be varied by the application of gradients along either the x, y, and z directions. Once this specific slice through the sample has been exited or selected, only nuclei within this slice are detected and their T_2 relaxation times determined similar to the multi-echo pulse sequence previously described in Chapter 2. After the 90° selective pulse and a τ delay, a 180° selective pulse rotates all the spins inside the selected plane around the x, y-axes. After a delay 2τ (T_E), the spins are refocused and are detected. After a delay 3τ, a second 180° selective pulse rotates the spins inside the slice around x, y-axes and after 4τ (2 x T_E), the signal is detected. Each echo is stored in the computer's hard drive as this echo train proceeds. The T_2 relaxation times are obtained by fitting

the acquired signal intensity in each pixel to obtain the corresponding T_2 to value from Equation 1.2 using the Bruker imaging software, ParaVision.

As was in the case of the one-dimensional imaging, the application of a magnetic field gradient encodes spatial information in the frequencies of the detected signal and is called frequency encoding gradient. In two-dimensional imaging, an additional gradient is applied that is called the phase encoding gradient that further resolves the NMR signal by providing a phase differentiation of the detected signal in addition to the frequency encoding. The progression of the spins in the experiment is shown in Figure 4.3. After the 90° selective pulse, the spins of a slice through the sample are in the x, y plane precessing at the Larmor frequency as shown in Figure 4.3 (a). The application of the phase encoding gradient along the y-direction results in a differentiation of precessional frequencies as shown in Figure 4.3 (b). The size of each arrow in each voxel represents the relative speed of precession and the larger the gradient, the faster the voxels' magnetization precesses. After the y-gradient is turned off, the spins are out of phase as shown in Figure 4.3 (c). During the detection period, or frequency encoding, the x-gradient is turned on, and the spins in each voxel are now differentiated on the basis of both their precessional frequency and phase. The second dimension is obtained by incrementing the phase encoding gradient strength through a series of N experiments producing an N x N pixel image. Each pixel or voxel in this case is indicative of the water signal intensity. When coupled together with the multi-echo pulse sequence, each voxel has a distinct T_2 relaxation time which can be converted into concentration.

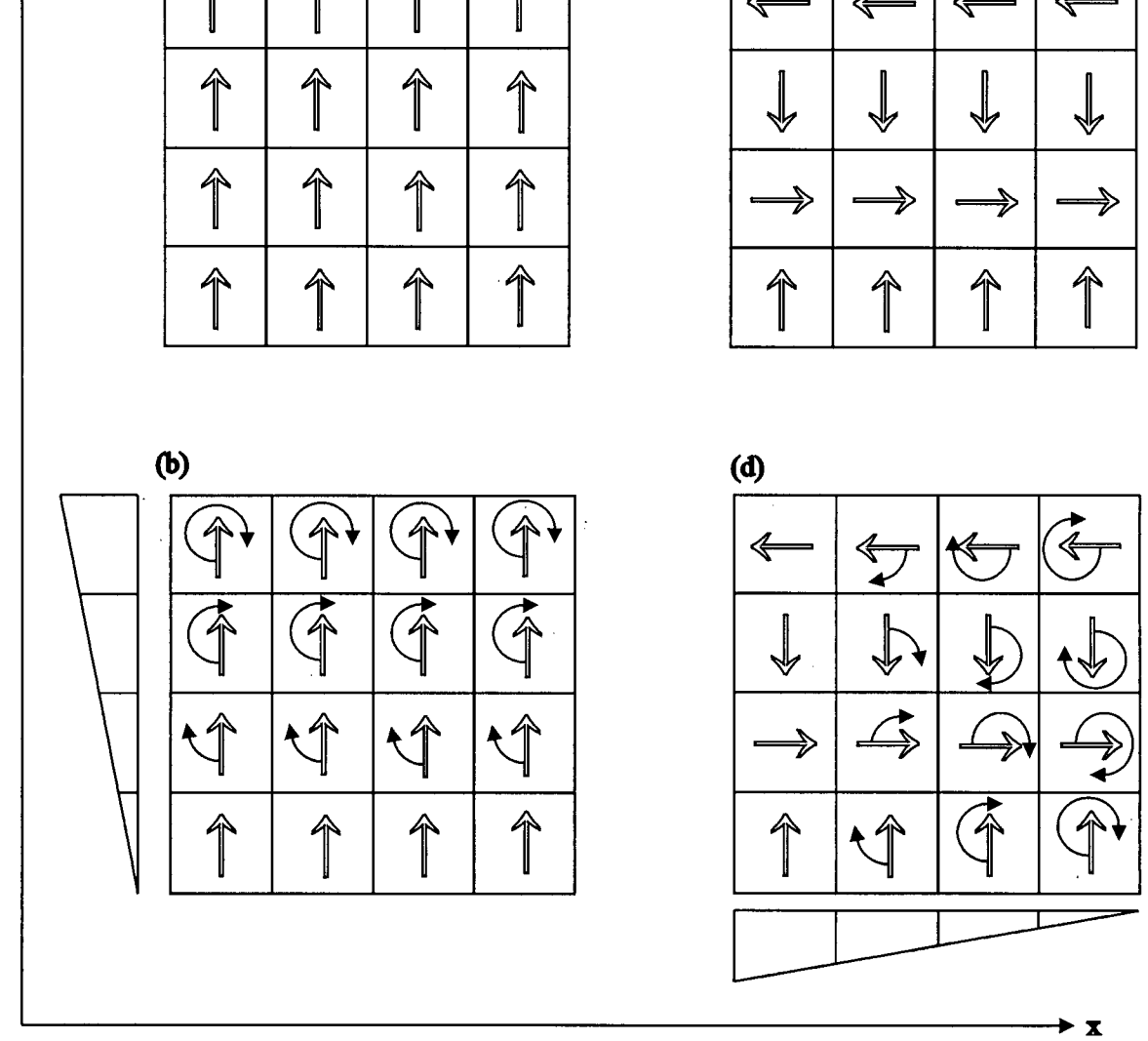

Figure 4.3 Phase and frequency encoding of a sample divided into 16 voxels (a) Representation of the nuclear spins after a 90° pulse (b) Application of the y-gradient causes a differentiation of precessional frequency as indicated by the size of the darkened arrows (c) Representation of the nuclear spins once the y-gradient is turned off resulting in the spins being out of phase (d) Frequency encoding of the spins as the x-gradient is applied. The result is a differentiation of each voxel identified by its phase and precessional frequency.

4.3 Experimental Setup for the Three-dimensional Swelling of Type 1 HPMC Tablets

The three-dimensional swelling experiment was carried out in a 27 x 55 mm (o.d.) glass vial held vertically inside a 30 mm rf coil. Prior to the imaging studies, the Type 1 tablet was evacuated for 10 minutes as previously discussed in Chapter 3 to remove any air trapped inside. The setup of the HPMC tablet is shown in Figure 4.4. The tablet was supported by a very small amount of glass wool to keep it suspended and a very small amount of glass wool was placed on top of the tablet to prevent it from floating to the top. Prior swelling experiments revealed that the use of glass wool to support and to prevent the tablet from floating to the top did not interfere with the swelling process and the imaging experiment. The glass vial was capped and a heating coil, Dewar, and a Bruker variable temperature unit were utilized to maintain the sample at a constant temperature of 37 °C. Two 1 mm thick slices were selected to be imaged as shown in

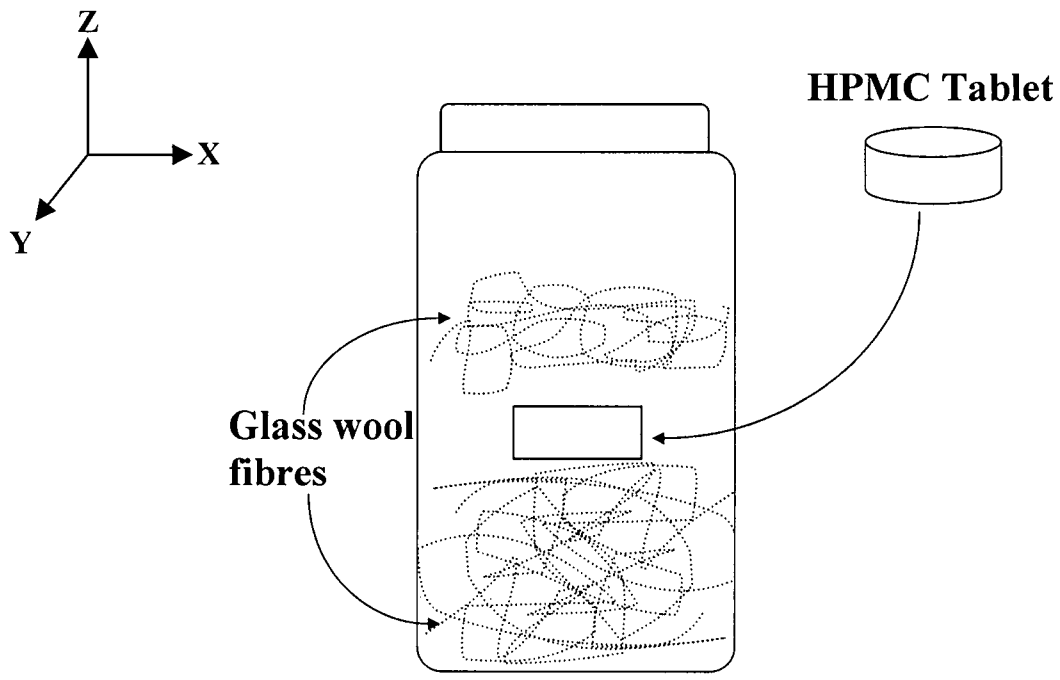

Figure 4.4 Three-dimensional swelling setup of a Type 1 HPMC tablet.

Figure 4.5. These slices, referred to as axial and sagittal are representative of the swelling in the radial and vertical swelling directions, respectively. The z, x slice perpendicular to the z,y sagittal slice would duplicate the information from the sagittal slice and therefore was omitted in the three-dimensional swelling experiment. Each slice was imaged with the shortest possible T_E

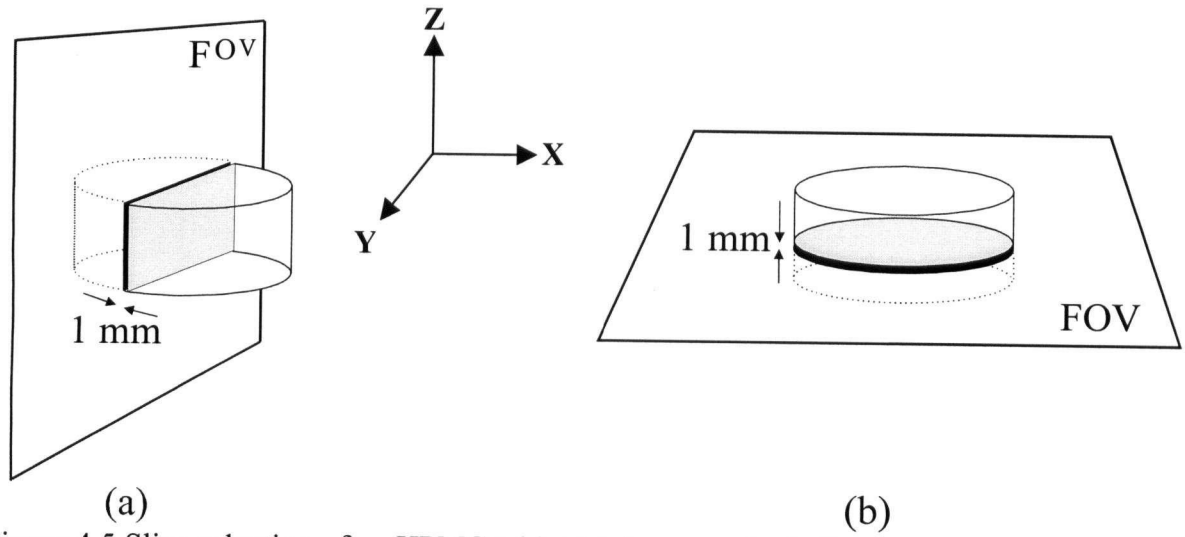

Figure 4.5 Slice selection of an HPMC tablet (a) 1 mm sagittal slice representing the swelling in the vertical direction (b) 1 mm axial slice representing the swelling in the radial direction.

of 6.7 ms which allowed for the detection of the shorter T_2 relaxation times. The total number of echoes or images acquired was 100 which allowed for the detection of the longer T_2 relaxation times. A longer T_E experimental protocol could not be combined together with the shorter T_E experimental protocol due to the long acquisition time involved. A single experimental protocol from the two-dimensional imaging took 8 times longer than the one-dimensional imaging or approximately 25 minutes to complete. If a long T_E experimental protocol was implemented, this would contribute to a significant variation in the tablet dimension and also concentration during the imaging. By also having only one experimental protocol, the subsequent analysis of the results was greatly simplified. The sagittal and axial slices were acquired in succession. Each image was 64 x 64 in size with each voxel in the image having a volume equal to 0.47 x 0.47 x 1.0 mm. A summary of the acquisition parameters for the two-dimensional imaging is

found in Table 4.1. All 100 intensity images for each slice were converted into a single T_2 image, each voxel representing a T_2 relaxation time as shown in Figure 4.6. The T_2 image was then converted to a concentration image by applying Equation 2.1 and represented as contour and mesh plots.

Table 4.1 Summary of the two-dimensional imaging parameters.

	T_E	Number of echoes	T_R	Image size (pixels)	FOV	Slice thickness	Slice selection gradient
Sagittal slice	6.7 ms	100	25 s	64 x 64	30.0 mm	1.0 mm	G_x
Axial slice							G_Z

4.4 Results and Discussion of the Three-dimensional Swelling of Type 1 HPMC Tablet

Although the one-dimensional investigation had a short echo time protocol with T_E equal to 5.6 ms and the three-dimensional investigation had a T_E equal to 6.7 ms, it was confirmed that this produced a variation of T_2 relaxation times of less than 5%. Therefore, Equation 2.1 was used to convert T_2 relaxation times obtained from the three-dimensional swelling experiment into concentrations as previously mentioned.

The concentration profiles of the three-dimensional swelling of the Type 1 HPMC tablet are shown as contour plots and also as mesh plots in Figures 4.7 and 4.8 respectively. Both of these plots give the same exact information; however, each plot presents this information from a different perspective. In all the distribution profiles shown for both plots, only HPMC concentrations below 35% HPMC are plotted. Polymer concentrations above 35% HPMC are considered semi-quantitative at best as discussed previously in Chapter 3.

The sagittal slice not only provides swelling information in the vertical direction but also in the radial direction. From the contour plots, this is possible if a row at z = 0 and parallel to the y-axis is compared to the axial slice. The swelling behaviour in this region is similar to that of

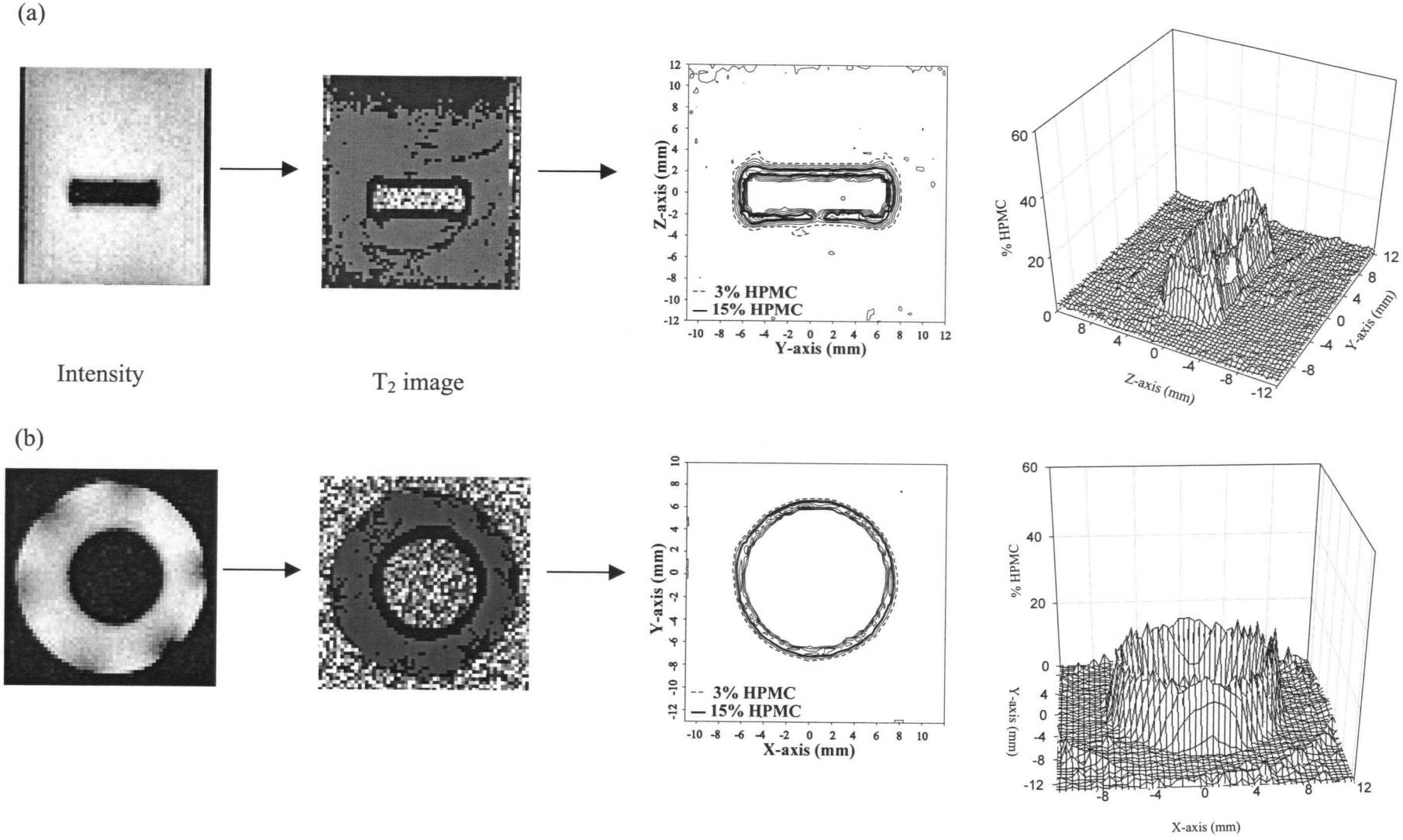

Figure 4.6 Type 1 HPMC tablet after one hour of swelling (a) The sagittal slice shows the vertical swelling direction. The first image shown is one of a hundred intensity images that are subsequently converted to a single T_2 image. The T_2 image is then converted to concentration using Equation 2.3 and shown as contour and mesh plots (b) The axial slice shows similar data from the radial swelling direction.

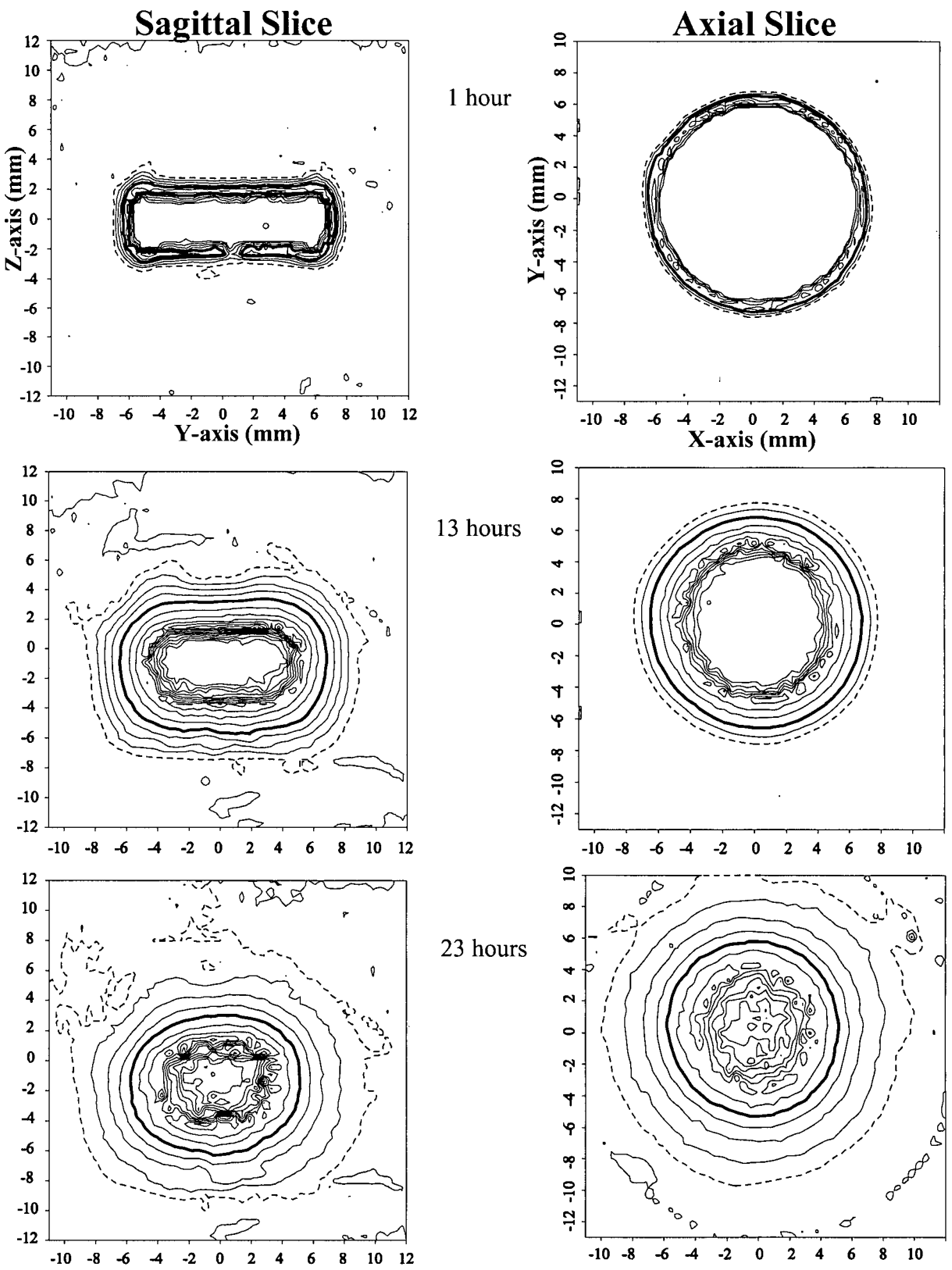

Figure 4.7 Contour plots of the vertical and radial swelling directions of the Type 1 HPMC tablet indicated by sagittal and axial slices respectively in 3% increments. The dashed and thick line in the plots represent the 3% and 15% polymer concentrations respectively.

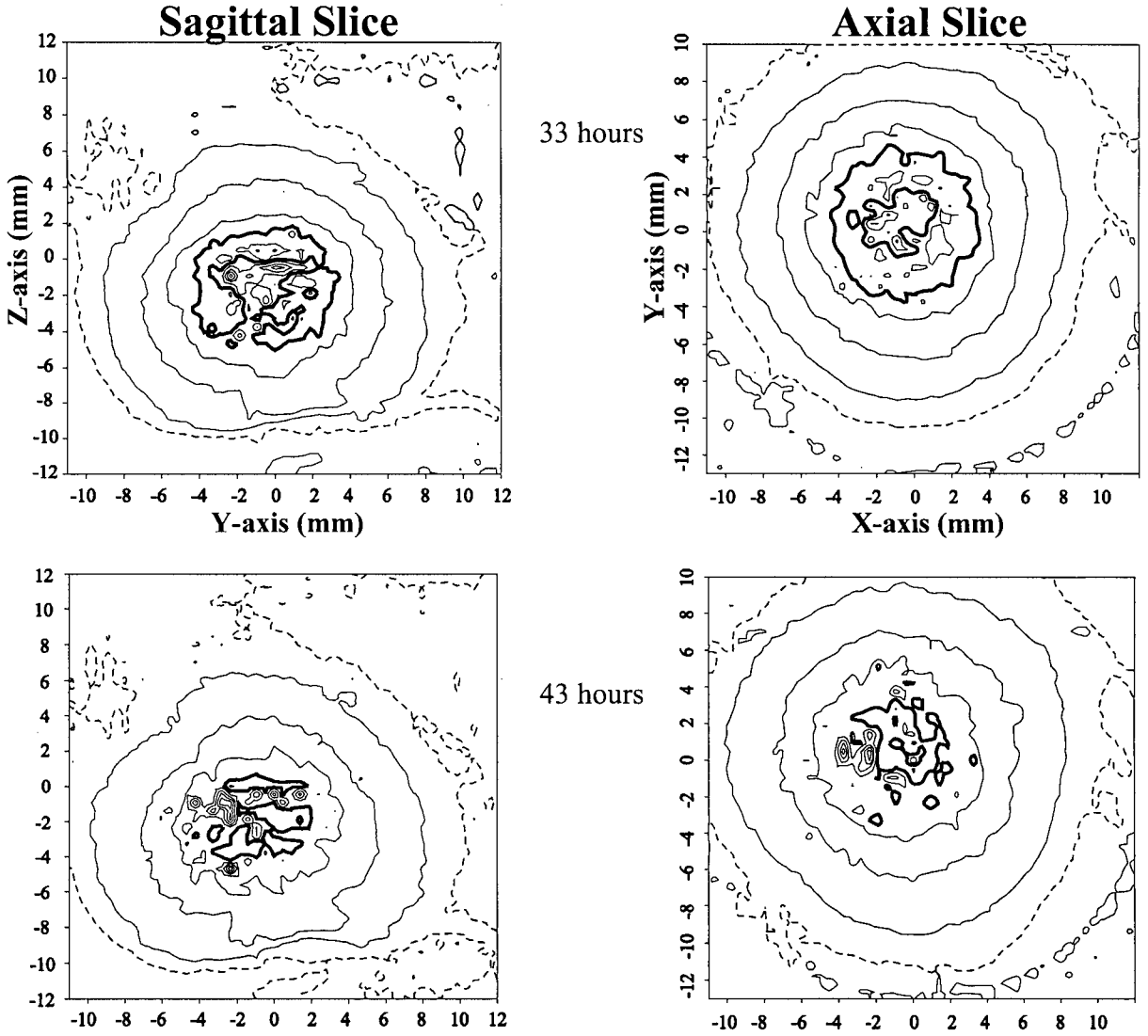

Figure 4.7 continued.

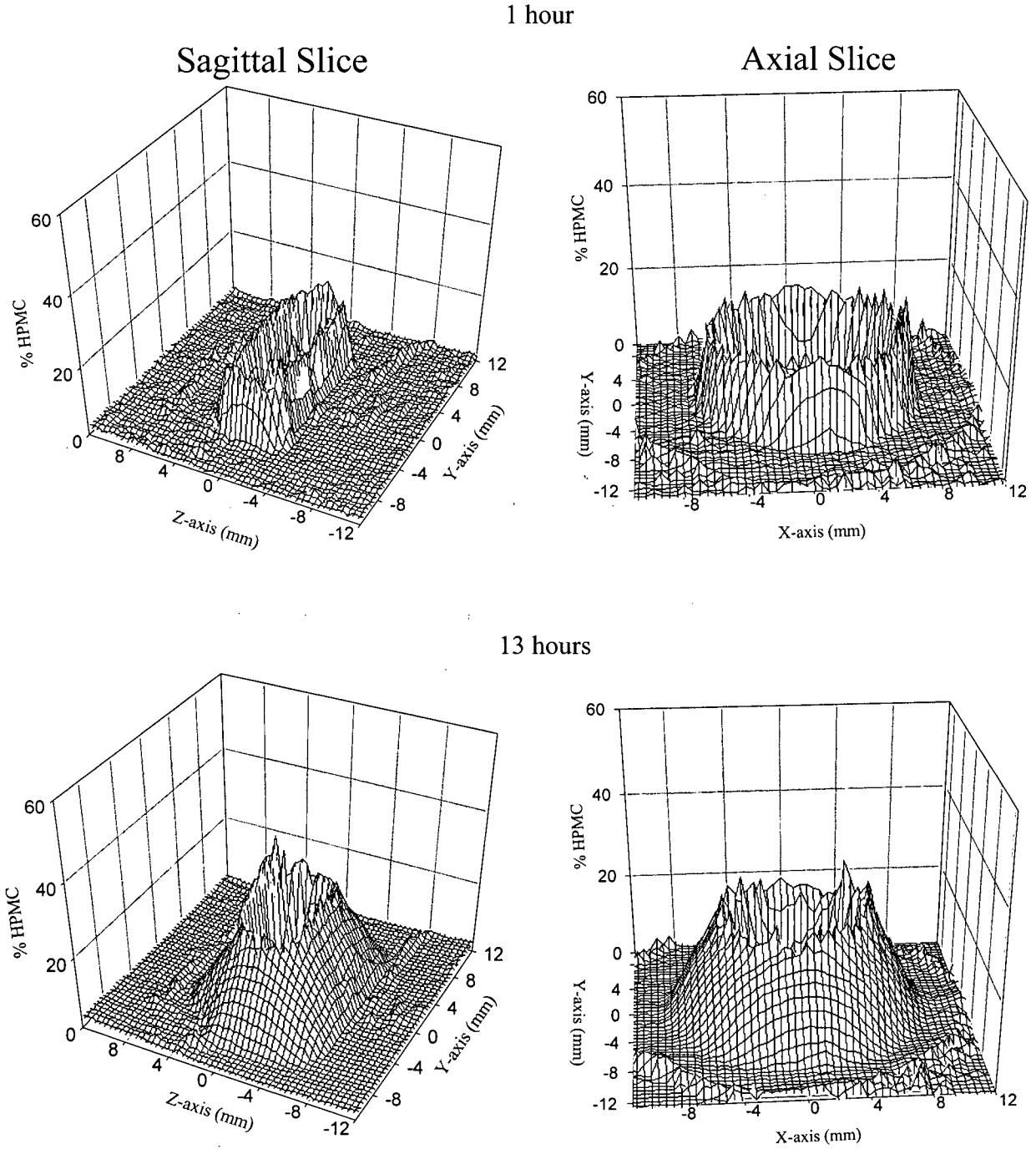

Figure 4.8 Corresponding concentration profiles as mesh plots for the three-dimensional swelling of the Type 1 HPMC tablet. The swelling in the vertical and radial directions is indicated by sagittal and axial slices respectively.

23 hours

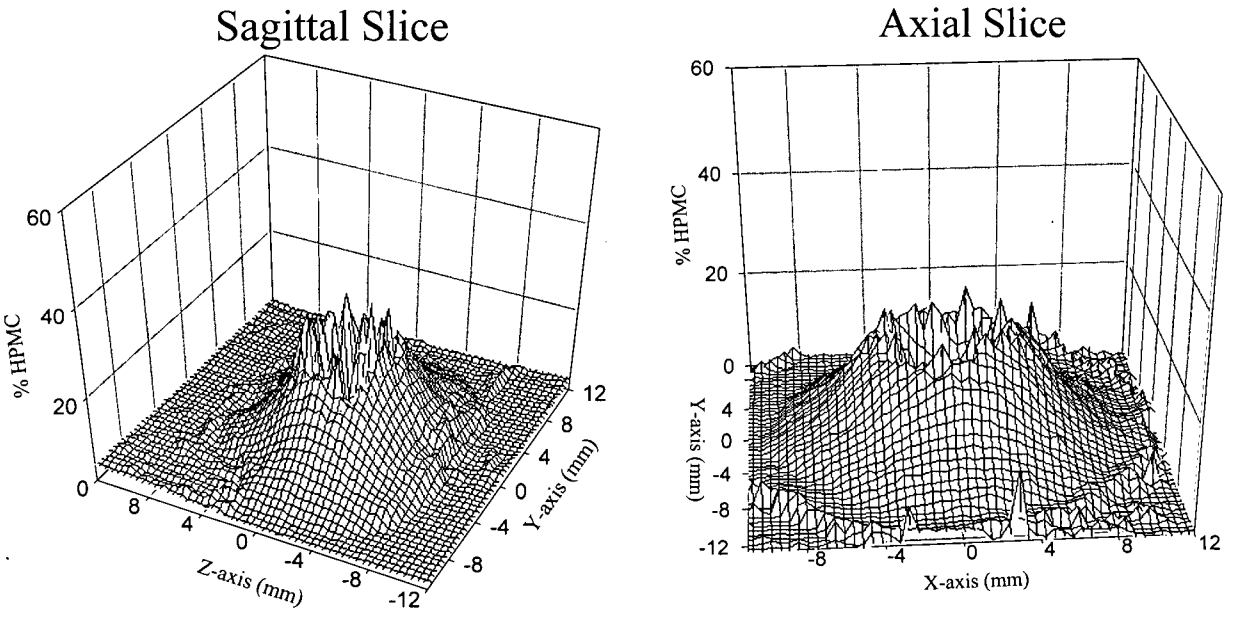

33 hours

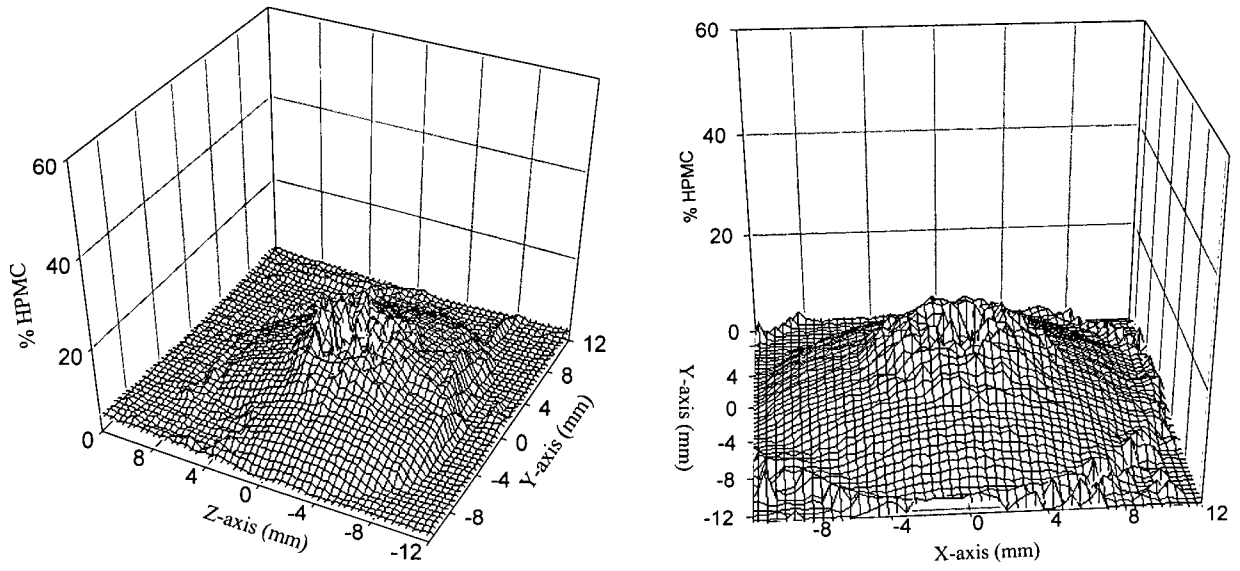

Figure 4.8 continued.

43 hours

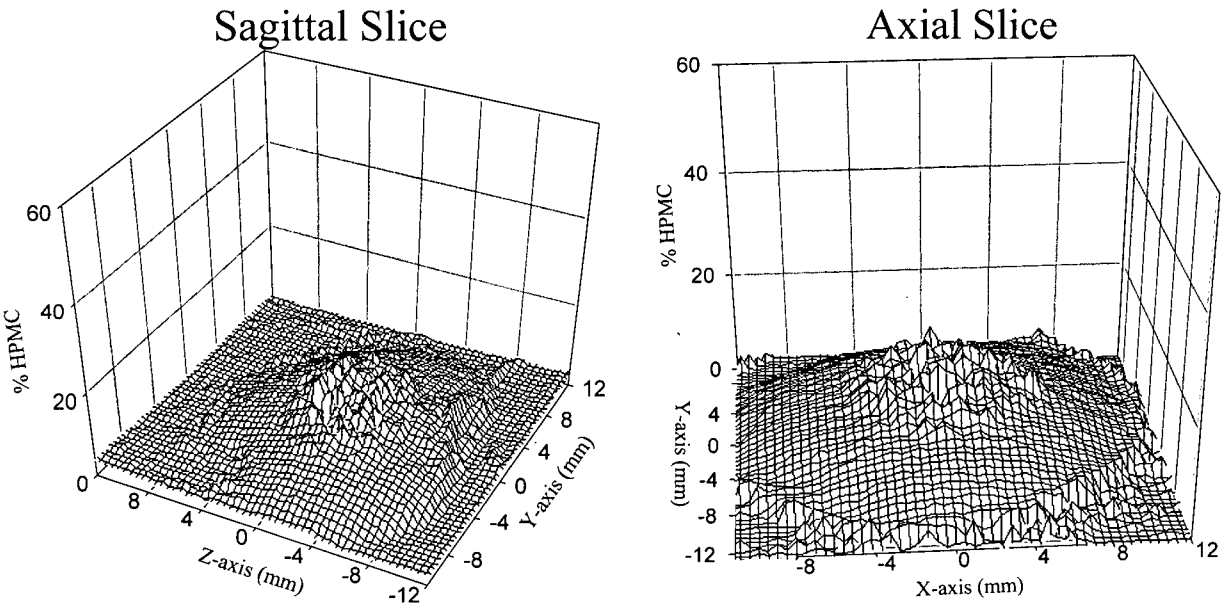

Figure 4.8 continued.

the axial slice only if the swelling behaviour in the radial direction in symmetrical. The volume expansion or swelling of the tablet in the vertical direction is very evident in that the 3% HPMC as indicated by the dashed line moves away from the center of the tablet. Polymer concentrations equal to 15% HPMC are indicated by the thick line. Initially (1 hour of swelling), there is a distinctively small concave shape that is clearly visible from the contour plot in the vertical swelling direction that has also been observed by other research groups [9, 10]. This higher rate of hydration followed by a greater expansion around the edges results from a more dense and tightly packed region of polymer around the edges due to the direct compression of the HPMC powder into a tablet. As the swelling of the tablet proceeds, the concentration within the core decreases as water continues to be imbibed by the tablet.

The swelling of the HPMC tablet in the radial direction is symmetrical as indicated by the radial slice in the contour plots. However, at 33 hours of swelling, the tablet has swelled to a point where the outermost region of polymer/water is in contact with the vial. It is clear from the contour plots that at the swelling time of one hour, the region at the center of the tablet for both the sagittal and axial slice shows zero concentration. There are three reasons that account for this observation. First, the T_2 relaxation times for the high polymer concentrations are too short to be detected and thus the higher polymer concentrations are not detected. Second, the size of each voxel has been reduced significantly compared to the voxel size in the one-dimensional swelling resulting in a decrease in the concentration of water per voxel and thus a decrease in the observed ^{1}H signal. This fact combined with the low water concentrations present at high polymer concentrations add further to the problem of a decreased ^{1}H signal. Third, only one scan was performed in the two-dimensional imaging compared to four in the one-dimensional imaging. The advantage of having more than one scan is each additional scan further improves the signal to noise ratio. The above three factors contribute to some degree the non-observation

of the higher HPMC concentrations. The polymer concentration within the core of the tablet gradually decreased as the swelling of the tablet proceeds. At 43 hours of swelling, the core of the tablet had decreased to approximately 10-15% HPMC and this is confirmed in the sagittal slice profile at this time.

The overall dimensional changes of the swelling tablet have been used specifically to monitor the swelling behaviour in the vertical and radial directions. These measurements are made by dividing the overall dimension at a particular swelling time by the dimension of the dry tablet. The overall dimension at a particular swelling time is defined as the boundary between 0% and approximately 1% HPMC. The overall dimensional changes in both the radial and vertical directions are shown in Figure 4.9. The vertical tablet dimension increased by approximately 200% as compared to approximately 100% for the radial dimension after only one hour of swelling. By the end of the swelling experiment, the swelling in the vertical direction had increased by approximately 800% compared to only 200% in the radial direction. One possible explanation as to why the vertical swelling occurs to a much greater extent than the radial swelling could be as a result of the release of the tablet compressional forces created during the tablet pressing process. A second explanation involves the variation of the surface area between the flat surface of the tablet and its sides. The surface area of the flat surface is much greater than the sides thus enabling more water penetration into the tablet and thus an increase in the swelling rate and dimension.

To compare the swelling in one-dimensional to the three-dimensional swelling, a column of T_2 relaxation times through the sagittal slice was converted into HPMC concentrations and plotted as shown in Figure 4.10. Plotted along with these profiles is the one-dimensional swelling distribution profiles not for the Type 1 tablet but for the Type 2 tablet also carried out at 37 °C which is half as thick as the Type 1 tablet. The three-dimensional swelling profiles

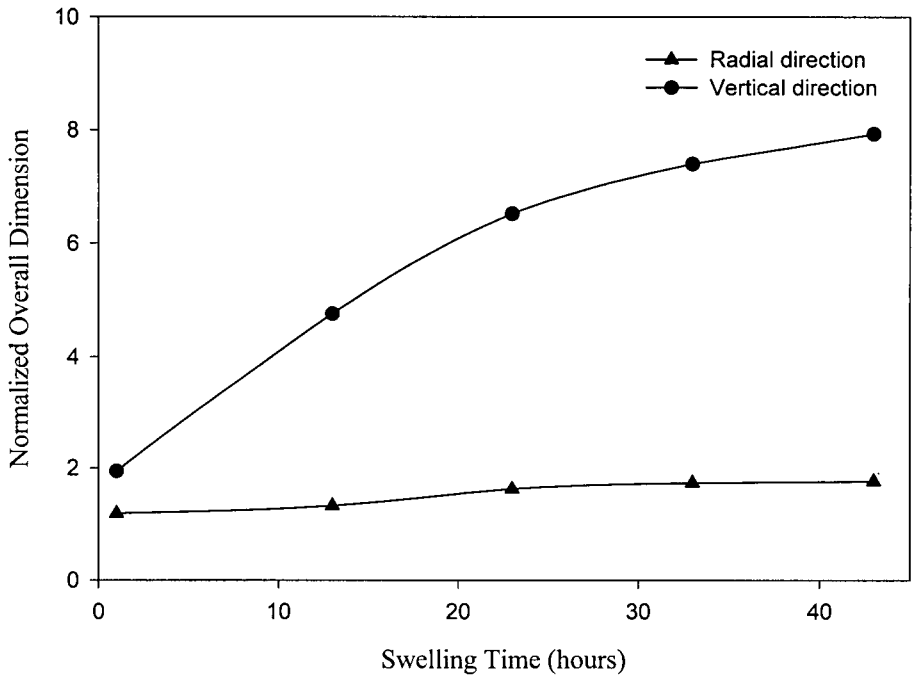

Figure 4.9 Normalized overall dimension changes for the radial and vertical swelling directions.

resemble the one-dimensional case at the earlier swelling times; however, at the later swelling times, the core of the tablet has a reduced polymer concentration compared to the one-dimensional case. This is attributed to the increased ability of water to access the core since the water is able to penetrate both flat faces of the tablet. One important characteristic that was present in the one-dimensional profiles and mentioned in Chapter 3 is the "bump" at approximately 25% HPMC which is also present in the three-dimensional swelling profiles from one hour until 23 hours. The presence of the "bump" will be examined in more detail when the one-dimensional modeling of HPMC tablets is discussed in Chapter 5. A suitable model for the one-dimensional swelling should be able to be generalized to fit the three-dimensional case.

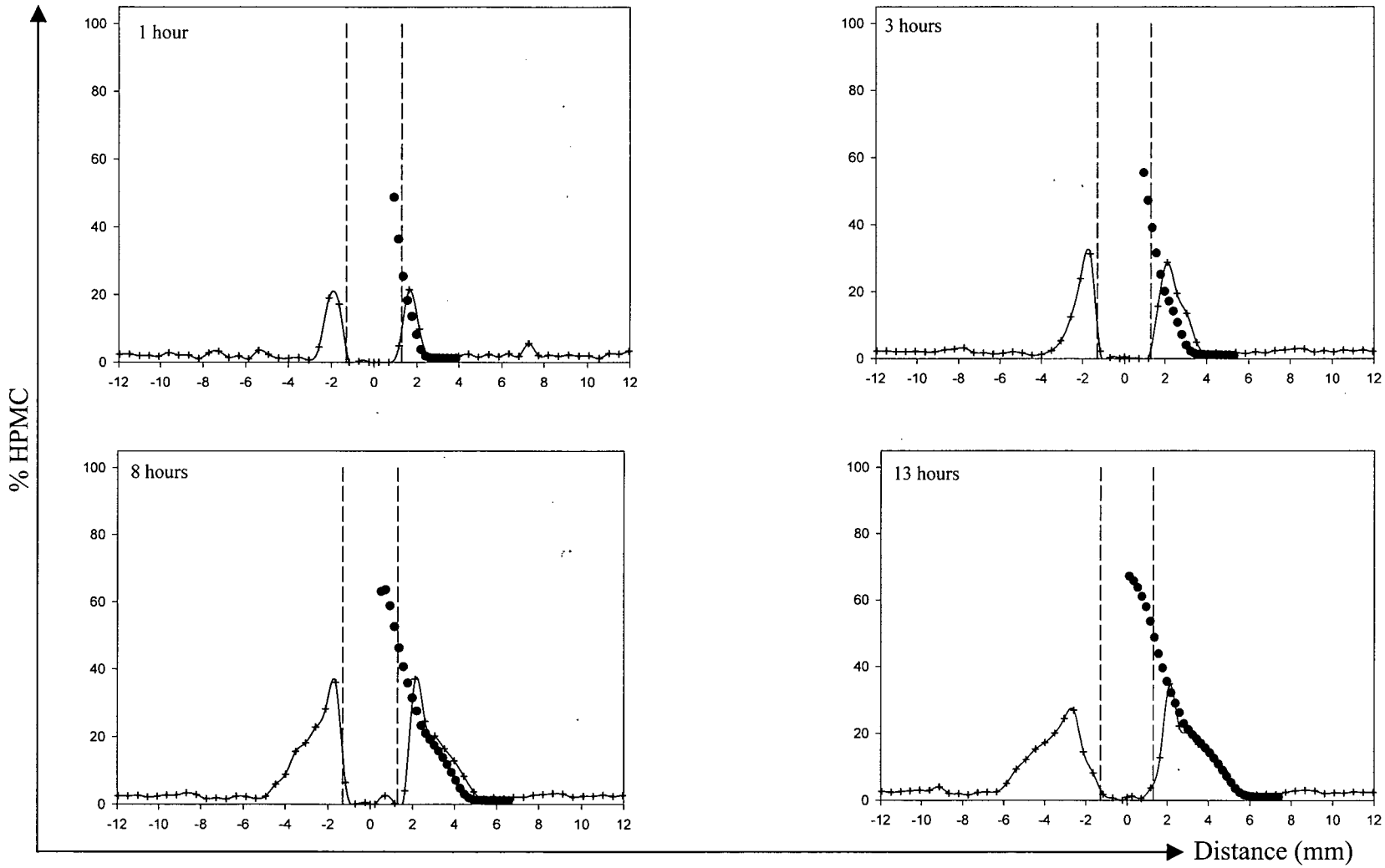

Figure 4.10 Column of concentration values through the sagittal slice of the Type 1 HPMC tablet. The crosshairs along with the solid line are obtained from the three-dimensional swelling. The darkened circles are from the one-dimensional swelling of the Type 2 HPMC tablet. The dashed vertical lines indicate the initial thickness of the Type 1 tablet. The concentration within the tablet is not the actual concentration but is as a result of the water T_2 relaxation times being too short to be detected in this region. The axes in the plots are defined by the arrows.

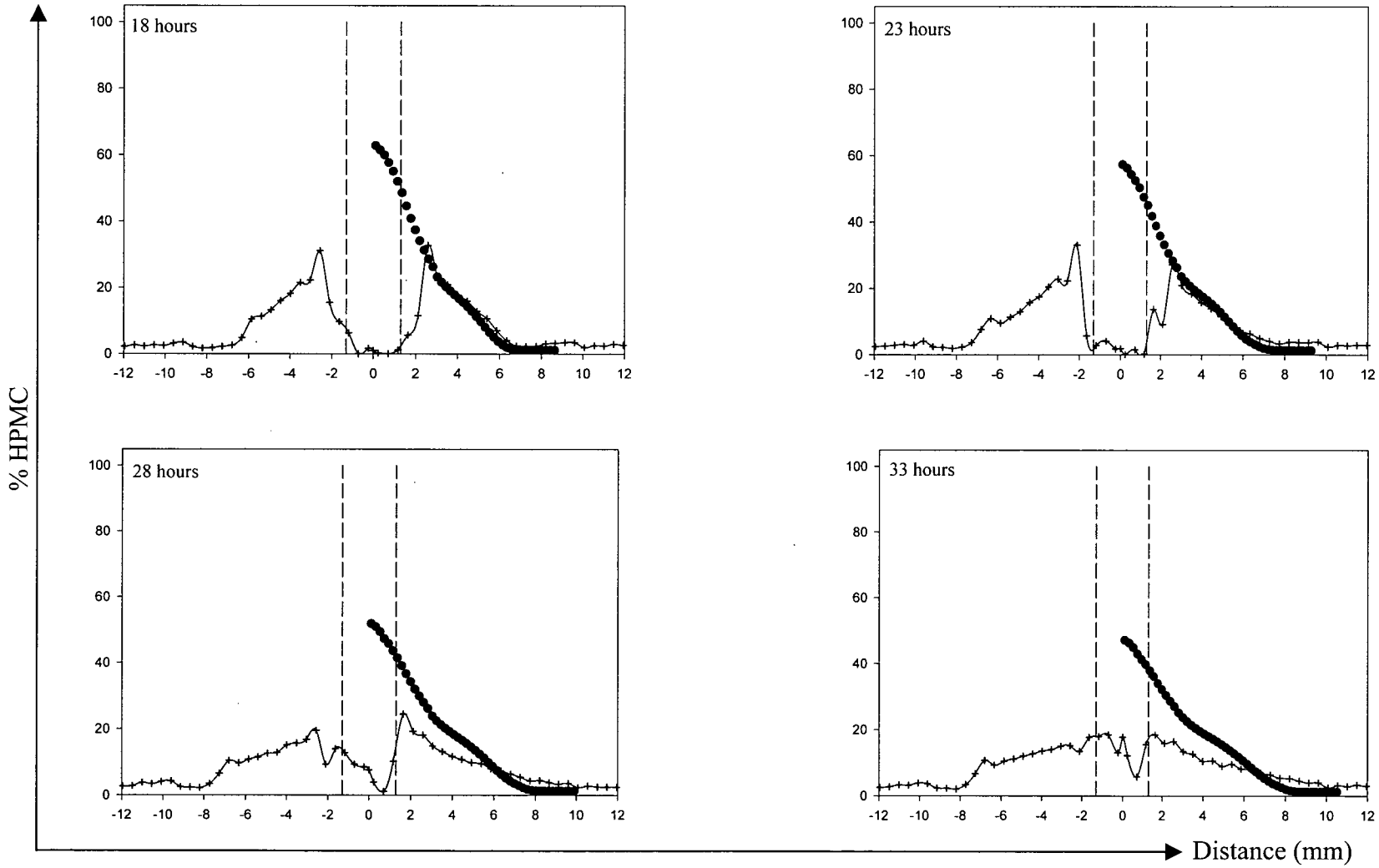

Figure 4.10 continued.

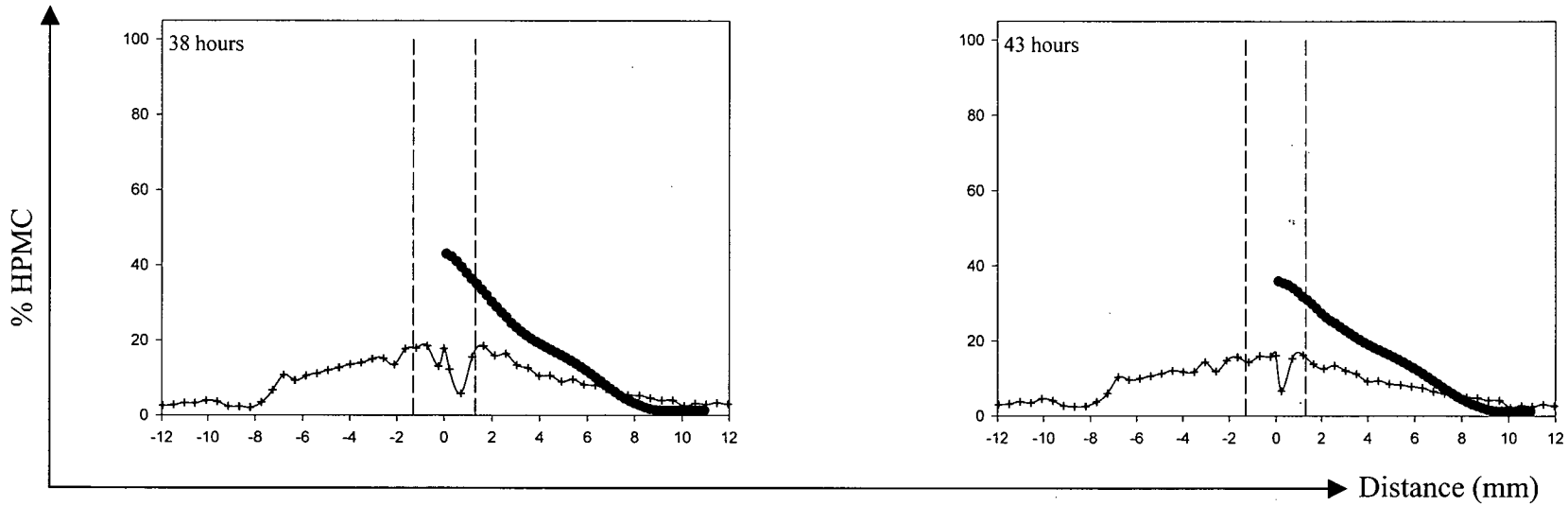

Figure 4.10 continued.

4.5 Summary

The three-dimensional swelling of a HPMC tablet using NMR imaging describe here is the first attempt to investigate the HPMC tablet swelling process quantitatively in terms of polymer concentration. The swelling in the vertical direction is several orders of magnitude greater than the radial direction. The swelling in the vertical direction as indicated by a column of T_2 relaxation times through the sagittal slice is similar to that of a tablet that is half as thick and constrained to swell in one-direction. The presence of the characteristic "bump" at the earlier swelling times is indicative that it is not relegated to only the one-dimensional swelling case but is an inherent characteristic of these tablet systems. In an attempt to predict these swelling tablet systems, the experimental one-dimensional profiles are compared to a proposed mathematical model in Chapter 5. The results from the modeling can determine the applicability of the model and if it is feasible to proceed to the three-dimensional modeling.

Chapter 5

Modeling the One-dimensional Swelling of HPMC Tablets

5.1 Introduction

To date, the only way to investigate the swelling of HPMC tablets in terms of the polymer concentration profiles is by NMR imaging. An alternative to the actual NMR imaging experiment would be a theoretical model that would be able to predict the swelling. The evaluation of a theoretical model could be accomplished by comparing the theoretical results to the actual experimental results. Not only must the model be able to predict the HPMC distribution profiles but also the drug release profiles. The model's ability to predict the swelling behaviour and drug release behaviour of these tablets must be flexible; it must be able to predict the effect of different tablet dimensions, different HPMC grades, and different drugs. A previous evaluation of a theoretical model involved the comparison of the experimental one-dimensional swelling profiles to the theoretical using a segmented tablet model that is discussed shortly. In the next section, a newer mathematical model is evaluated by comparing the HPMC theoretical swelling distribution profiles to the experimental profiles for different tablet thicknesses to test its applicability and validity.

The segmented tablet model was originally designed to fit the change in thickness of a swelling tablet [22]. The model was subsequently extended and modified to predict the polymer concentration distribution for the case of one-dimensional swelling of HPMC tablets [3]. The model involved the dry tablet being divided into segments of equal thickness in which case the sum of the individual segments corresponded to the thickness of the tablet. The swelling of the tablet at each time was the result of the water penetration into the dry segments and the subsequent volume expansion of these segments. Each segment swelled with respect to the amount of water present that resulted in a new thickness and position. The amount of polymer

remained constant within each segment; however, due to the unique volume expansion of each segment, the polymer concentration decreased. The generation of the one-dimensional swelling theoretical profiles therefore required the calculation of distances and polymer concentrations. The distance each segment expanded was calculated by the sum of the previous individual segments. The fitting procedure involved several variables that included the thickness of the dry tablet, the swelling time, and diffusion coefficient of water. The first two variables were fixed and the diffusion coefficient was incremented through a series of steps to obtain best fits to the experimental data determined by finding the smallest sum of χ^2 or the minimum sum of the squares of the differences between the theoretical and experimental concentration distributions.

From this previous work by Blazek [3], the results for the fitting that produced the best fit results are shown in Figure 5.1. A water diffusion coefficient was obtained by varying the diffusion coefficient to yield the best overall-fit. The theoretical fits seemed to more closely match the experimental data at the earlier swelling times. However, at the swelling time of 37 hours, the theoretical polymer distribution over-estimated the degree of swelling compared to the experimental results. The deviation of the theoretical from the experimental results suggests that a new mathematical model is needed to take into account more complex interactions between water and polymer.

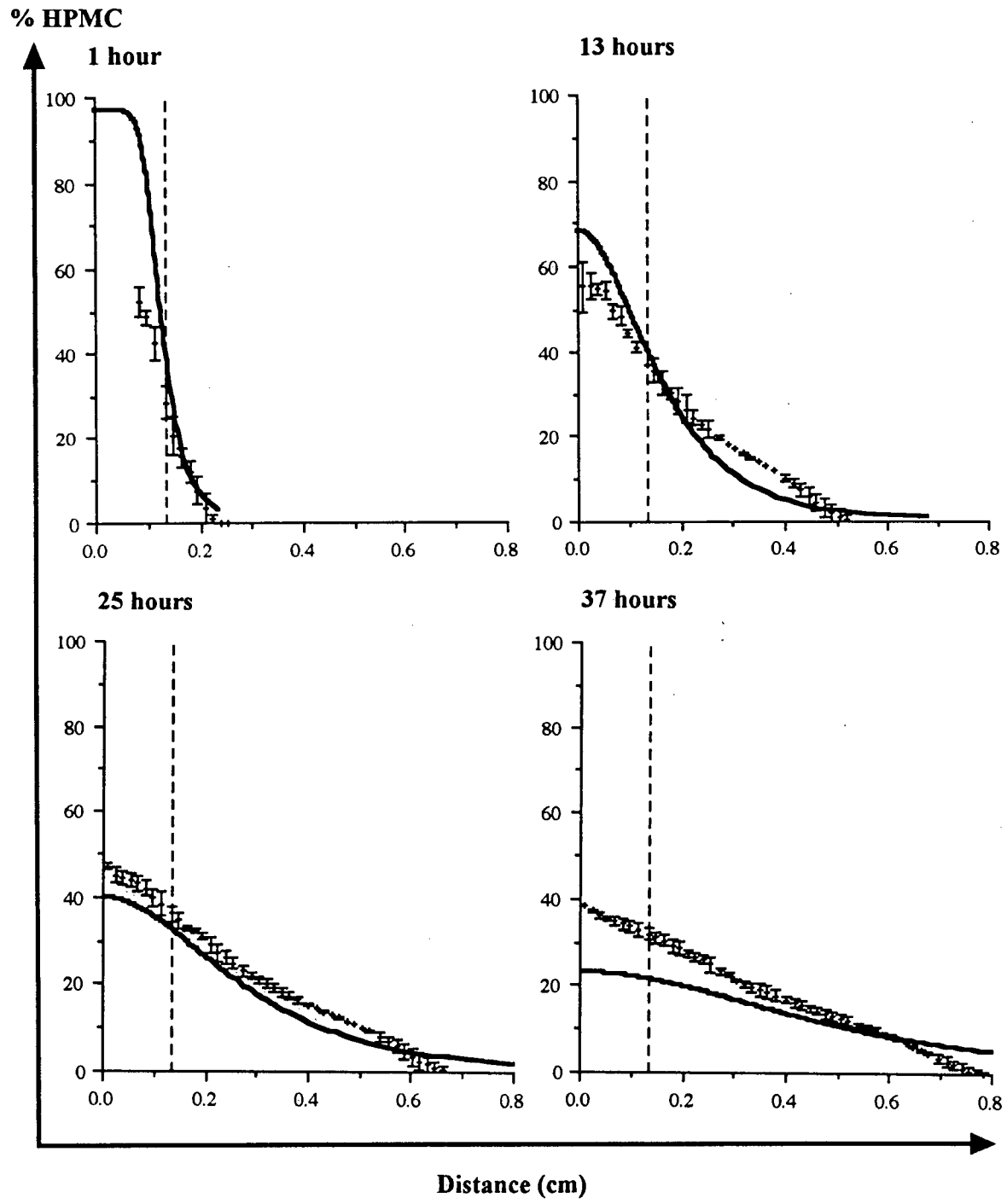

Figure 5.1 One-dimensional theoretical distribution profiles indicated by the solid line coupled together with the experimental distribution profiles carried out at 22 °C by Blazek [3] as indicated by the crosshairs. The dashed vertical line indicates the original tablet thickness. The axes in the plots are indicated by the arrows.

5.2 A Newer Mathematical Model Describing the Swelling of HPMC Tablets

5.2.1 Background

Previous mathematical models have attempted to provide a realistic description that took into account all the important phenomena that occurred during the drug release process [23, 24]. However, due to various assumptions made such as a constant water diffusion coefficient and neglect of the swelling process, these models were unable to provide a detailed account of the swelling of the tablet and the subsequent drug release. A newer mathematical model was proposed by Siepmann et al. [25] that took into account the water penetration, the subsequent swelling, and the resulting drug release. Although the model allowed for the study of drug release, the current investigation of HPMC is focussed on the study of the swelling process in terms of polymer concentration. The model was designed to be applicable for the case of three-dimensional swelling of cylindrical shaped devices such as tablets that involved the water penetration into both flat faces and the sides. There are four assumptions the model makes:

(1) Dissolution of the polymer is ignored.

(2) Swelling is ideal (the total volume of tablet at any given time is equal to the sum of the volumes of polymer and water), isotropic, and homogeneous.

(3) The water concentration at the surface of the tablet is equal to its equilibrium value.

(4) Water imbibing in the vertical/radial direction leads to volume increase in the corresponding vertical/radial direction that is proportional to the relative surface area.

The equation describing the concentration of water as a function of time, diffusion constant, and position within a three-dimensional swelling tablet is given by 5.1.

$$\frac{\partial c_1}{\partial t} = \frac{\partial}{\partial r}\left(D_1 \frac{\partial c_1}{\partial r}\right) + \frac{D_1}{r}\frac{\partial c_1}{\partial r} + \frac{\partial}{\partial z}\left(D_1 \frac{\partial c_1}{\partial z}\right) \qquad (5.1)$$

In the above equation, D_1 is the diffusion coefficient, r is the radial coordinate, and z is the

vertical coordinate measured from the center point of the cylinder. However, since only the one-dimensional swelling of HPMC tablets will be considered in the present work, Equation 5.1 can be simplified to describe the water penetration and subsequent swelling in only one-dimension as in Equation 5.2.

$$\frac{\partial c_1}{\partial_t} = \frac{\partial}{\partial_z}\left(D_1 \frac{\partial c_1}{\partial_z}\right) \tag{5.2}$$

One important improvement that this model attempts to take into account is concentration dependent diffusion coefficients of water which is described by an exponential dependence relationship [26] as in Equation 5.3.

$$D_1 = D_{1eq}\, e^{\left(-\beta_1\left(1 - \frac{c_1}{c_{1eq}}\right)\right)} \tag{5.3}$$

β_1 is a dimensionless constant describing this concentration dependence and D_{1eq} is the diffusion coefficient of water in the "equilibrium swollen state" of the system. The purpose and importance of the D_{1eq} constant is discussed in Sections 5.2.3 and 5.2.4.

At time ($t = 0$), the tablet is dry and the water concentration is equal to zero and written as:

$$t = 0 \qquad c_1 = 0 \qquad 0 \le z \le Z_0 \tag{5.4}$$

where Z_0 is the initial thickness of the tablet. At the surface of the tablet, the concentration of water is assumed to be equal to c_{1eq} or 1 g/mL. At $t > 0$, this is written as:

$$t > 0 \qquad c_1 = c_{1eq} \qquad 0 \le z \le Z_t \tag{5.5}$$

where Z_t represents the time dependent thickness of the HPMC tablet. There are two unknown parameters that have to be determined: β_1 and D_{1eq}. These unknown parameters were determined by Siepmann et al. [25] by using water uptake data for HPMC tablets by Tahara [27] calculated by a least-squares method [28]. The β_1 and D_{1eq} constants thus determined are given

as 2.5 and 5.6 x 10^{-6} cm^2/s (this value is less than the self diffusion coefficient for water, Section 5.2.3) respectively.

Due to the concentration dependence of the diffusion coefficients, the equations were solved numerically using the method of finite differences. This involved the discretization of the tablet into a finite number of space intervals similar to the segmented tablet model. In addition, a particular swelling time was also divided into a finite number of time intervals. The concentration of a space interval at a particular swelling time, e.g. 1 hour, was calculated when the concentration of this space interval at the previous time interval was known.

A second research paper published by Siepmann et al. [29] incorporated a dissolution mechanism. A constant characterizing this process was obtained by determining the dry tablet mass at $t = 0$ and t and fitting the results to an equation. However, the mathematical treatment remained unchanged from the original research paper. The most recent research paper by Siepmann et al. [30] redefined Equation 5.3 but the basic equation remained unchanged. D_{1eq} and c_{1eq} were redefined to D_{1crit} and c_{1crit} to describe the diffusion and concentration at the polymer/water interface. However, the present work involves the evaluation of the original paper published by Siepmann et al. [25].

5.2.2 Evaluation of the Mathematical Model

The results from the model were compared to the results obtained from the one-dimensional swelling experiments for Types 1 to 3 HPMC tablets at 37 °C. Present in all these profiles is the characteristic "bump" that appears to be a genuine feature that must be taken into account when attempting to model the one-dimensional swelling of HPMC tablets. The results of the theoretical distribution profiles along with their corresponding experimental profiles are shown in Figures 5.2 to 5.4. As was discussed in Chapter 3, the limit of reliability for the

determination of polymer concentration is considered to be approximately 35% HPMC. Therefore, when comparing the theoretical distribution profiles to the experimental results, only the region less than 35% HPMC as indicated by the dashed horizontal line in all the plots should be considered. The model provides very poor fits, consistently predicting less swelling at the longer swelling times for the three different tablet thicknesses.

It is important to note that one claim the model by Siepmann et al. [25] makes is that it is applicable to pure HPMC tablets like those studied here. However, the original water uptake data by Tahara [27] which Siepmann et al. [25] used to calculate the β_1 and D_{1eq} constants was obtained from tablets that contained 33% lactose as well as HPMC! Lactose is very water soluble and when incorporated together with HPMC into a tablet which is placed in water, the lactose should dissolve as water penetrates the tablet. This should result in the water having a greater accessibility to HPMC and therefore a faster penetration rate into the core of the tablet. One-dimensional experiments carried out with a tablet containing lactose confirmed that the core of the tablet became very water concentrated after approximately 28 hours compared to the behaviour of a pure HPMC tablet. The incorporation of lactose together with HPMC further complicates the swelling process but more importantly the swelling behaviour cannot be equivalent to that of a pure HPMC system. The β_1 and D_{1eq} constants are suspect and must be considered when trying to improve the theoretical distribution profiles.

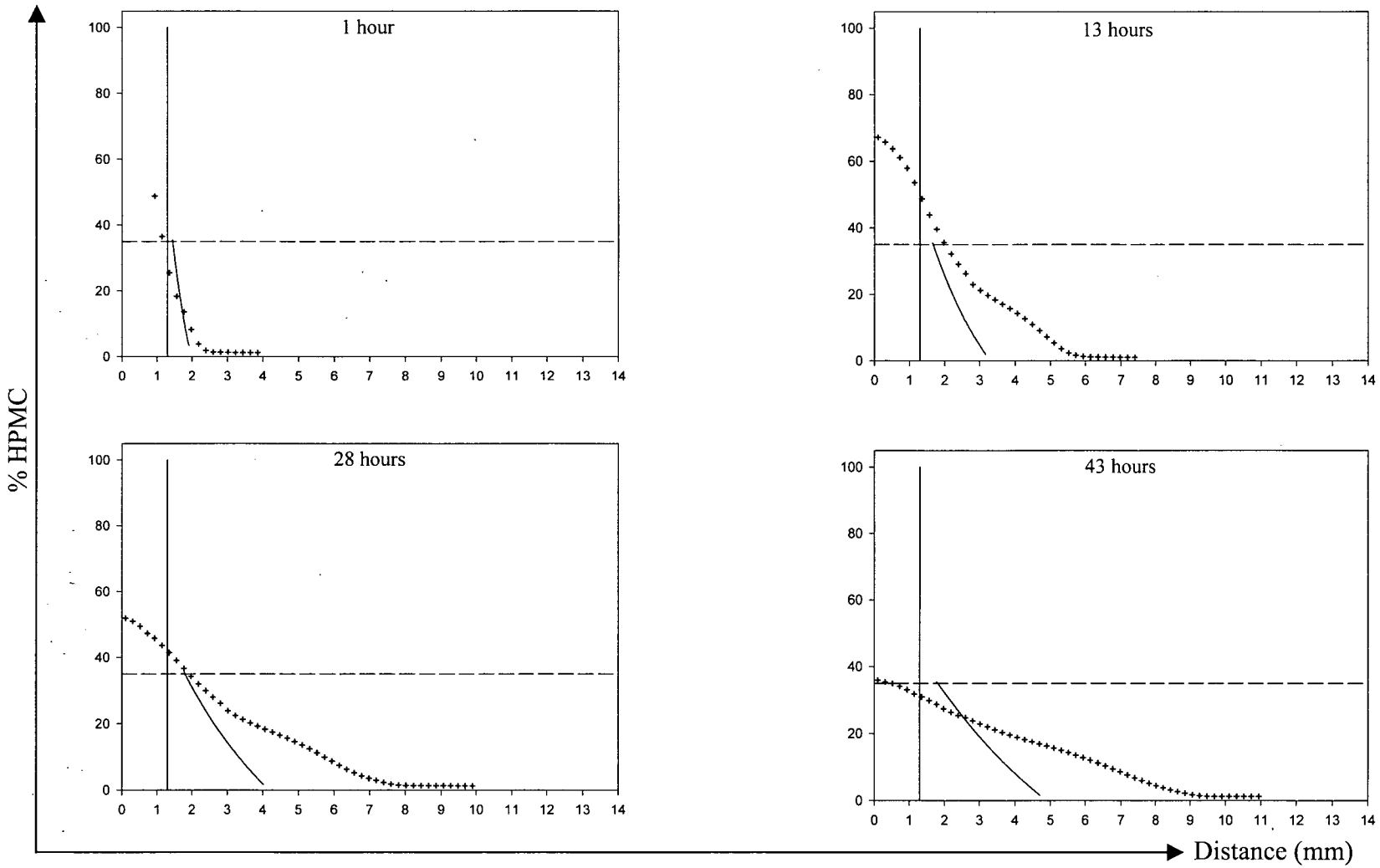

Figure 5.2 Experimental swelling distributions (crosshairs) and the theoretical swelling distribution profiles (solid line) of Type 2 HPMC tablet at 37 °C. $\beta_1 = 2.5$ and $D_{1eq} = 5.6 \times 10^{-6}$ cm^2/s given by Siepmann et al. [25]. The vertical line at 1.35 mm indicates the original tablet thickness. The dashed horizontal line at 35% HPMC indicates the limit of reliability of the results from the swelling experiment. The axes in the plots are defined by the arrows.

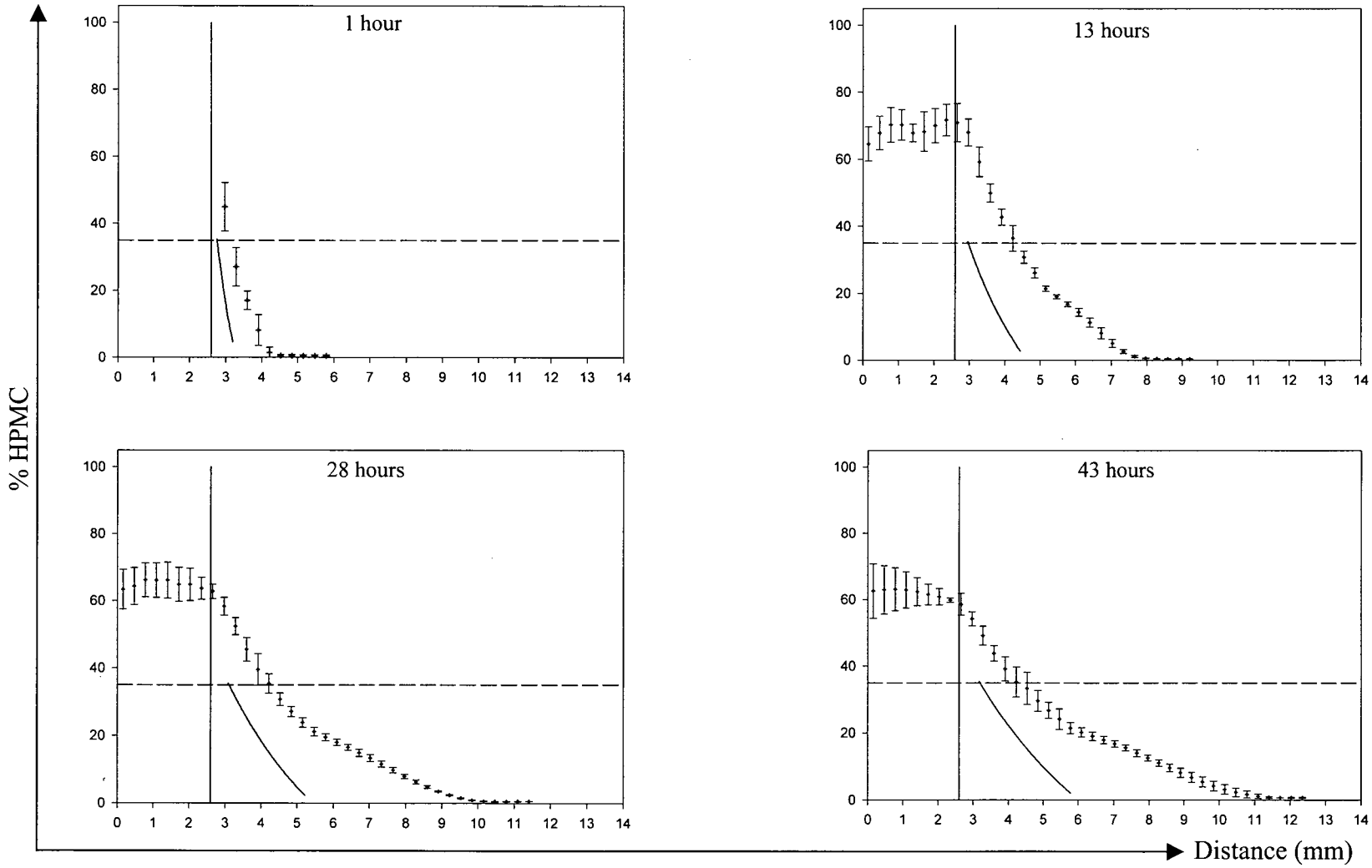

Figure 5.3 Average experimental swelling distributions (crosshairs) and the theoretical swelling distribution profiles (solid line) of Type 1 HPMC tablet at 37 °C. $\beta_1 = 2.5$ and $D_{1eq} = 5.6 \times 10^{-6}$ cm^2/s given by Siepmann et al. [25]. The vertical line at 2.66 mm indicates the original tablet thickness. The dashed horizontal line at 35% HPMC indicates the limit of reliability of the results from the swelling experiment. The axes in the plots are defined by the arrows.

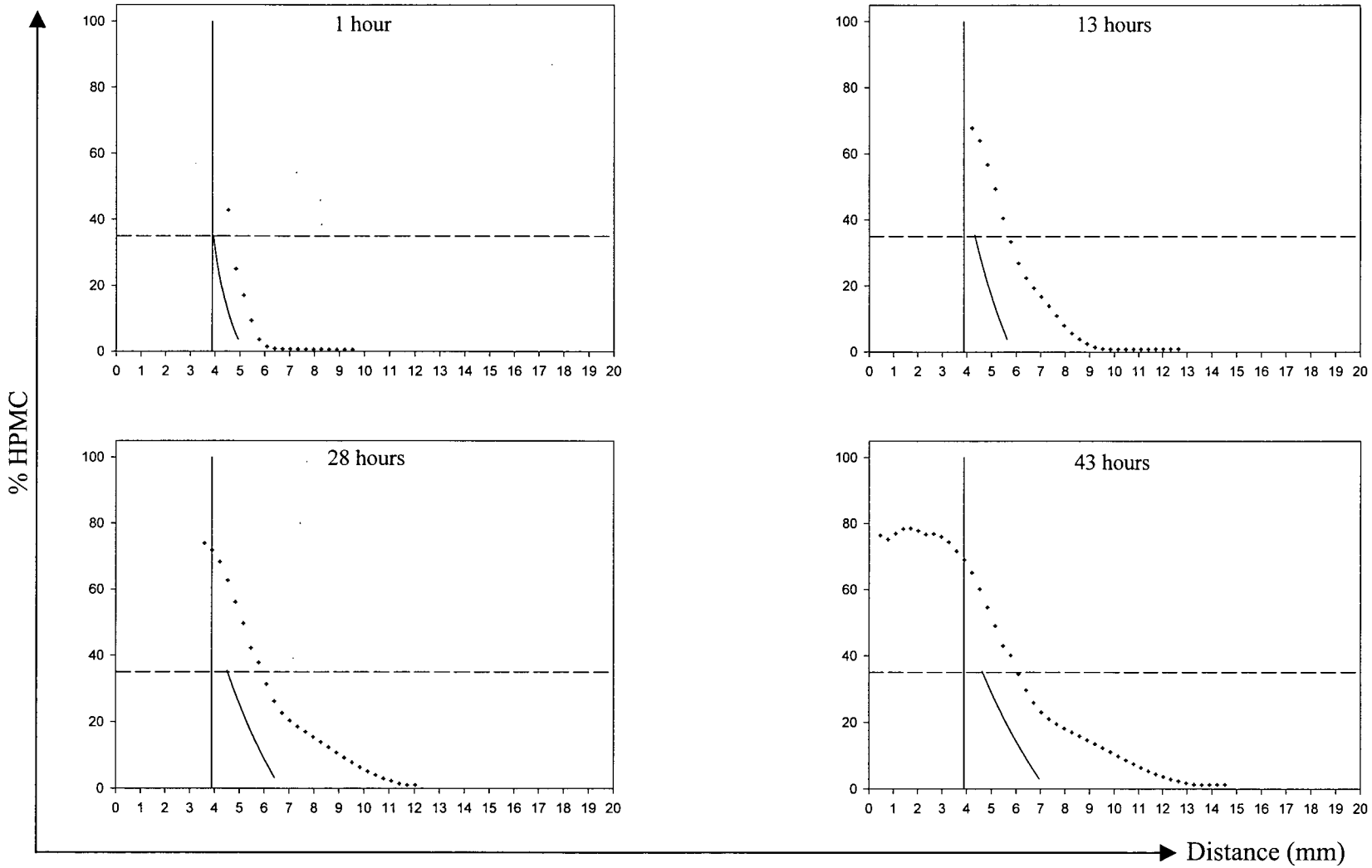

Figure 5.4 Experimental swelling distributions (crosshairs) and the theoretical swelling distribution profiles (solid line) of Type 3 HPMC tablet at 37 °C. $\beta_1 = 2.5$ and $D_{1eq} = 5.6 \times 10^{-6}$ cm^2/s given by Siepmann et al. [25]. The vertical line at 3.89 mm indicates the original tablet thickness. The dashed horizontal line at 35% HPMC indicates the limit of reliability of the results from the swelling experiment. The axes in the plots are defined by the arrows.

5.2.3 Further Evaluation of the Mathematical Model: A Modified Version

In an attempt to determine more realistic D_{1eq} and β_1 constants, a series of experimental water self-diffusion coefficients, D, for known polymer/water mixtures were measured. The pulse sequence used to measure these self-diffusion coefficients is called the pulsed gradient spin echo and is shown in Figure 5.5. It is similar to the spin-echo pulse sequence in Figure 1.5

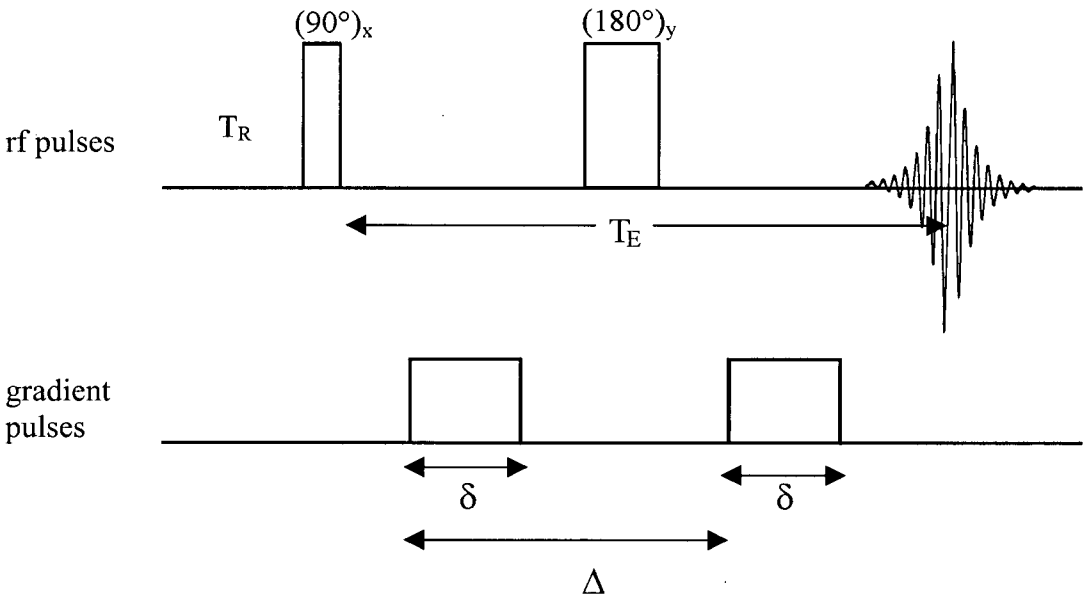

Figure 5.5 Pulsed gradient spin-echo sequence used to measure self-diffusion coefficients.

except for the application of two magnetic field gradient pulses. The application of the gradients purposely causes an inhomogeneous magnetic field. The effect of diffusion in an inhomogeneous magnetic field on the spin-echo experiment was first described by Hahn [18] and Carr [19]. In terms of only the rf pulses, after the 90° pulse, the spins begin to dephase and the 180° pulse refocuses the magnetization so that they are coherent. The complete refocusing of the magnetization only occurs when all the spins precessing at their Larmor frequency have not moved for the duration of the experiment. However, when a spin diffuses in an inhomogeneous magnetic field, the refocusing of the magnetization is reduced due to the change in its precessional frequency as it has moved to a different position in the field gradient. The result of

the refocusing pulse is thus a decrease in the echo amplitude. The decrease in the echo amplitude is as a result of varying one of several factors: δ, Δ, or G. δ is the duration of the magnetic field and Δ is the time delay between the application of the first and second gradient. In this case, the gradient strength (G) was incremented through a series of steps and the signal intensity, $I[G]$, was measured. The self-diffusion coefficient was determined by fitting the results to Equation 5.6. The resulting self-diffusion coefficients for water obtained from these

$$\frac{I[G]}{I[O]} = e^{\left[\left(-D^2\right)\left(2\pi\gamma G\delta\right)\left(\Delta-\frac{\delta}{3}\right)\left(10^4\right)\right]} \tag{5.6}$$

measurements for the different polymer/water mixtures are given in Table 5.1. These were fitted to Equation 5.3 using a two parameter fit and a new D_{1eq} constant was obtained equal to 3 x 10^{-5} cm^2/s. The new D_{1eq} constant is approximately ten times greater than the original value given. The resulting β_1 constant obtained was equal to 5.7 which is approximately twice as big as the original β_1 constant given by Siepmann et al. [25]. The model was modified to include these changes and new theoretical swelling profiles were generated for the three different tablet types as shown in Figures 5.6 to 5.8. Again, emphasis should be placed in the region below 35%

Table 5.1 Water self-diffusion coefficients for the different HPMC concentrations at 37 °C.

% HPMC	D (x 10^{-5}) cm^2/s
0	3.94
4.47	2.03
8.98	1.79
17.8	1.39
27.4	0.941
37	0.719

HPMC due to the limit in reliability of the experimental polymer concentrations. Compared to the previous theoretical treatment, the current fits are considerably improved. An increase in D_{1eq} by a factor of ten and an increase in β_1 by a factor of more than two increases the swelling of the theoretical profiles. However, for the three different tablet types, the model still predicts a lesser degree of swelling compared to the experimental profiles. To illustrate the effects that D_{1eq} and β_1 have on the outcome of the theoretical distribution profiles, these constants were varied as shown in Figure 5.9. In Figure 5.9 (a) three theoretical profiles are shown along with the experimental profile at 43 hours for the Type 2 tablet. Each of the profiles has the same D_{1eq} constant but varying β_1 constants. Shown in Figure 5.9 (b) are three theoretical distribution profiles; however, this time β_1 is fixed and D_{1eq} is varied. From these figures, it is clear that both of these two constants affect the theoretical profiles in terms of the degree of swelling. The β_1 value is defined as a dimensionless constant describing the concentration dependent water diffusivities. Because it is a poorly defined constant, it could be optimized to fit the experimental distribution profiles while keeping D_{1eq} constant as determined from the experimental data. This is discussed in the next section.

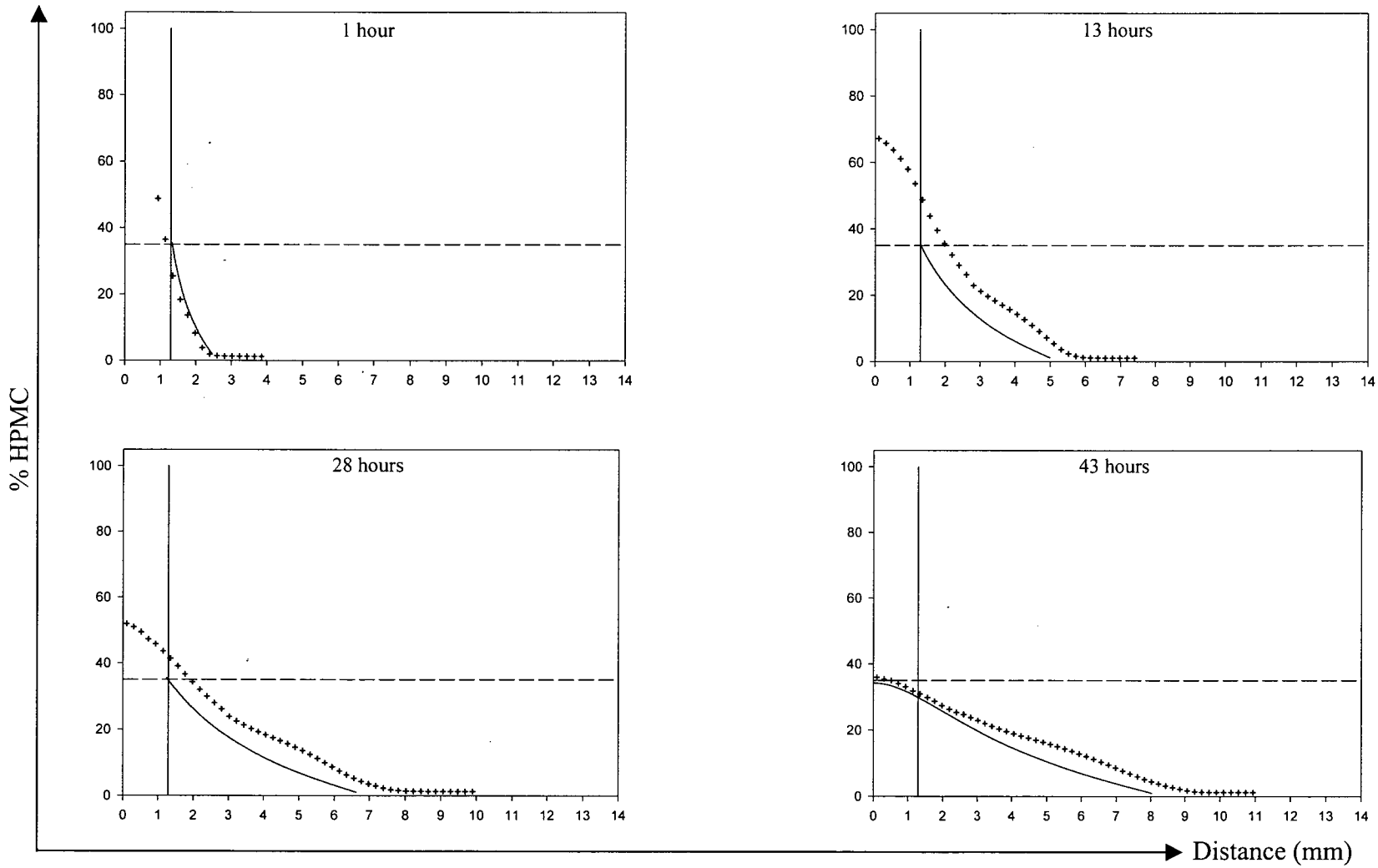

Figure 5.6 Experimental swelling distributions (crosshairs) and the theoretical swelling distribution profiles (solid line) of Type 2 HPMC tablet at 37 °C. $\beta_1 = 5.7$ and $D_{1eq} = 3.0 \times 10^{-5}$ cm^2/s. The vertical line at 1.35 mm indicates the original tablet thickness. The dashed horizontal line at 35% HPMC indicates the limit of reliability of the results from the swelling experiment. The axes in the plots are defined by the arrows.

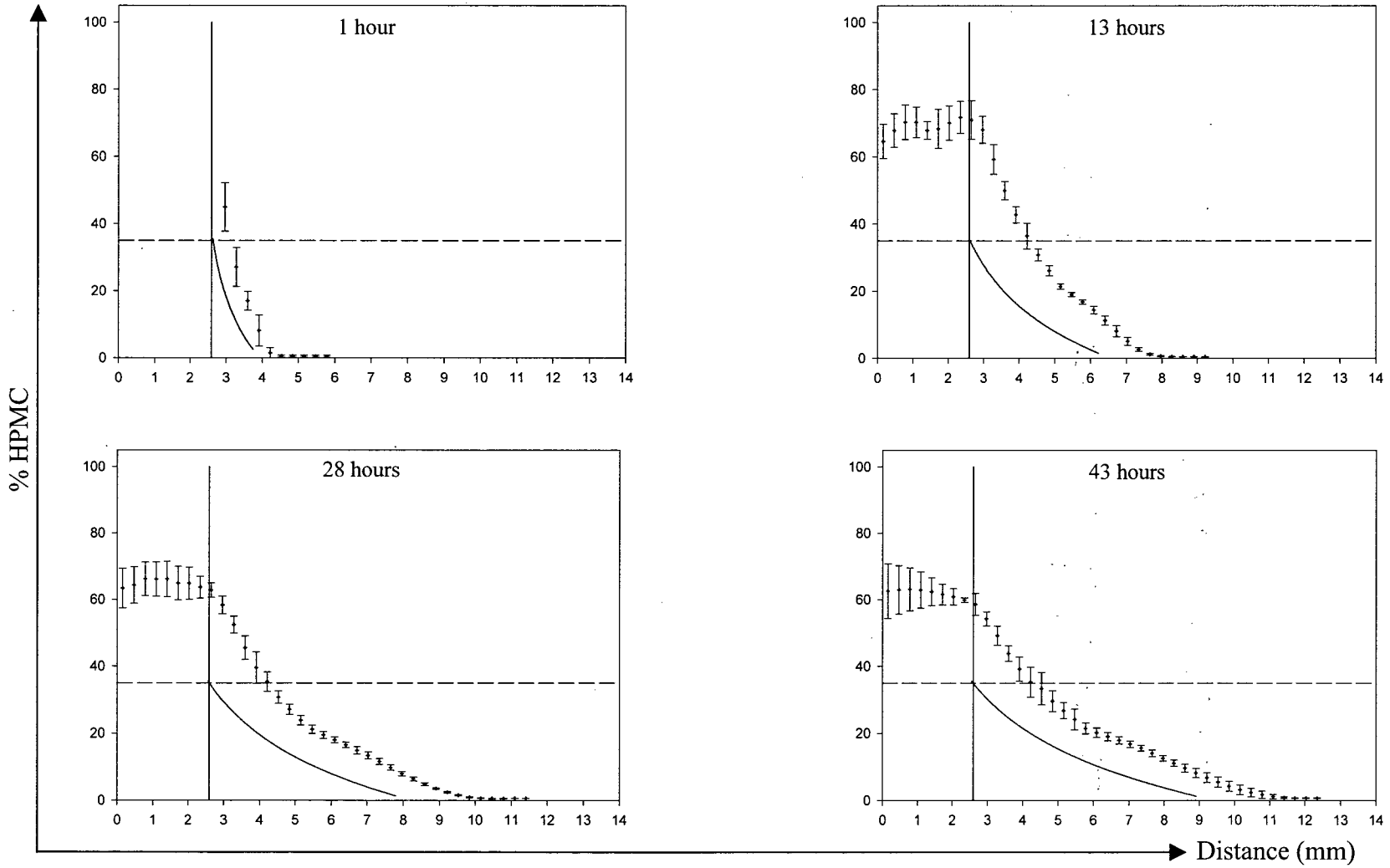

Figure 5.7 Average experimental swelling distributions (crosshairs) and the theoretical swelling distribution profiles (solid line) of the Type 1 HPMC tablet at 37 °C. $\beta_1 = 5.7$ and $D_{1eq} = 3.0 \times 10^{-5}$ cm^2/s. The solid vertical line at 2.66 mm indicates the original tablet thickness. The dashed horizontal line at 35% HPMC indicates the limit of reliability of the results from the swelling experiment. The axes in the plots are defined by the arrows.

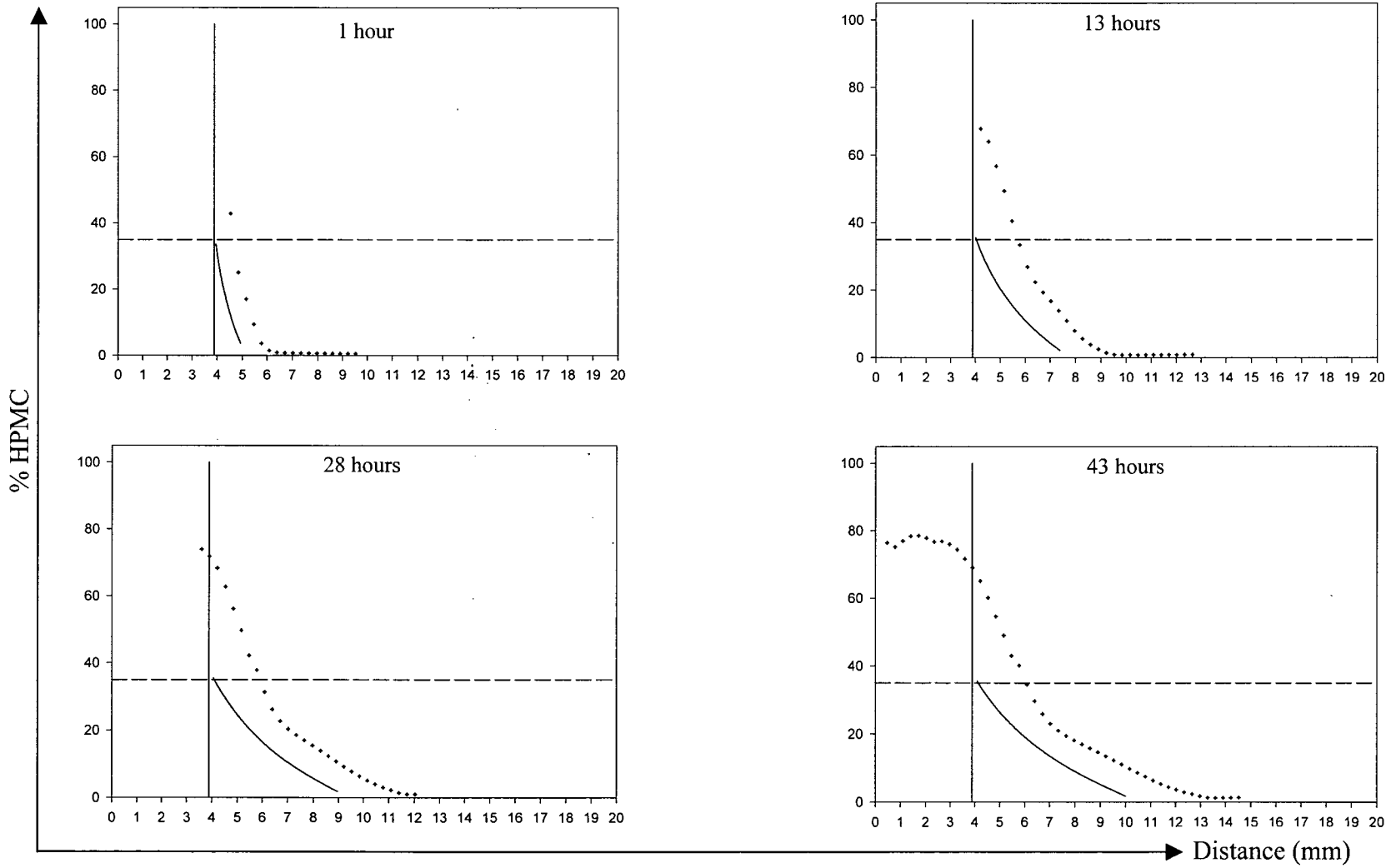

Figure 5.8 Experimental swelling distributions (crosshairs) and the theoretical swelling distribution profiles (solid line) of Type 3 HPMC tablet at 37 °C. $\beta_1 = 5.7$ and $D_{1eq} = 3.0 \times 10^{-5}$ cm^2/s. The vertical line at 3.89 mm indicates the original tablet thickness. The dashed horizontal line at 35% HPMC indicates the limit of reliability of the results from the swelling experiment. The axes in the plots are defined by the arrows.

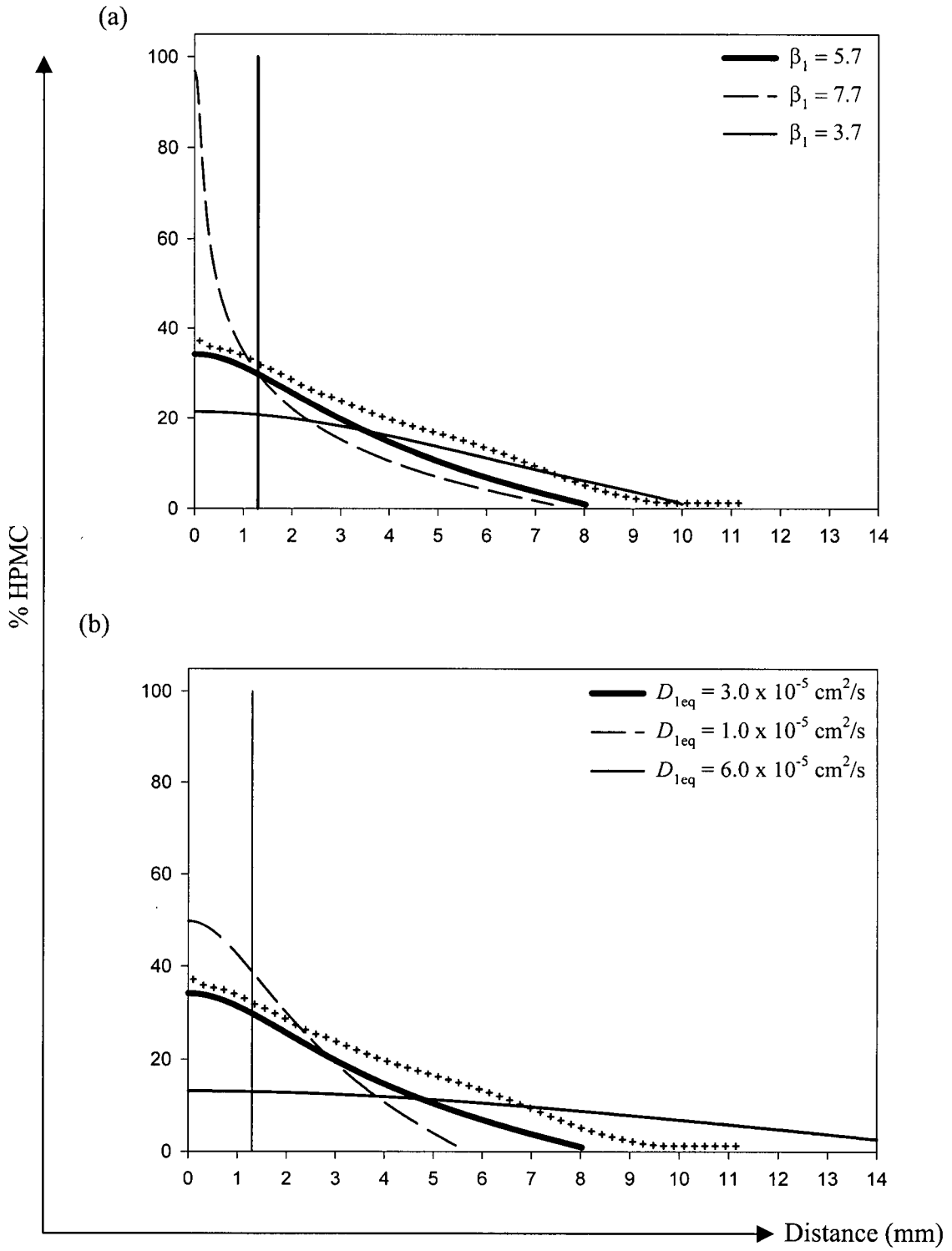

Figure 5.9 Effects on the theoretical distribution profiles when β_1 and D_{1eq} are varied and shown alongside the experimental distribution profiles (crosshairs). (a) D_{1eq} is fixed and equal to 3.0 x 10^{-5} cm^2/s; β_1 is varied. (b) β_1 is fixed and equal to 5.7; D_{1eq} is varied. The axes in the plots are defined by the arrows.

5.2.4 Further Evaluation of the Mathematical Model: An Optimized Version

The best possible theoretical distribution profiles were achieved by varying β_1 while keeping D_{1eq} constant. The optimal theoretical distribution profiles are described as having the minimum sum of χ^2 between the theoretical and experimental polymer concentrations. As a result, new β_1 constants were generated for each of the different tablet thicknesses for each of the swelling times and these were averaged to produce a single β_1 value for a specific tablet thickness. The results for the theoretical distribution profiles using average β_1 values are shown in Figures 5.10 to 5.12.

From the profiles shown, there appears to be a large improvement in the fitting of the profiles for all three tablet thicknesses compared to the fits in Figures 5.6 to 5.8. The model attempts to predict a swelling process for a single phase one component system. However, it must be noted that the swelling process is more complex than it appears. This is reflected by the optimized β_1 constant being quite different for each tablet thickness. Further, in all the experimental profiles for the different tablet thicknesses, a characteristic "bump" was present at approximately 25% HPMC. This "bump" could be described as a boundary dividing two regions having two different components and is indicative of a heterogeneous system. The first region that was less than 25% HPMC is usually classified as a transparent gel region ranging from a semi-dilute solution to a viscous solution. The second region that was greater than 25% HPMC is usually classified as an opaque region resembling wetted powders rather than a gel. This region would have a much reduced mobility of the polymer chains resulting in a more restricted rotational motion of these chains. It is clear that the constants: β_1 and D_{1eq} or the equations given by Siepmann et al. [25] or both are questionable. Siepmann et al. [25] in their research claimed they had included in their calculations a new mathematical model which took into account concentration dependent water diffusivities as indicated by Equation 5.3. However, included in

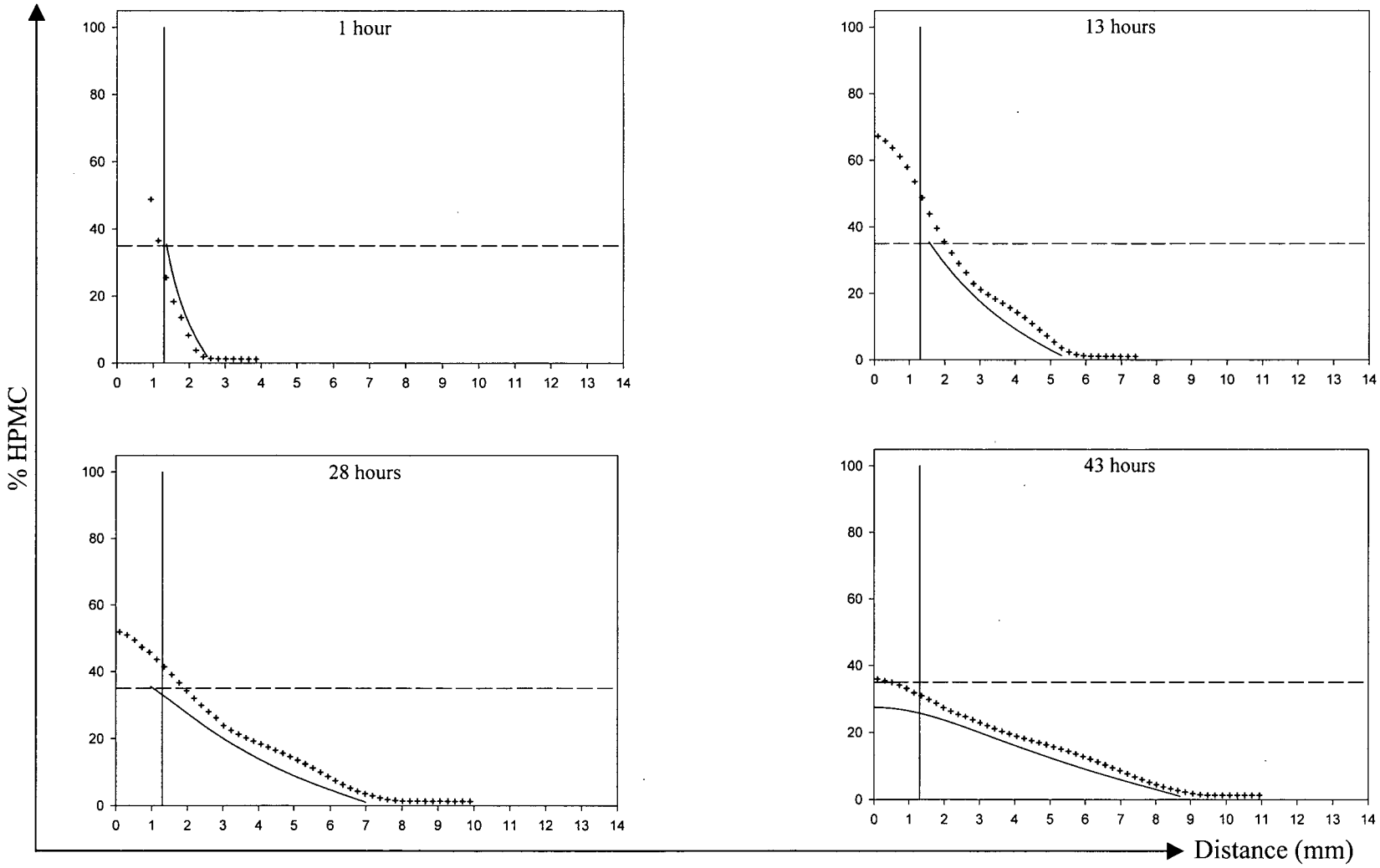

Figure 5.10 Experimental swelling distributions (crosshairs) and the optimized theoretical swelling distribution profiles (solid line) of Type 2 HPMC tablet at 37 °C. $\beta_1 = 4.9$ and $D_{1eq} = 3.0 \times 10^{-5}$ cm^2/s. The vertical line at 1.35 mm indicates the original tablet thickness. The dashed horizontal line at 35% HPMC indicates the limit of reliability of the results from the swelling experiment. The axes in the plots are defined by the arrows.

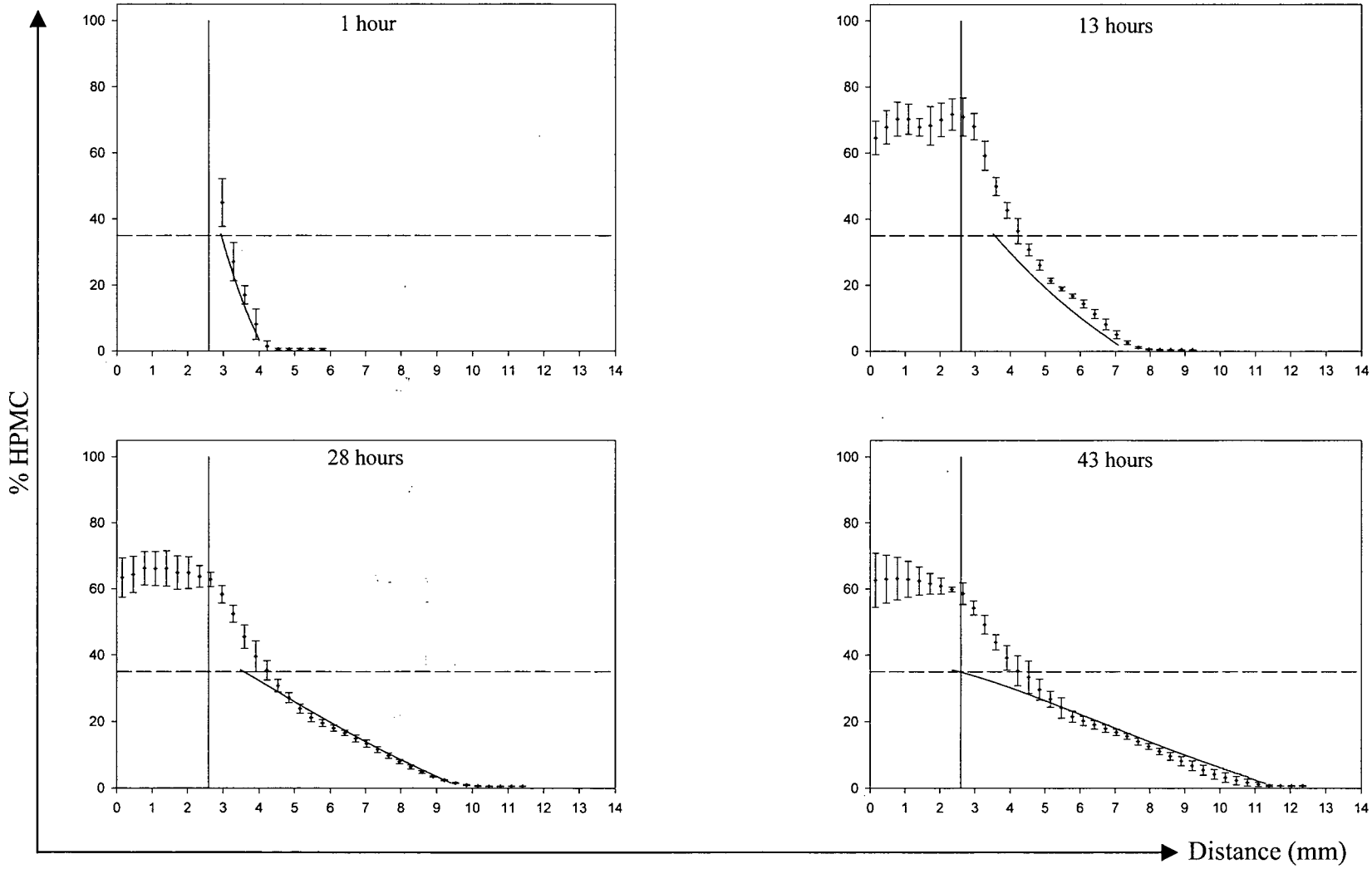

Figure 5.11 Average experimental swelling distributions (crosshairs) and the optimized theoretical swelling distribution profiles (solid line) of Type 1 HPMC tablet at 37 °C. $\beta_1 = 2.1$ and $D_{1eq} = 3.0 \times 10^{-5}$ cm^2/s. The vertical line at 2.66 mm indicates the original tablet thickness. The dashed horizontal line at 35% HPMC indicates the limit of reliability of the results from the swelling experiment. The axes in the plots are defined by the arrows.

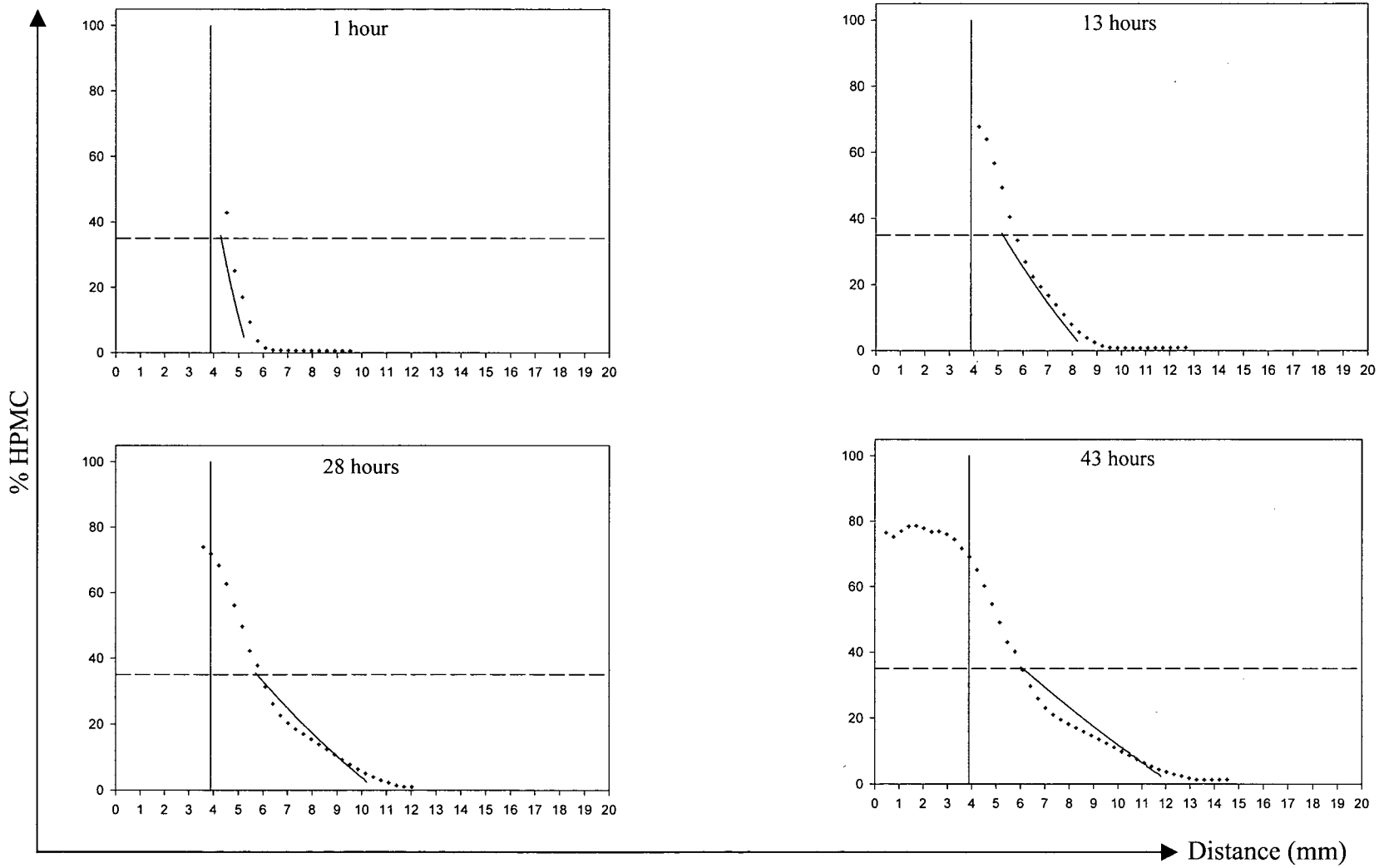

Figure 5.12 Experimental swelling distributions (crosshairs) and the optimized theoretical swelling distribution profiles (solid line) of Type 3 HPMC tablet at 37 °C. $\beta_1 = 1.9$ and $D_{1eq} = 3.0 \times 10^{-5}$ cm^2/s. The vertical line at 3.89 mm indicates the original tablet thickness. The dashed horizontal line at 35% HPMC indicates the limit of reliability of the results from the swelling experiment. The axes in the plots are defined by the arrows.

this same equation is a D_{1eq} constant that describes the diffusion coefficient in the equilibrium swollen state.

The evaluation of the one-dimensional swelling theoretical profiles against the experimental data showed several deficiencies. The ability of the proposed model to therefore predict the three-dimensional swelling would result in the same outcome and as such, the three-dimensional theoretical distribution concentrations were not calculated.

5.3 Summary

The model proposed by Siepmann et al. [25] could not simulate the one-dimensional swelling profiles at all but could do so only with certain modifications, in particular to the D_{1eq} and β_1 constants. For the optimized version, the D_{1eq} constant was determined using actual water diffusivities for various polymer/water mixtures and β_1 was determined from the fits to the profiles. The D_{1eq} constant differed by a factor of ten from the original constant given by Siepmann et al. [25]. One clear observation from all the results of the theoretical one-dimensional swelling distribution profiles is the model's inability to generate the characteristic "bump" that was present in the experimental distribution profiles and the fact that different β_1 values had to be used to fit the results from different tablet thicknesses. Just as with previous theoretical models, the assumption was made that the swelling process of HPMC is a single phase one component system. However, as indicated by the experimental distribution profiles, it is a distinct two component system and this must be taken into account when attempting to simulate the one-dimensional swelling behaviour of HPMC tablets.

Chapter 6

Conclusions and Suggestions for Future Work

6.1 Conclusions

Although the work presented in this thesis was restricted to the investigation of swelling HPMC tablets and was not combined with the investigation of the drug release process, it is essential to understand the swelling process first since this determines the release profile of a drug. With the present imaging equipment and the implementation of the multi-echo pulse sequence, it was possible to investigate the three-dimensional swelling of a HPMC tablet. The ability of NMR imaging to monitor the changes in the concentration and dimension of a swelling tablet proved to be an invaluable tool. However, in order to gain a better understanding of the swelling process, the swelling of the tablet was limited to one-direction to simplify the interpretation of the results. The one-dimensional swelling distributions provided a better insight into a complex swelling process that was previously considered to be in a homogeneous one component system. Attempts made to provide a theoretical model that is able to accurately describe this swelling have not been successful. However, the recently proposed theoretical model by Siepmann et al. [25] includes several important considerations when attempting to describe the swelling process that could be incorporated in a future mathematical model.

6.2 Suggestions for Future Work

Further advancements in the current mathematical model by Siepmann et al. [25] such as including a two component description and the ability to generate the characteristic "bump" would allow a more accurate prediction of the swelling process. This would involve a more complex set of equations containing twice as many variables.

The three-dimensional swelling is the precursor to the three-dimensional drug release investigation. Fluorine containing compounds or fluorine substituted drugs would allow for the

study of this release process by ^{19}F NMR imaging. However, the ultimate goal for the investigation of these systems is to monitor these tablets *in vivo*. This could be accomplished by first investigating these tablets in a simulated gastric fluid medium which would be able to provide direct information of these tablets *in vivo*. The next step would be to carry out a whole body imaging study where the swelling of the tablet could be monitored as it passes through the gastrointestinal tract of a person. Important information would be obtained on how closely the *in vitro* flow cell experiments mirror the actual *in vivo* swelling of tablets.

Bibliography

[1] D. L. Sackett, J. C. Snow, in R. B. Haynes, D. W. Taylor, D. L. Sackett (Eds.): *Compliance in Health Care*, John Hopkins University Press, Baltimore 1979, p. 11.

[2] R. Langer, *Science 249* (1990) 1527.

[3] A. Blazek, *Department of Chemistry*, The University of British Columbia, Vancouver 1998.

[4] P. Colombo, U. Conte, A. Gazzaniga, L. Maggi, M. E. Sangalli, N. A. Peppas, A. L. Manna, *Int. J. Pharm. 63* (1990) 43.

[5] N. A. Peppas, P. Colombo, *J. Controlled Release 45* (1997) 35.

[6] V. Vigoreaux, E. S. Ghaly, *Drug Dev. Ind. Pharm. 20* (1994) 2519.

[7] N. A. Peppas, R. Gurny, E. Doelker, P. Buri, *J. Membr. Sci. 7* (1980) 241.

[8] U. Conte, L. Maggi, P. Colombo, A. L. Manna, *J. Controlled Release 26* (1993) 39.

[9] A. R. Rajabi-Siahboomi, R. W. Bowtell, P. Mansfield, A. Henderson, M. C. Davies, C. D. Melia, *J. Controlled Release 31* (1994) 121.

[10] R. Bowtell, J. C. Sharp, A. Peters, P. Mansfield, A. R. Rajabi-Siahboomi, M. C. Davies, C. D. Melia, *Magnetic Resonance Imaging 2* (1994) 361.

[11] E. M. Purcell, H. C. Torrey, R. V. Pound, *Phys. Rev. 69* (1946) 37.

[12] F. Bloch, W. W. Hansen, M. Packard, *Phys. Rev. 69* (1946) 127.

[13] R. K. Harris, *Nuclear Magnetic Resonance Spectroscopy*, Longman Scientific & Technical, Essex, UK 1987.

[14] C. Dybowski, R. L. Licter, *NMR Spectroscopy Techniques, Vol. 5*, Marcel Dekker, Inc., New York, NY 1987.

[15] A. Abragam, *Principles of Nuclear Magnetism*, Clarendon Press, Oxford, UK 1983.

[16] R. Freeman, *A Handbook of Nuclear Magnetic Resonance*, Longman Scientific & Technical, Essex, UK 1983.

[17] R. L. Vold, J. S. Waugh, M. P. Klein, D. E. Phelps, *J. Chem. Phys. 48* (1968) 3831.

[18] E. L. Hahn, *Phys. Rev. 80* (1950) 580.

[19] H. Y. Carr, E. M. Purcell, *Physical Rev. 94* (1954) 630.

[20] P. C. Lauterbur, *Nature 242* (1973) 190.

[21] P. Mansfield, P. K. Grannell, *J. Phys. C: Solid State Phys. 6* (1973) L422.

[22] T. Koizumi, S. P. Panomsuk, T. Hatanaka, K. Katayama, *Pharm. Res. 13* (1996) 329.

[23] D. Hariharan, N. A. Peppas, R. Bettini, P. Colombo, *Int. J. Pharm. 112* (1994) 47.

[24] P. Gao, P. R. Nixon, J. W. Skoug, *Pharm. Res. 12* (1995) 965.

[25] J. Siepmann, K. Podual, M. Sriwongjanya, N. A. Peppas, R. Bodmeier, *J. Pharm. Sci. 88* (1999) 65.

[26] H. Fujita, *Fortschr. Hochpolym.-Forsch 3* (1961) 1.

[27] K. Tahara, K. Yamamoto, T. Nishihata, *J. Controlled Release 35* (1995) 59.

[28] U. Hoffmann, H. Hoffmann, *Einfuehrung in die Optimierung, Verlag Chemis GmbH*, Weinheim, Germany 1971.

[29] J. Siepmann, H. Kranz, R. Bodmeier, N. A. Peppas, *Pharm. Res. 16* (1999) 1748.

[30] J. Siepmann, N. A. Peppas, *Pharm. Res. 17* (2000) 1290.